

**“Design and Synthesis of Novel Scaffolds as B-Raf Kinase
Inhibitors for the Treatment of Skin Cancer.”**

A PROJECT SUBMITTED TO

NIRMA UNIVERSITY

in Partial Fulfillment for the Award of the Degree of

Master of Pharmacy

IN

Pharmaceutical Chemistry

BY

CHAVDA JAYDEEPSINH P. (17MPH402), B.Pharm

UNDER THE GUIDANCE OF

DR. HARDIK G. BHATT

**Associate Professor & Head,
Department of Pharmaceutical Chemistry**



INSTITUTE OF PHARMACY

NAAC ACCREDITED 'A' GRADE

**Department of Pharmaceutical Chemistry
Institute of Pharmacy
Nirma University
Ahmedabad-382481
Gujarat, India.**

May 2019

CERTIFICATE

This is to certify that the dissertation work entitled "Design and Synthesis of Novel Scaffolds as B-Raf Kinase Inhibitors for the Treatment of Skin Cancer." submitted by Mr. Jaydeepsinh Chavda with Regn. No. 17MPH402 in partial fulfillment for the award of Master of Pharmacy in "Pharmaceutical Chemistry" is a bonafide research work carried out by the candidate at the Department of Pharmaceutical Chemistry, Institute of Pharmacy, Nirma University under my/our guidance. This work is original and has not been submitted in part or full for any other degree or diploma to this or any other university or institution.

Guide



Dr. Hardik G. Bhatt

M. Pharm., Ph.D., MRSC

Associate Professor & Head,

Department of Pharmaceutical Chemistry,

Institute of Pharmacy,

Nirma University



Prof. Manjunath Ghate

M. Pharm., Ph.D.

Director

Institute of Pharmacy,

Nirma University

24/5/2019

CERTIFICATE OF ORIGINALITY OF WORK

This is to undertake that the dissertation work entitled "Design and Synthesis of Novel Scaffolds as B-Raf Kinase Inhibitors for the Treatment of Skin Cancer" Submitted by Mr. Jaydeepsinh Chavda (17MPH402) in partial fulfillment for the award of Master of Pharmacy in "Batch of 2017" is a bonafide research work carried out by me at the "Department of Pharmaceutical Chemistry", Institute of Pharmacy, Nirma University under the guidance of "Dr. Hardik G. Bhatt". I am aware about the rules and regulations of Plagiarism policy of Nirma University, Ahmedabad. According to that, this work is original and not reported anywhere as per best of my Knowledge.



Mr. Jaydeepsinh Chavda (17MPH402)
Department of Pharmaceutical Chemistry,
Institute of Pharmacy,
Nirma University

Guide



Dr. Hardik G. Bhatt
M. Pharm., Ph.D., MRSC
Associate Professor & Head,
Department of Pharmaceutical Chemistry,
Institute of Pharmacy,
Nirma University

24/5/2019

DECLARATION

I hereby declare that the dissertation entitled "Design and Synthesis of Novel Scaffolds as B-Raf Kinase Inhibitors for the Treatment of Skin Cancer." is based on the original work carried out by me under the guidance of Dr.Hardik G. Bhatt, Head & Associate Professor, Department of Pharmaceutical Chemistry, Institute of Pharmacy, Nirma University. I also affirm that this work is original and has not been submitted in part or full for any other degree or diploma to this or any other university or institution.



Mr. Jaydeepsinh Chavda (17MPH402)
Department of Pharmaceutical Chemistry,
Institute of Pharmacy,
Nirma University,
Sarkhej - Gandhinagar Highway,
Ahmedabad-382481,
Gujarat, India

24/5/2019

ACKNOWLEDGEMENTS

Man is an inexhaustible spring of potential. The endowments of intelligence and the resultant creativity, accords him the epithet “Crest jewel” of creation. Creativity proffers him the opportunity to bask in the delight of the divine effulgence within him.

This further leads him to the wondrous discovery and realization that the world around him is a glorified reflection of the same effulgence.

To gratefully and appreciatively acknowledge the blessings of the Almighty whose very existence has helped me sail smoothly so far ,I bow my head before him and thank him from the core of my heart for being there every time and anytime I needed him.

I am grateful to the blessings of the Almighty whose very existence helped me to sail smoothly so far. I bow my head before him and thank him from the core of my heart for being there every time and anytime I needed him.

But this journey of my success would not be possible without motivational and consistent support of **Dr. Hardik G. Bhatt**, Associate Professor and Head, Department of Pharmaceutical Chemistry, Nirma University. His guidance was priceless and I express my sincere thanks to him for being my guiding force throughout my research work. Without them this work could not be the same. I would like to express my humble and whole hearted thanks to Dr. Bhumika D. Patel, for her unremitting supervision, consistent guidance, enthusiastic encouragement and critical evaluation in this research work and expressing her faith in me.

I thank **Dr. Manjunath Ghate**, Director of IPNU for his helping hand throughout my work.

I would extend my thanks to Dr. Vivek Vyas, Dr. Jignasa Savjani and Ms. Palak Parikh for their motivational guidance.

My jovial gratitude is to Mr. Jignesh bhai and Shreyash bhai (Laboratory Assistants) for providing immeasurable and non-formal help and advice whenever needed.

I sincerely thanks to to Mr. Udit Chaube for being immeasurably considerate, non-formal and open in offering priceless and timely own advices during my dissertation work. His trust in me also inspired me to push myself beyond the limits. I am also thankful to Keerti Vishwkarma, Piyush Gediya their support and critical advice.

Thanks to Harshil, Karan, Kevin, Mitali, Priyancy, Rushabh, Sapna, Shivangi, Shreya, and Silvi for giving me such a pleasant time when working together with them since I knew them and creating such a great friendship at the Lab. It was indeed my pleasure to work with you all.

Sincere and deep hearted thanks to Tushar Sir, Vikas sir, Jignesh Sir, Vinod Sir, Atulbhai, Mayankbhai for inculcating the skills of chemistry laboratory within me during my training tenure at Piramal Discovery Solution (PDS).

Where would I be without my family? My parent deserves special mention for their inseparable support and prayers. Last but not the least we should not overlook, what lies behind our success, it is strength of my parents who had scarified their present to secure future for us.

Finally, I would like to thank everybody who was important to the successful realization of thesis, as well as expressing my apology that I could not mention personally one by one.

It is my immense pleasure to wind up my thesis with these beautiful lines of Robert Frost - “Woods are lovely, dark and deep but I have promises to keep miles to gobefore I sleep”

Thank you

Thank You

Jaydeepsinh Chavda

TABLE OF CONTENT

Contents	
Chapter 1 Introduction	1
Chapter 2 Literature Review	6
Chapter 3 Aim & Objectives	80
Chapter 4 Computational Analysis	81
4.1 Introduction to Computer-aided drug design	81
4.2 Pharmacophore modelling	82
4.3 Materials and Methods	90
4.4 Results and Discussion	94
4.5 Virtual Screening	97
4.6 Material and Methods	98
4.7 Results and Discussion	98
4.7 3D QSAR (Three Dimensional Quantitative Structural Activity Relationship)	102
4.8 Material and Methods	103
4.9 Result and Discussion	108
Chapter 5 Design of Novel B-Raf Inhibitors	125
5.2 Molecular Docking	127
5.3 In silico Pharmacokinetic properties	130
Chapter 6 Experimental Section	134
Chapter 7 In Vitro Pharmacological Screening	163
Chapter 8 In-Vivo Pharmacological Screening:	167
Chapter 9 Conclusion	178
Chapter 10 References	179

LIST OF FIGURES

Fig. 1	Pathophysiology of Melanoma Cancer
Fig. 2	Structure of Raf proteins: A-Raf, B-Raf and C-Raf; Three conserved regions (CR) -CR1, CR2 and CR3; RBD - Ras Binding Domain; CRD - Cysteine-rich domain and KD - Kinase domain; G-loop - A conserved glycine loop; and AS - the activation segment; C: Carboxyl-terminal domain; N: Amino-terminal domain.
Fig. 3	Progression in growth of cells through MAPK pathway (RAS-RAF-MEK-ERK pathway) in: A – Normal growth of cells involving wild type of B-Raf (B-Raf ^{WT}); B – Abnormal growth of cells (cancerous cells) involving V600E bearing B-Raf (B-Raf ^{V600E}).
Fig. 4	Pharmacophore model A) 3D pharmacophore model B) 2D pharmacophore model with distance between two features in Å.
Fig. 5	ROC curve with their AUC
Fig. 6	Steps for virtual screening
Fig. 7	Different alignment methods with common core scaffold of purinylpyridine derivatives: (a) Distill based alignment; (b) Pharmacophore based alignment; (c) Docking based alignment.
Fig. 8	The plot of experimental versus predicted activity of training and test set based on: (a) CoMFA model; (b) CoMSIA model (SHD); (c) CoMSIA model (SH); (d) HQSAR model; (e) Topomer CoMFA model
Fig. 9	Statistical comparison of 25 different combinations of descriptors for the CoMSIA model.
Fig.10	CoMFA contour map analysis: (a) Steric contour maps; (b) Electrostatic contour maps.
Fig. 11	Contour maps of CoMSIA analysis: (a) Steric; (b) Hydrophobic; (c) Hydrogen bond donor (HBD)
Fig. 12	Important fragments of purinylpyridine derivatives obtained from HQSAR model.
Fig. 13	Atom contribution map for: (a) Compound 190 ; (b) Compound 197 . The green or yellow colour indicates that positive contribution while grey or white colour indicates intermediate contribution in the biological activity.
Fig. 14	3D contour maps of Topomer CoMFA model for: (a) R ¹ ; (b) R ² of potent compound 190 (IC ₅₀ = 0.669 nM) and least potent compound 197 , (IC ₅₀ = 6430 nM). a1 and b1 shows steric contour maps, while a2 and b2 shows electrostatic contour maps. Colour coding of all these contour maps were same as CoMFA and CoMSIA steric and electrostatic

	contour maps.
Fig. 15	General outcome of 3D-QSAR study: (a) CoMFA & CoMSIA contour maps output; (b) output of HQSAR contribution maps and Topomer CoMFA contour maps.
Fig.16	Available B-Raf inhibitors for treatment of melanoma cancer
Fig. 17	Design of Novel B-Raf Inhibitors
Fig. 18	Flowchart of Docking Process
Fig.19	Measurement of serum biomarkers after the treatment with 5-FU and compounds HB-JC-206 and HB-JC-304 where each bar represents Mean \pm SEM, n = 6 mice (Oneway ANOVA followed by Dunnett's multiple comparison test), * = p < 0.05 vs normal control group: (A) Lactate dehydrogenase level; (B) Gamma glutamyl transferase level; (C) C-reactive protein level.
Fig.20	Measurement of oxidative stress parameters after the treatment with 5-FU and compounds Hb-JC-206, and HB-JC-304 where each bar represents Mean \pm SEM, n = 6 mice (Oneway ANOVA followed by Dunnett's multiple comparison test), * = p < 0.05 vs normal control group: (A) Malondialdehyde level; (B) Glutathione level; (C) Super oxide dismutase level.
Fig. 21	Photographs of caudal region skin of the mice (A) Normal control group; (B) Disease control group; (C) Skin cancer treated with 5-FU; (D) Skin cancer treated with synthesized compounds.
Fig. 22	Photographs of histopath analysis of caudal region skin of the mice (A) Normal control group; (B) Disease control group; (C) Skin cancer treated with 5-FU; (D) Skin cancer treated with HB-JC-206. (E) Skin cancer treated with HB-JC-304.

LIST OF TABLES

Table 1	List of Most Dangerous Types of Cancer
Table 2	List Most Common Causes of Cancer Death
Table 3	Top Five Cancer in Men and Woman as per NCIPR
Table 4	Clark model for various melanoma levels
Table 5	Breslow Level
Table 6	Description of B-Raf Mutation
Table 7	Clinical Trial Studies of Drug/Molecule or Combination of Two Molecules and Their Status; Active But Not Recruiting
Table 8	Clinical Trial Studies of Drug/Molecule or Combination of Two or More Molecules as Inhibitors of B-Raf ^{V600E} Mutation with Their Year of Starting and Completion
Table 9	Various programs for pharmacophore modelling (including ligand-based and structure-based methods)
Table 10	Reported B-Raf Inhibitors used to develop Pharmacophore model
Table 11	Results of DiscoTech Pharmacophore model
Table 12	Results of GASP pharmacophore after refining of DiscoTech model (Model_006)
Table 13	Statistical parameter for GH scoring method
Table 14	Top 20 virtual hits with their Q_{fit} value
Table 15	Reported B-Raf Inhibitors with IC_{50} and PIC_{50} values (nM).
Table 16	Statistical Parameters of a Comparative Study by Different Alignment Methods Using PLS Analysis
Table 17	Experimental and Predicted pIC_{50} with Residual of Training and Test Sets using CoMFA, CoMSIA, HQSAR and Topomer CoMFA Models (Distill Alignment).
Table 18	Molecular Docking Studies of Designed Compounds with marketed B-Raf Inhibitors.
Table 19a	In-silico ADMET studies of series I/II compounds
Table 19b	<i>In-silico</i> ADMET studies of series III/IV compounds
Table 20a	Contribution of different parameters on drug score of series I/II compounds
Table 20b	Contribution of different parameters on drug score of series III/IV compounds
Table 21	List of chemicals/Solvents required for synthesis
Table 22	List of Synthesized Novel Benzoxazole derivatives
Table 23	Anti-proliferative activity of synthesized compounds with their IC_{50} value
Table 24	Effect of 5-FU (5%), Compound HB-JC-206, and HB-JC-304 on serum biomarkers:
Table 25	Effect of 5-FU (5%), Compound HB-JC-206, and HB-JC-304 on oxidative stress parameters

LIST OF ABBREVIATIONS

Raf- Rapidly Accelerated Fibrosarcoma

RAS- Retrovirus-associated DNA sequences

MAPK- Mitogen-Activated Protein Kinase

RTK- Receptor Tyrosine Kinase

ERK- Extracellular Regulated Kinase

ROC- Receiver operating characteristic

3D-QSAR- Three-dimensional Quantitative Structural Activity Relationship

CoMFA- Comparative Molecular Field Analysis

CoMSIA- Comparative Molecular Similarity Indices Analysis

HQSAR- Molecular Hologram QSAR

MTT- Dimethyl Thiazolyly Diphenyl Tetrazolium Bromide

Abstract

Cancer is the second leading cause of death after cardiovascular disease. Melanoma is more aggressive than most other types of cancer. B-Raf belongs to the serine/threonine kinase family playing an essential role in cell growth proliferation. Almost 70% B-Raf mutation found in melanoma cancer. Hence, B-Raf is the excellent target for the treatment of melanoma cancer. To design novel B-Raf kinase inhibitors, various computational approaches like pharmacophore modelling, virtual screening, 3D-QSAR (CoMFA, CoMSIA, HQSAR, and Topomer CoMFA) and molecular docking were used. Pharmacophore model was generated using 10 structurally diverse molecules using DiscoTech module and best-generated model was refined with GASP module of Sybyl X. The refined best pharmacophore model with nine features; one hydrophobic region, three donor sites, three acceptor atom, one donor atom, and one acceptor site, was used as a query for virtual screening in the NCI database. Virtual hits from NCI database was further screened by applying the Lipinski's filter, removal of counter ions / duplicate structures that resulted into 11485 hits. 3D-QSAR study was also performed on purinyl-pyridine derivatives. Benzoxazole moiety was selected from features of best pharmacophoric model and bioisosteric replacement of core ring of virtual hit molecules, while various substitutes were incorporated based upon contour map analysis of 3D-QSAR studies. Molecular docking study of novel benzoxazole derivatives were carried out by using GOLD 5.2. Among, all designed molecules, few compounds showing good docking score as compared to the marketed available B-Raf inhibitor, Vemurafenib, were synthesized and characterised. All synthesized molecules were evaluated for *in vitro* cytotoxicity studies on various cell lines and potent molecule is under investigation for *in vivo* pharmacological models for skin cancer. In future, this study will be explored to develop hit to lead generation of novel inhibitor against mutated B-Raf for effective skin cancer therapy.

1. Introduction

In worldwide, all peoples are frightening against diagnosis and treatment of cancer due to the problem of more side effects during chemotherapy. Cancer is considered as a not curable, unbearably painful disease with no guaranty for a complete diagnosis. As per the World Health Organization (WHO) statistics, cancer is the 2nd most leading cause of death after that cardiovascular disease. As per WHO, 9.6 million peoples are dying due to cancer in 2018.¹

The human body is made up of millions of tiny normal cells and each cell has the ability for self-proliferation process. Typically, each cell combines with other and form tissue followed by body organ. These cells can reproduce new cells and replace with dying cells (old cells). Cancer is a disease characterized by uncontrolled cell growth proliferation and the name cancer is given to a collection of related diseases caused by internal or external factors. It may start from any part of the body, and the progression of the disease leads to the primary tumor, which in turn converted into the malignant tumor and spread into other parts of the body. These cells penetrate to normal body tissues and organ and origin of the body tissues determined the type of cancer.²

Benign and malignant these are the two types of cancer. A benign tumor is not spread into the other part of body tissue. Thus it is not dangerous. A malignant tumor is considered a more dangerous type of cancer compared to benign tumor because in malignant tumor grow and spread to other parts of body tissue.^{2,3}

Cancer can cause by two factors viz. internal factor and external factor. In internal factor cancer can be caused by the body's internal factors likes Mutation, DNA damage, inheridity from parents, etc. In external factor includes an environmental factor, tobacco, etc. the abnormal growth due to DNA damage in cells as well as a mutation in the gene. The genetic changes that add to growth results into three fundamental type of gene— proto-oncogenes, tumor suppressor gene, and repair DNA gene. These progressions known as "drivers" of disease.⁴

Proto-oncogenes are included in typical cell development and division. However, changes in these heredities are more dynamic than ordinary. However, they might be progress toward disease bringing on protein sequence, permitting cells to develop and survive.

Oncogenes are likewise required in controlling cell development and division. Cells with specific adjustments in oncogenes may grow in an uncontrolled way. DNA repair genes are included in settling damaged DNA. Cells alterations in these genes tend to build up extra changes in a different gene. These transformations may make the cells end up noticeably dangerous.²⁻⁴

Change the shape of body tissue and grow in uncontrolled manner are also called as cancer. Here are a few examples of tissue changes leads to development of malignancy are follow:

Hyperplasia is a type of cancer where cells are divided faster than normal cells within the body tissue, and new cells are building up in the form of the ulcer. Dysplasia is more dangerous compared to hyperplasia, it is an uneven growth formation and lead to the formation of extra cell layer on particular body tissue leads to change in the tissue functioning. Conversions of Normal cell into hyperplasia followed by dysplasia and lastly lead to the formation of cancer.³

1.1 Types of cancer

Carcinoma: - It is the most common type of cancer. Carcinoma developed on epithelial cells, which are the cells of the uppermost surface of the body. Name of carcinoma depends on the type of specific epidermal cell likes....

Adenocarcinoma is cancer that forms in the outer most layers of mucus or fluids. Most of the colon, breast, and prostate are under adenocarcinoma.

Basal cell carcinoma is cancer that begins from the lower of the epidermis.

Squamous cell carcinoma forms in squamous cells of the outer surface of the skin. They lie in many organs likes stomach, intestine, lung, bladder, and kidney.⁵

Sarcoma: - Cancer that forms in bone and soft tissues including muscle, fat bold vessels, lymph vessels are called sarcoma. Cancer cells are found in the bone tissue are called osteosarcoma.

Leukemia: - Cancer that starts from blood tissues and bone marrow is called leukemia. In this type of cancer instead of a solid tumor, various form of white blood cells are build up in blood and bone marrow.

Lymphoma: - It is a type of cancer that begins in lymphocytic cells. There are two types of lymphoma viz. Hodgkin lymphoma and Non-Hodgkin lymphoma. Hodgkin lymphoma usually form in B-cells. While Non-Hodgkin lymphoma forms in B cells or T-cells.

Melanoma: - It is a type of skin cancer, which is more dangerous compared to the other types of skin cancer. The significant difference between melanoma compares to other skin cancer that, the formation of pigment on the skin due to a deficiency of melanin. If it does not diagnose early which leads to primary tumor converted into the malignant tumor and they spread to the other part of body tissues.

1.2 Cancer Statistics

As per the World Health Organization (WHO)

Cancer is the second leading cause of death globally and is responsible for an estimated 9.6 million deaths in 2018. Globally, about 1 in 6 deaths is due to cancer. Approximately 70% of deaths from cancer occur in low- and middle-income countries. Around one-third of deaths from cancer are due to the five leading behavioral and dietary risks: high body mass index, low fruit and vegetable intake, lack of physical activity, tobacco use, and alcohol use. Tobacco use is the most critical risk factor for cancer and is responsible for approximately 22% of cancer deaths. Cancer-causing infections, such as hepatitis and human papillomavirus (HPV), are responsible for up to 25% of cancer cases in low- and middle-income countries. Late-stage presentation and remote diagnosis and treatment are common. In 2017, only 26% of low-income countries reported having pathology services generally available in the public sector. More than 90% of high-income countries reported that treatment services are available compared to less than 30% of low-income countries. The economic impact of cancer is significant and is increasing. The total annual economic cost of cancer in 2010 was estimated at approximately US\$ 1.16 trillion. Only 1 in 5 low- and middle-income countries have the necessary data to drive cancer policy. Cancer is a leading cause of death worldwide, accounting for an estimated 9.6 million deaths in 2018.¹ The most common cancers are:

Table 1. List of Most Dangerous Types of Cancer

Name of Cancer	No. of Cases (in million)
Lung	2.09
Breast	2.09
Colorectal	1.80
Prostate	1.28
Skin cancer	1.04
Stomach	1.03

Table 2. List Most Common Causes of Cancer Death

Name of Cancer	No. of deaths (Million)
Lung	1.76
Colorectal	862000
Stomach	783000
Liver	782000
Breast	627000

As per the National Cancer Institute (NCI)

In 2018, an estimated 1,735,350 new cases of cancer will be diagnosed in the United States and 609,640 people will die from the disease. The most common cancers (listed in descending order according to estimated new cases in 2018) are breast cancer, lung and bronchus cancer, prostate cancer, colon and rectum cancer, melanoma of the skin, bladder cancer, non-Hodgkin lymphoma, kidney and renal pelvis cancer, endometrial cancer, leukemia, pancreatic cancer, thyroid cancer, and liver cancer. The number of new cases of cancer (cancer incidence) is 439.2 per 100,000 men and women per year (based on 2011–2015 cases). The number of cancer deaths (cancer mortality) is 163.5 per 100,000 men and women per year (based on 2011–2015 deaths). Cancer mortality is higher among men than women (196.8 per 100,000 men and 139.6 per 100,000 women). When comparing groups based on race/ethnicity and sex, cancer mortality is highest in African American men (239.9 per 100,000) and lowest in Asian/Pacific Islander women (88.3 per 100,000).

In 2016, there were an estimated 15.5 million cancer survivors in the United States. The number of cancer survivors is expected to increase to 20.3 million by 2026. Approximately 38.4% of men and women will be diagnosed with cancer at some point during their lifetimes (based on 2013–2015 data). In 2017, an estimated 15,270 children and adolescents ages 0 to 19 were diagnosed with cancer, and 1,790 died of the disease. Estimated national expenditures for cancer care in the United States in 2017 were \$147.3 billion. In future years, costs are likely to increase as the population ages and cancer prevalence increases. Costs are also likely to increase as new, and often more expensive, treatments are adopted as standards of care.⁵

As per National Institute of Cancer Prevention and Research (NCIPR)

One woman dies of cervical cancer every 8 minutes in India. For every two women newly diagnosed with breast cancer, one woman dies of it in India. As many as 2,500 persons die every day due to tobacco-related diseases in India. Tobacco (smoked and smokeless) use accounted for 3,17,928 deaths (approx) in men and women in 2018. 7,84,821 peoples were died due to cancer in 2018. Cancers of the oral cavity and lungs account for over 25% of cancer deaths in males and cancer of the breast and oral cavity account for 25% cancers in females. The top five cancers in men and women (**Table 3**) account for 47.2% of all cancers; these cancers can be prevented, screened for and/or detected early and treated at an early stage. This could significantly reduce the death rate from these cancers.⁶

Table 3:- Top Five Cancer in Men and Woman as per NCIPR

	Men	Women
1	Lip, Oral Cavity	Breast
2	Lung	Lip, Oral
3	Stomach	Cervix
4	Colorectal	Lung
5	Esophagus	Gastric

1.4 Skin Cancer

Skin cancer is the most common type of cancer specifically in western countries. The most common alarming situation of skin cancer is a change in the appearance of skin such as ulceration and pigmentation. Mainly two types of skin cancer viz. Non-melanoma and Melanoma. Non-melanoma also subdivided into Basal Cell Carcinoma (BCC) and Squamous Cell Carcinoma (SCC).⁵

Basal Cell Carcinoma (BCC)

It is the most common type of skin cancer in which cell proliferation observed in the outer most layer of the skin. It is also called as carcinoma epithelioma. In BCC, sometime presence of ulceration is a characteristic of this cancer.

Squamous Cell Carcinoma (SCC)

Cancer arises from squamous cells called as SCC. Primary sign and symptoms of this kind of cancer are firm hard nodules and dome shape ulcer on the skin. Ulceration and bleeding may occur which lead to the development of large mass. It is a more dangerous type of skin cancer compared to BCC but not nearly as dangerous as melanoma.⁷

Melanoma

Melanoma cancer arises due to a deficiency of melanin in melanoma cells. Most of the melanoma consisting of various pigments in different color codes like brown and black. A small number of pink, red pigments are called amelanotic melanoma which to be more aggressive. The alaramic situation in melanoma includes a change in size, shape, and color. An often-used mnemonic is "ABCDE", where A is for "asymmetrical", B for "borders" (irregular: "Coast of Maine sign"), C for "color" (variegated), D for "diameter" (larger than 6 mm – the size of a pencil eraser) and E for "evolving."^{7,8}

1.5 Melanoma

Melanoma cancer considered one of the major cause of death among all other types of skin cancer, 75% of peoples are die in due to melanoma cancer. It is a malignant tumor of melanocytes. When the melanoma cancer arises first symptoms arises from the skin, as the progression of the disease leads to spreading of pigments in the lymph, eye, lung, etc.

Melanoma cells consisting of melanocytes responsible for the production of the dark pigment melanin and also protects the deeper layers of the skin from the UV rays. When people spend time in the sunlight, skin exposed to UV light may lead to abnormality in the melanocytic cells, and it becomes cancer. This condition is called melanoma.⁵⁻⁸

Around 60,000 new cases of melanoma were diagnosed in the United States each year. According to a WHO report, about 48000 melanoma-related deaths occur worldwide per year. As per the National Cancer Institute (NCI) statistics in 2018, around 91,270 new cases of melanoma will be estimated, and 9,320 people will die of this disease.⁷⁻⁸

1.5.1 Pathophysiology

Ecological introduction (UV light) in addition to genetic weakness (CDKN2A, CDK4, MC1R, BRAF, p16/ARF qualities) prompts the accumulation of genetic mutation in melanocytes that activate oncogenes, inactivate tumor suppressor gene and impair DNA repair components. This prompts melanocyte proliferation, vein development, tumor attack, avoidance of immune response, and eventually metastasis.

Melanoma tumor progression given Clark model depicts a moderate but steady development of being melanocytic nevi to metastatic melanoma. The progression starts with a controlled expansion of normal melanocytes to yield a benign nevus. The evolution proceeds with abnormal development of the melanocytes in a previous nevus or another area bringing about a pre-malignant injury with random cytologic atypia, this is referred to as atypical/dysplastic nevi. These lesions show up as levels of macules, more prominent than five mm in size, with unpredictable border, and variable pigmentation. With time the melanocytes secure the capacity to multiply horizontally in the epidermis (outspread development) and histologically demonstrate constant atypia (melanoma in situ). E-cadherin limits the cells intra-epidermally however a couple of cells may attack the papillary dermis. Various biochemical occasions including articulation of N-cadherin and the loss of E-cadherin permit cancerous cells to attack the storm cellar film and multiply vertically in the dermis as an extending knob with metastatic potential (vertical development). Cancerous melanocytes spread to different areas of the body generally start from lymph nodes and then to the skin, subcutaneous soft tissue, lungs and the brain

(metastatic melanoma). The graphical representation of progression of melanoma cancer are shown in **fig. 1**.⁸

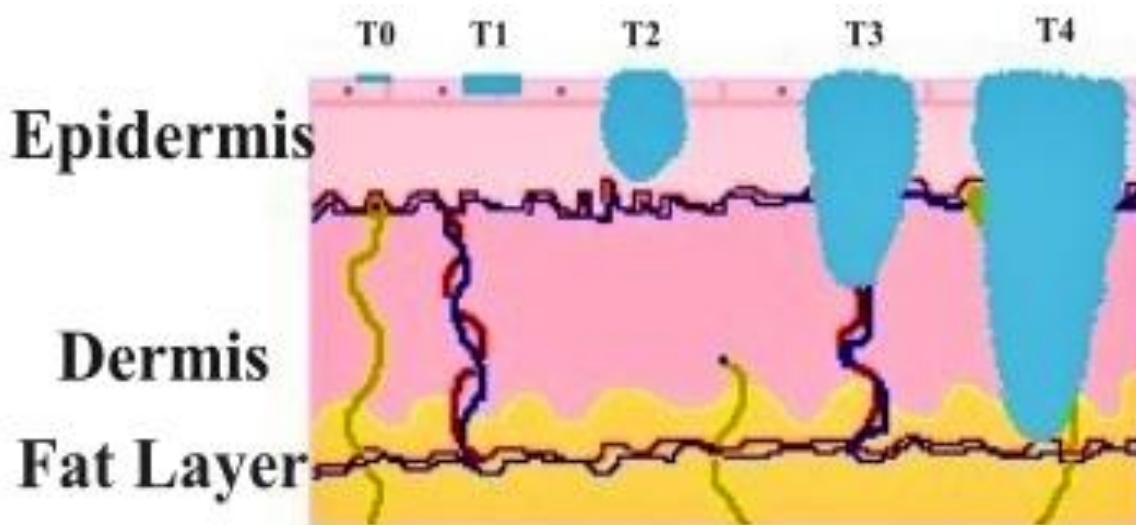


Fig. 1 Pathophysiology of Melanoma Cancer

1.5.2 Classification

Melanoma is classified based on the histopathology, development, and spreading of melanoma cancer. Concerning histopathology, it is classified based on spreading of the tumor during the malignant stage of melanoma. There are four main types of melanoma based on the histopathological patterns described in descending order of their frequency which includes superficial spreading melanoma, nodular melanoma, lentigo maligna melanoma and acral lentiginous melanoma.

Superficial spreading melanoma considered as most common subtype of melanoma and 75% incidence among all malignant melanoma. It has found in a pre-existing nevus. In this type of cancer radical growth pattern occurs as the progression of disease and growth occurs. This melanoma cancer generally found in white peoples. Variation in color, irregular borders, and the irregular surface is the characteristics of this type of melanoma.

Lentigo malignant melanoma is responsible for about 4% to 15% of all melanoma cases. Generally, it grew in an area where the skin damage observed due to sun damage found in geriatric (older people) peoples. Histological pattern of this kind of cancer includes radical and vertical growth pattern of the epidermal cell of the uppermost layer of skin.

The underlying growth in the epidermal cell usually called atrophic while dominant type vertical of growth called epithelioid cells.

Acral lentiginous melanoma represents 2-8% of all melanoma in white people and 29-72% in dark skin people. It is commonly developed in planar regions, palms region and occasionally surfaces. It arises from the nail matrix generally found in dark skin peoples. It occurs on the palms, soles of the feet or beneath the nail beds. It is extremely aggressive and large, with an average diameter of three centimeters.

Nodular melanoma represents 15-30% of all melanoma. The lesions are darker and dome-shaped. The progression of this type of melanoma is quicker compared to other types of melanoma.

Mucosal melanoma occurs in mucosal tissue, which lines body cavities and hollow organs. The most common sites of this type of melanoma are head and neck regions as well as rectum urinary tract and vagina. It occurs in mucosal tissue of the skin layer.

Uveal melanoma is the tumor arises from pigment cells that reside within the uvea giving color to the eye. It is the cancer of the eye involving the iris, ciliary body or choroid part of the eye region. It is distinct from the epithelium cell of the retina, which leads to they do not form melanoma.⁷

1.5.3 Causes

Ultraviolet (UV) light is the major environmental factor that causes melanoma. The following risk factors those are responsible for melanoma cancer.

1. Dysplastic moles (nevi):- It is the most common type of nevi present in the melanoma cell. A very few individuals are lack of this kind of moles which leads to progression of melanoma cancer.
2. Fair skin:- Occurrence of melanoma is quicker compared to people having fair skin compared to the dark skin.
3. Personal history of melanoma or other skin cancers:- People who have a higher risk of second melanoma those who have been treated for melanoma. People who are suffering from BCC and SCC are at increased risk of melanoma.

4. Weakened immune system:- Those people who have weakened the immune system or by giving specific drug during organ transplantation or several infectious diseases are a higher risk of developing melanoma.
5. The family history of melanoma:- Cancer is considered a genetic disease which comes from family hereditary or family history. Sometimes melanoma runs in families. 10% of cases of melanoma have a family member with this disease.
6. Severe, blistering sunburns:- people who have severe, blistering sunburn are increased risk of melanoma.
7. Ultraviolet radiation (UV):- In today's world, due to change in the several environmental changes increasing the UV radiation on the earth which leads to the increase the risk of melanoma cancer.

1.5.4 Signs and Symptoms of Melanoma:-

The first sign of melanoma is a change in the size, shape, color or feel of an existing mole. In most cases, dark-brown and black pigments are characteristics of initiation of melanoma cancer.

1. Asymmetry
2. Border
3. Colour
4. Diameter

Melanomas can be grouped given the level of intrusion through the diverse layers of the skin (VGP, for example, Clark Level and Breslow Level, which associate with five-year survival (**Table 4 & 5**))

Table 4. Clark model for various melanoma levels

Clark Level	The degree of Tumor Invasion	5-Year Survival (%)
Level I	Threatening melanocytes are bound to the epidermis	99
Level II	Malignant melanocytes infiltrate papillary dermis singly or in small nests	95
Level III	Harmful melanocytes fill and extend papillary dermis, with augmentation of the tumor to the papillary-reticular dermal interface (as a rule meaning vertical development stage)	82
Level IV	Malignant melanocytes infiltrate reticular dermis in a significant fashion	71
Level V	Malignant melanocytes infiltrate subcutaneous fat	49

Table 5. Breslow Level

Clark Level	The degree of Tumor Invasion
Level I	<1 mm
Level II	1 – 2 mm
Level III	>2 – 4 mm
Level IV	>4 mm

1.5.5 Treatment of Melanoma Cancer

The rate of melanoma has quickly expanded over recent years. Around 10% of all patients who are diagnosed with melanoma. When it ends up with metastatic, melanoma frequently prompts death within a year.

The US-FDA has approved a couple of therapies for the treatments of melanoma cancer, all of which have insignificant advantageous impacts on patient survival. A significant number of these have been immunologic, including interferon (IFN)- a2b, high-dosage interleukin (IL)- 2 and, as of March 2011, ipilimumab. IFN-a2b is related with a 10–15% lessening in the danger of relapse in the adjuvant setting, while IL-2 produces a physical

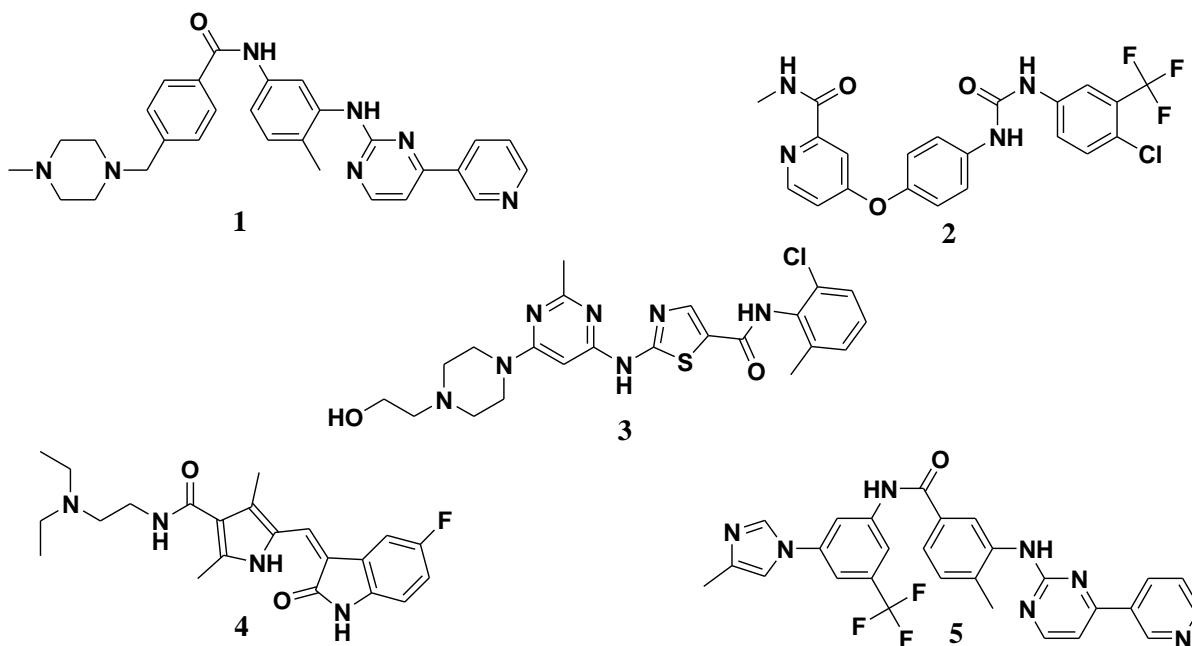
reaction in 15% of metastatic patients. An older FDA-approved melanoma treatment is the alkylating agent's dacarbazine (DTIC), which accomplishes reactions in under 10% of patients, a profile like other accessible agents, for example, carmustine (BCNU), temozolomide, taxanes, and, platinum analogs. Even with these constrained alternatives, there has been a sea change in melanoma medications introduced by recent molecular advances.

Targeted agents aimed for oncogenic drivers that have been identified over the past decade give an open door for novel melanoma therapeutics. This audit concentrates on the central molecular system that fuels melanoma development and recent medication improvement advance towards targeting these essential proteins and signaling pathways.

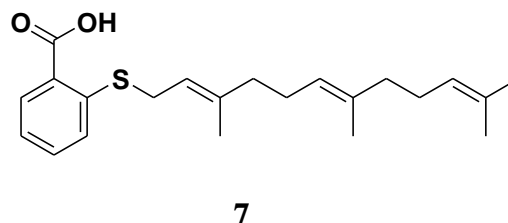
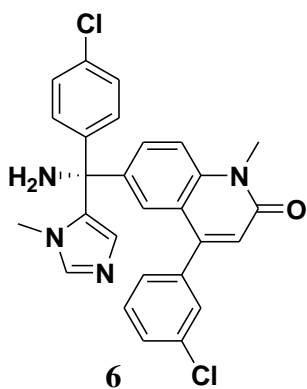
Over the previous decade, much has been found out about genetic injuries that stimulate development and signaling pathways in melanomas. Numerous segments of the RAS pathway are either activated through oncogenic changes or inactivated through injurious modifications. From this composite view, activation of a KIT–NRAS– BRAF–MEK–ERK central axis (Figure 4, shaded in green) is by all accounts critical in all types of melanoma.⁹

Targeted therapy includes:

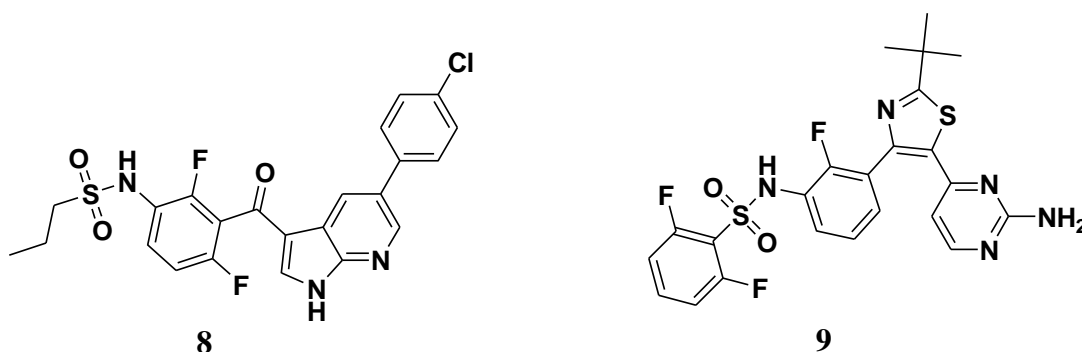
i. Receptor Tyrosine Kinases Inhibitors (RTKIs): - EGFR, PDGFR, and KIT are the types of RTKs growth factor overexpressed in melanoma cell due to activation of gene mutation. Among all these types of growth factors, c-KIT plays a significant role in melanocyte differentiation, but overexpression appears during melanoma disease progression. Approximately 10-20% of c-KIT mutation is observed in gastrointestinal stromal tumors(GISTs). RTKIs are the class of chemotherapeutic which are used in the treatment of cancer by inhibiting or by blocking the enzyme tyrosine kinase. Imatinib (**1**) was the first drug candidate in this class and then followed by the sorafenib (**2**), dasatinib (**3**), sunitinib (**4**), nilotinib (**5**), etc.¹⁰



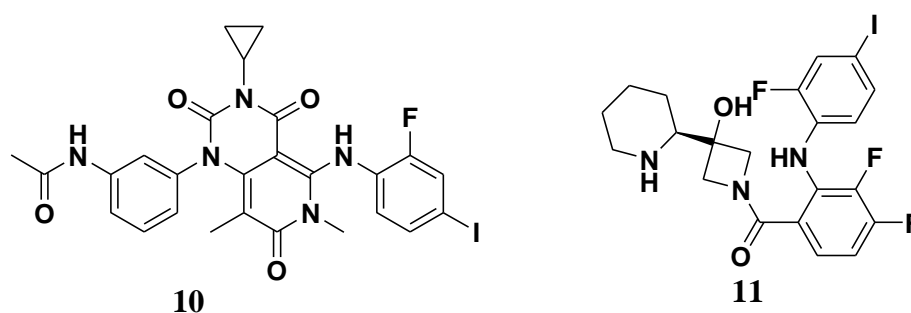
ii. Retrovirus-associated DNA sequences inhibitors (RASIs): - The RAS oncogenes (HRAS, NRAS, and KRAS) comprise the more efficient mutation in human cancers (33%). Among all these isoforms of RAS, NRAS is considered the most common affected oncogene in melanoma after B-Raf. All RAS inhibitors are inhibiting the RAS by blocking the activity of the farnesyltransferase enzyme. The group of a compound to inhibit RAS were farnesyltransferase inhibitors (FTIs), such as tibifarnib (**6**) and salirasib (**7**). Both inhibitors were designed to block the post-translational lipid modification of RAS.¹¹



iii. Rapidly accelerated fibrosarcoma inhibitors (RAFI): - Raf inhibitors play an essential role in the treatment of melanoma cancer. The Raf oncogenes have three isoforms viz. A-Raf, B-Raf, C-Raf. Among all these Raf isoforms, B-Raf mutation 80-85% contribution to the development of melanoma cancer. So, B-Raf is a prominent target for the treatment of melanoma cancer. The first B-Raf inhibitor which went in the clinical trial viz. sorafenib (**2**), which was targeting multiple kinases like B-Raf, C-Raf, VEGFR, and RTKs. After 1st B-Raf inhibitor, other B-Raf inhibitors includes Vemurafenib (**8**), Dabrafenib (**9**).



iv. Metiogen Extracellular Kinase Inhibitors (MEKIs): - MEK is the primary downstream regulator of MAPK kinase pathway. All MEK inhibitors are generally used with a combination of B-Raf inhibitors to avoid drug resistance as well as to increase the effectiveness of the chemotherapy during treatment of cancer. The MEK inhibitor was trametinib (**10**) and then followed by the cobimetinib (**11**).¹²



1.6 Rapidly Accelerated Fibrosarcoma (Raf) Kinase

The Mitogen-Activated Protein Kinase (MAPK) pathway is the most prominent pathway for normal and uncontrolled cell growth during the cell cycle and also called the RAS-RAF-MEK-ERK pathway.¹³ During RAS activation, extracellular growth promoting

ligand binds to tyrosine kinase receptor which leads to the occurrence of trans-auto-phosphorylation via downstream activation of the MAPK pathway. Conversion of RAS-GDP to RAS-GTP stimulates the MAPK pathway. RAS-GTP then promotes the activation of Raf kinase. During activation, Raf undergoes phosphorylation process which leads to conformational changes in Raf subtypes by the formation of homodimer and heterodimer.¹⁴ RAF is composed of three isoforms, viz. A-Raf, B-Raf, and C-Raf, which are related to retroviral oncogenes discovered in 1983. The first Raf isoform (C-Raf) was found in 1985¹⁵ and A-Raf was found in the following year (i.e. 1986), while most important B-Raf was found in 1988.¹⁶ All Raf isoforms share MEK1/2 kinases as substrates.

1.6.1 Raf Kinase Structure

All Raf isoforms have a typical structure consisting of 3 conserved regions (CR) with unique functions of each domain. CR1 contains the cysteine-rich domain (CRD) and the RAS-binding domain (RBD). Both these domains are required for dealings of CR1 with the kinase domain for Raf auto-inhibition.¹⁷ CR2 region is essential for negative regulation through inhibition of phosphorylation sites. CR3 is the kinase domain and fundamental domain for all Raf kinase activity during cell division. Overall, Raf structure can be divided as N-terminal region and C-terminal region. N-terminal region contains the RBD which is crucial for Raf activity as well as to inhibit phosphorylation sites; while C-terminal region comprises of kinase domain to regulates kinase activity and constitutive oncogenic activation.¹⁸

In the following section, the necessary structural information of all three Raf isoforms is demonstrated as per sequence of discovery. The structural features of all three Raf isoforms are also shown in **Fig.2**.

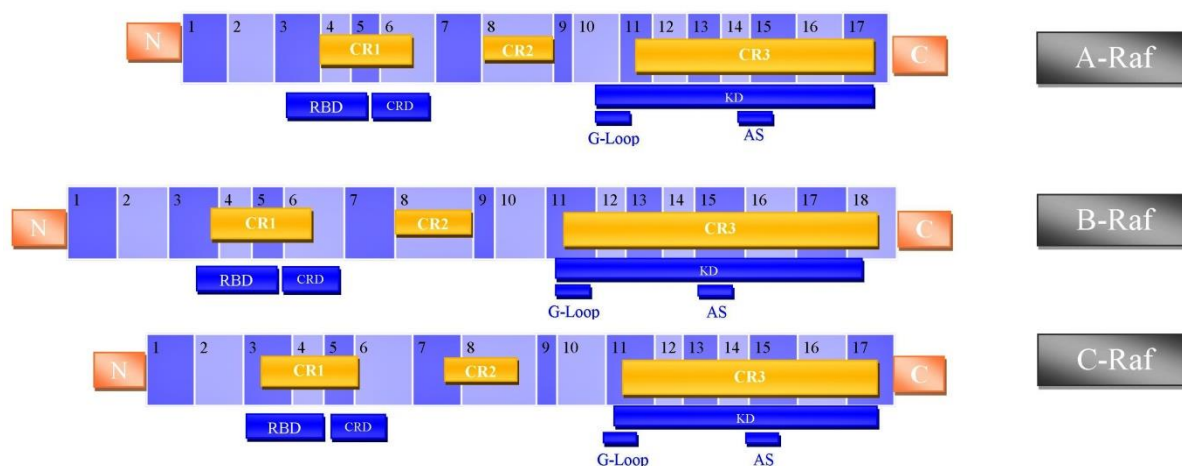


Fig.2. Structure of Raf proteins: A-Raf, B-Raf and C-Raf; Three conserved regions (CR) - CR1, CR2 and CR3; RBD - Ras Binding Domain; CRD - Cysteine-rich domain and KD - Kinase domain; G-loop - A conserved glycine loop; and AS - the activation segment; C: Carboxyl-terminal domain; N: Amino-terminal domain.

1.6.1.1 C-Raf

The first Raf isoform discovered was C-Raf and was found in 1985. Structurally, C-Raf contains two isoforms of mRNA. It included 17 exons and 648 amino acids. C-Raf is a "gatekeeper" of the ERK1/2 (Extracellular Signal-Regulated Kinase) pathway. This critical regulatory mechanism involves the direct, physical link of the N-terminal in the kinase domain. C-Raf plays a vital role in kinase activity. Failure in phosphorylation of C-Raf leads to fully shutdown of kinase activity and inhibition of cell growth proliferation. All Raf isoforms have unique characteristics to make a dimer formation during activation.¹⁹

1.6.1.2 A-Raf

A-Raf was found in the year 1986. It has unique phosphorylation sites to regulate its functions. Mutation of the non-CR residue, Tyrosine296, within the N-region to arginine leads to constitutive stimulation of A-Raf. Tyrosine296 is located between the kinase domain and N-region and therefore, plays a significant role to mimic the kinase activity of A-Raf. Two alternative A-Raf splice forms are discovered viz. DA-Raf1 and DA-Raf2 and are found in mouse, monkey and human cells. Subsequently, A-Raf_{short} is another

subtype which is also found in human cells. The distinction between all these Raf isoforms contrast with the A-Raf, as there was an absence of CR2 and CR3 domain. DA-Raf is activated by binding to the RAS and interferes in the ERK pathway. All Raf isoforms bind and activate MEK, but A-Raf has the weakest activity towards MEK as compared to C-Raf.

1.6.1.3 B-Raf

B-Raf was found in 1988 and exhibits higher kinase activity as compare to the other two Raf isoforms. RAS and 14-3-3 protein (necessary cofactor for Raf kinase activation) binding play a vital role in the activation of B-Raf. B-Raf is the most prominent protein of all other RAF isoforms having 18 exons, 766 amino acid residues and molecular weight of 84436 Da. Location of this gene is at 7q34 chromosome.²⁰ It contains three conserve regions, viz. CR1, CR2, and CR3. B-Raf is expressed in most tissues with high expression in neuronal tissue.

The CR1 of N-terminal contains the RAS-binding domain. It contains 131 amino acid residues. The function of this domain is to initiates the interaction with an arginine residue (R188) in the plasma membrane. CR1 also includes cysteine-rich domain (CRD) and can bind with two zinc ions as a cofactor.

The CR2 region is rich with serine amino acid residues and plays a critical role during phosphorylation. The S365 residue, when phosphorylated and bind with 14-3-3, it produces negative contribution during cell proliferation. During cell growth, S365 and S729 amino acids are phosphorylated, while during cell growth inhibition, both S365 and S729 are dephosphorylated which leads to the formation of inactive conformation of B-Raf and stops the cell proliferative activity.

The CR3 domain is the kinase domain which contains 293 amino acids located near the C-terminus. The structural representation of the kinase domain indicates that the N-terminal lobe fits in the form of antiparallel β -sheet structure and the anchor side, which orients ATP or the inhibitor. This ATP binding is sometimes also called as P-loop and α C-helix. This activation loop is a very flexible loop, but when it is in an inactivated state, it blocks kinase and catalytic activity.²¹

1.7 B-Raf Mutation

Development of cancers, due to the MAPK pathway, are noted to around 30% of all cancers in which the majority is due to B-Raf mutation. The frequency of B-Raf mutation is more in melanoma cancer (50-80%); but apart from this, it is also found in the thyroid (36-53%), colorectal (5-22%) and ovarian cancer (30%).

Approximately, 50 % of melanoma cancers activate B-Raf transformations. From the mutations observed in B-Raf, more than 90 % are at codon 600, and among these, majority is a single nucleotide transformation bringing about the substitution of valine by glutamic acid (B-Raf^{V600E}). The second most regular transformation is B-Raf^{V600K}, substituting lysine for valine that speaks to 5-6 % which is trailed by B-Raf^{V600R} (substitution of valine by arginine). The pervasiveness of B-Raf^{V600K} has been accounted as higher in few populaces.²⁰ The lists of important B-Raf mutations are shown in **Table 6**.

Table 6. Description of B-Raf Mutation

The Position of B-Raf Mutation	Description of B-Raf Mutation
462	From Arginine (R) to Isoleucine (I) at position 462 (R462I, p.Arg462Ile)
463	From Isoleucine (I) to Serine (S) at position 463 (I463S, p.Ile463Ser).
464	From Glycine (G) to Glutamate (E) at position 464 (G464E, p.Gly464Glu).
466	From Glycine (G) to Valine (V) at position 466 (G466V, p.Gly466Val).
597	From Leucine (L) to Arginine (R) at position 597 (L597R, p.Leu597Arg).
600	From Valine (V) to Glutamate (E) at position 600 (^{V600E} , p.Val600Glu). also found in sarcoma, metastatic melanoma, ovarian serous carcinoma, pilocytic astrocytoma; somatic mutation; most common mutation; constitutive and elevated kinase activity; efficiently induces cell

transformation; suppression of mutation in melanoma causes growth arrest and promotes apoptosis; loss of regulation by PMRT5.

601

From Lysine (K) to Glutamate (E) at position 601 (K601E, p.Lys601Glu).

1.7.1 B-Raf^{V600E} Mutation

In 2002, for the first time, B-Raf mutation (B-Raf^{V600E}) was identified for the development and spread of cancer in human. There is change in the amino acid position in B-Raf^{V600E} i.e. valine (V) is substituted by glutamic acid (E) at position 600. B-Raf^{V600E} is overexpressed in various human cancers which predominantly include melanoma, colorectal, thyroid, and ovarian. The progression of disease occurs due to the level of expression of B-Raf^{V600E} mutation, which leads to conversion of benign tumor into the malignant tumor. In many cases, the development of cancer with primary tumor was due to B-Raf^{V600E} mutation and this developed primary malignant tumor potentiated K-Ras mutations without APC (Adenomatous polyposis coli) mutation. These results into the mutant allele which played an important role in the development of initial tumor formation followed by the development of late-stage cancer¹⁹⁻²¹.

Mutation in Raf isoforms; specifically in B-Raf, is correlated with cell dysfunctions and uneven cell growth proliferation. B-Raf^{V600E} mutation gives the freedom to cell growth stimulation by upstream regulation which leads to the negative feedback regulation in the MAPK pathway. B-Raf^{V600E} plays an important role in melanoma progression by activation of the MAPK pathway, avoidance of senescence and apoptosis, unchecked replicative potential, angiogenesis (through MEK-dependent activation of HIF-1 α and VEGF), tissue intrusion and metastasis and additionally, the evasion of immune reaction.^{20,21}

The development of different stages of cancer is strongly accompanied by DNA mismatch repair (MMR) system deficient genes and mutant B-Raf^{V600E}. The presence of B-Raf mutant gene is at higher percentage in melanoma and colorectal MMR-deficient carcinomas which showed tumorigenic involvement of mutation within the cell itself and leads to expansion of tumor growth in different body tissues. In addition to this, the absence of K-Ras and B-Raf mutations are alternative genetic events occur in melanoma as well as in colorectal cancer genesis.

Both B-Raf^{V600E} and K-Ras mutations are important for the development of cancer. During the development of cancer, about 30% of the B-Raf inactive mutants (viz. D594) occur which also potentiate Ras mutation leading to the suppression of excessive MAPK pathway. Therefore, the MAPK pathway plays a prominent role in a wide array of cancer types and helps out to find occurrence of first mutation in the progression of particular cancer. With a seemingly growing importance in tumorigenesis, B-Raf^{V600E} is being carefully studied as a potential target for more effective oncologic therapies. **Fig. 3** demonstrated that the B-Raf is the up-regulator gene for the MAPK pathway in normal as well as in cancer cells. The role of B-Raf^{WT} in MAPK pathway is to regulate the proliferation of normal cell growth. On the other hand, the high frequency of B-Raf^{V600E} results in the formation of uneven cell growth proliferation which lead to the development of cancer.

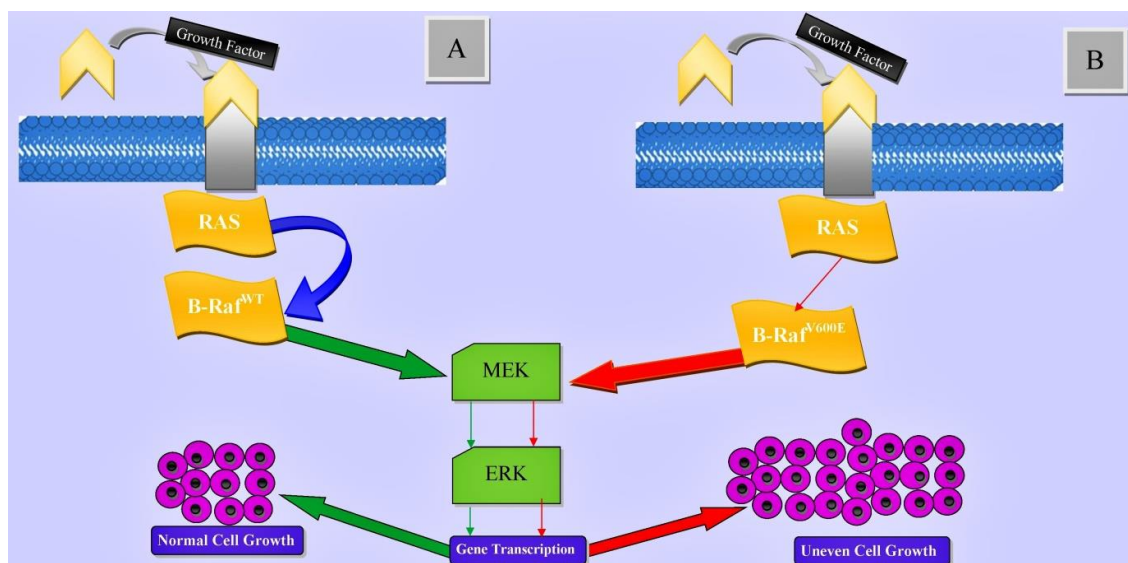


Fig. 3 Progression in growth of cells through MAPK pathway (RAS-RAF-MEK-ERK pathway) in: A – Normal growth of cells involving wild type of B-Raf (B-Raf^{WT}); B – Abnormal growth of cells (cancerous cells) involving V600E bearing B-Raf (B-Raf^{V600E}).

1.7.2 B-Raf Mutation in Melanoma

Melanoma is considered as a malignant tumor arises due to the deficiency of melanocyte. MAPK pathway is habitually mutated in melanocytes and plays an important role in the development of melanoma cancer. B-Raf^{V600E} is most prominent mutation in melanoma. The intensity of B-Raf mutation in melanoma is extreme but, it was scarce in both types of melanoma cancer viz. chronic sun-induced damage melanoma and in low sun exposure area. B-Raf mutation is specifically associated with low UVR dose and melanocortin-1 receptor (MC1R). The B-Raf mutation is observed with low rate in mucosal lining, an area with the low sun exposure, such as palms and the soles of the feet, which directly indicates that sun exposure is required for the development of B-Raf mutated melanoma cancer. Non-chronic sun induced damaged melanoma is caused by B-Raf transformation due to high force of UV light. This prompts skin containing melanin to oxidize and to deliver lethal oxidizing operator which ultimately causes DNA damage in melanoma cells and responsible for transformation of normal B-Raf to mutant one²¹.

MC1R receptors plays an important role in the development of pigment. It is different in human and other specific subjects which are linked to the phenotypic behavior of the human body. This phenotypic behavior is sometimes responsible for the development of melanoma cancer. MC1R is the type of G-protein-coupled receptor and its isoforms affects signaling through the MAPK pathway. B-Raf mutation is also cause by

dissimilarity in the melanocortin-1 receptor (MC1R). Wild-type MC1R is mainly responsible for the accumulation of eumelanin over pheomelanin in the presence of UV-light. However, variations in this lead to change in receptor functions which are not able to change eumelanin from pheomelanin and results in the accumulation of pheomelanin. The higher concentration of the pheomelanin increase the production of free radical in the presence of UV-light, and it is responsible to do DNA damage in the melanocytes and results in B-Raf mutation¹⁹⁻²¹.

Human melanoma cell proliferation depends on adhesion to the extracellular matrix (ECM) for activation of B-Raf kinase followed by the activation of ERK1/2. The mutation occurred in B-Raf protein results into the activation of the ERK1/2 without the need of ECM signalling. B-Raf^{V600E} mutation has power of self-establishing cells without the involvement of ECM signalling, which results into the up regulation of cyclin D1 and down regulation of cyclin dependant kinase (CDK) in the absence of ECM pathway. Thus, B-Raf^{V600E} mutation destabilizes the growth factor which is required for the activation of ERK1/2 in melanoma cells and thereby allows uneven cell progression in G₁/S phase of cell growth cycle²¹.

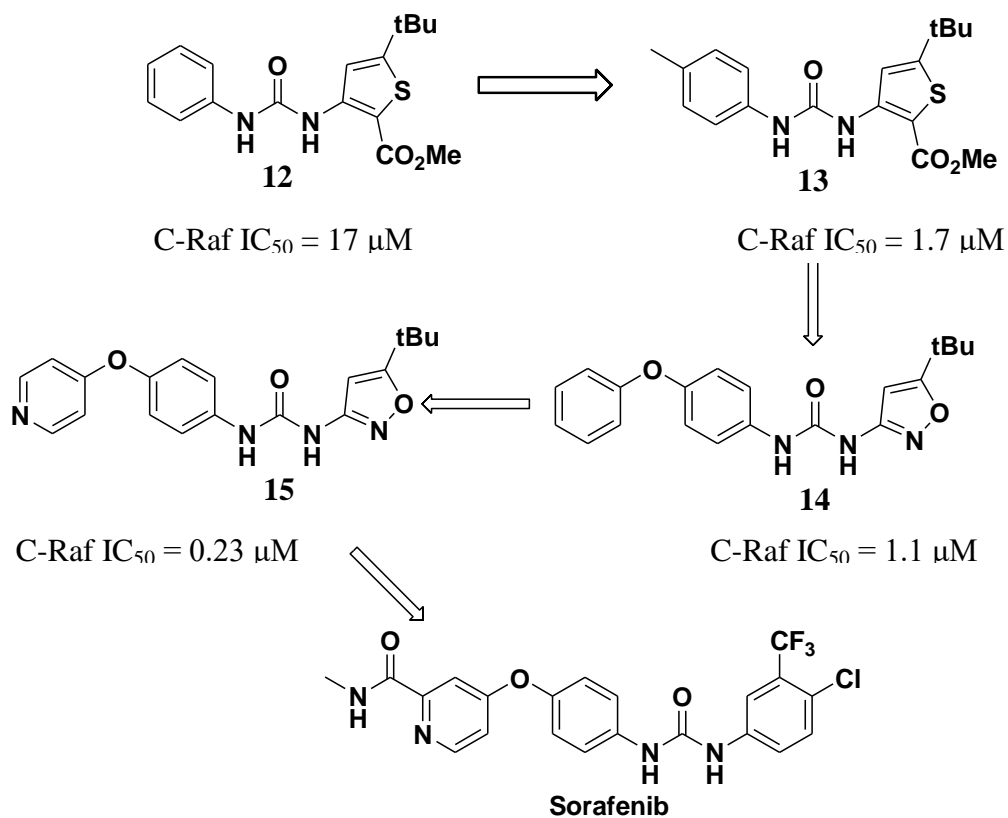
1.8 B-Raf Inhibitors for the Treatment of Melanoma Cancer:-

As described above, the role of B-Raf mutation in the development of melanoma cancer is more prevalent among all other Raf isoforms. Approximately 40-50% of B-Raf mutation is involved in melanoma cancer. B-Raf^{V600E} mutation plays a vital role in the development of melanoma cancer. The details of various B-Raf inhibitors are shown below...

Sorafenib (Nexavar): -

Sorafenib is a novel pyridyl biaryl urea scaffold identified by Bayer and Onyx for targeting dual inhibitors viz. Raf and Ras in the MAPK signaling pathway. US FDA approved it in December 2005 for the treatment of advanced renal cancer and then followed by October 2007 for the treatment of liver cancer and in November 2007 for the treatment of hepatocellular carcinoma (HCC). Sorafenib was failed in the treatment of melanoma cancer in a clinical trial.^{22,23}

Chemical Discovery of Sorafenib: -

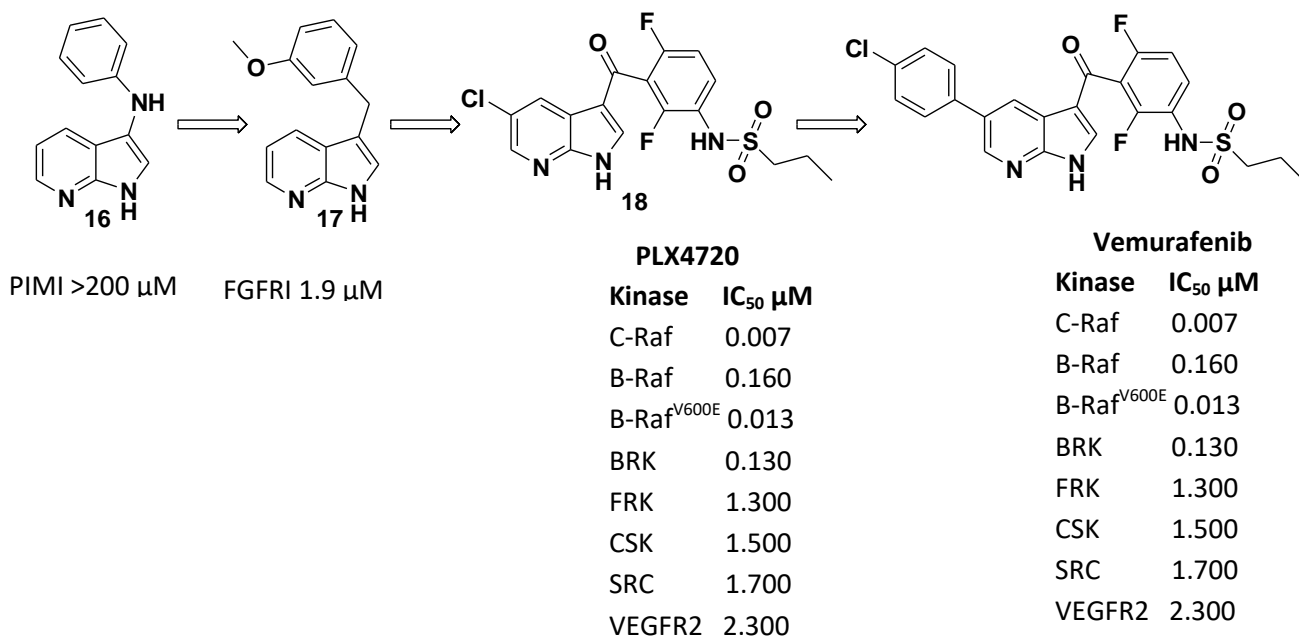


Kinase	IC ₅₀ μM
C-Raf	0.006
B-Raf	0.025
B-Raf ^{V600E}	0.038
VEGFR	0.090
PDGFR	0.057

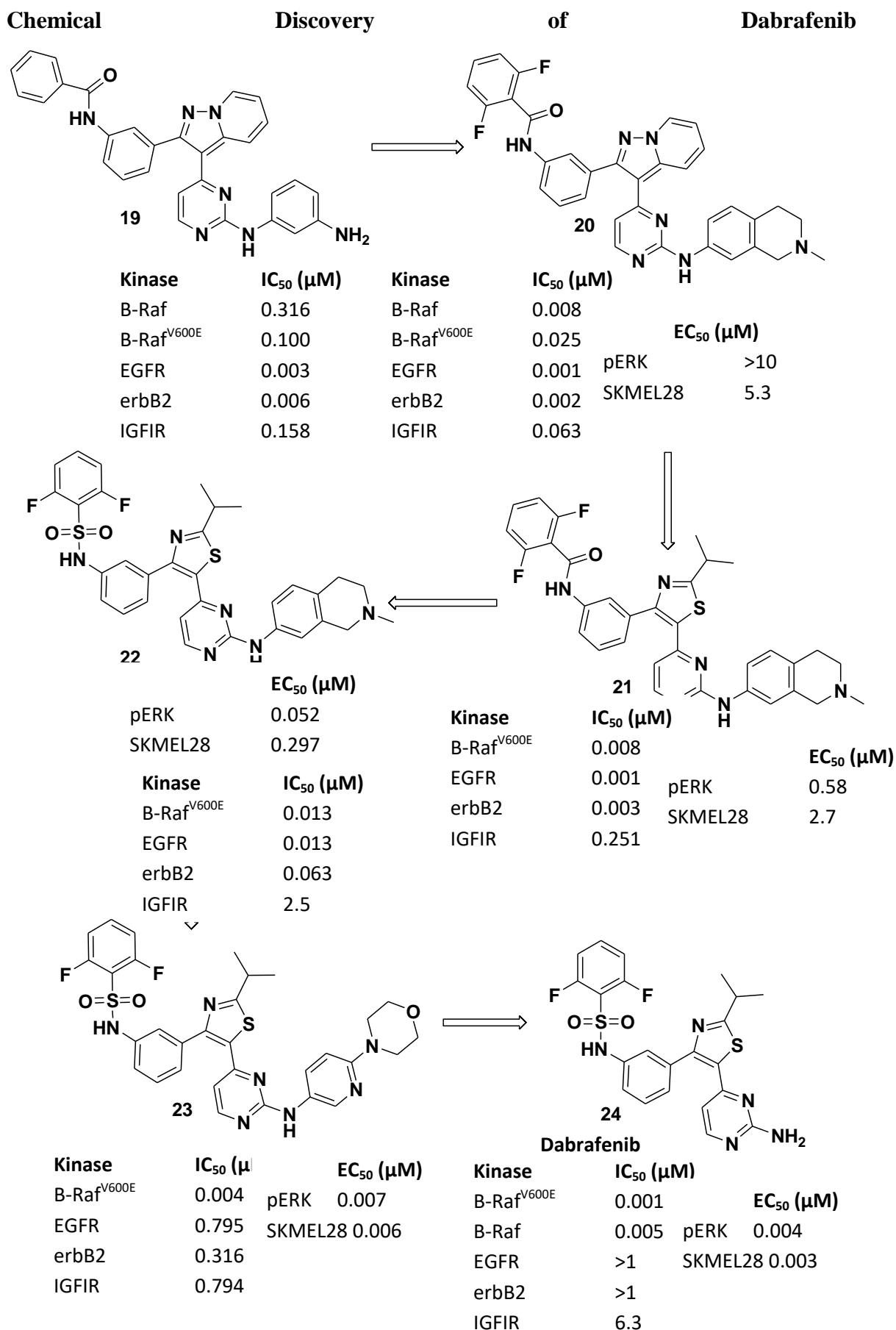
Vemurafenib (Zelboraf[®], or PLX4032)

Vemurafenib is the 1st selective B-Raf kinase inhibitor approved in August 2011 by US FDA, and in Europe in February 2012 for targeting B-Raf^{V600E} mutation in the treatment of melanoma cancer. It was discovered by Plexxicon.²⁴⁻²⁶

Chemical Discovery of Vemurafenib

Dabrafenib (Tafinlar[®] or GSK2118436)

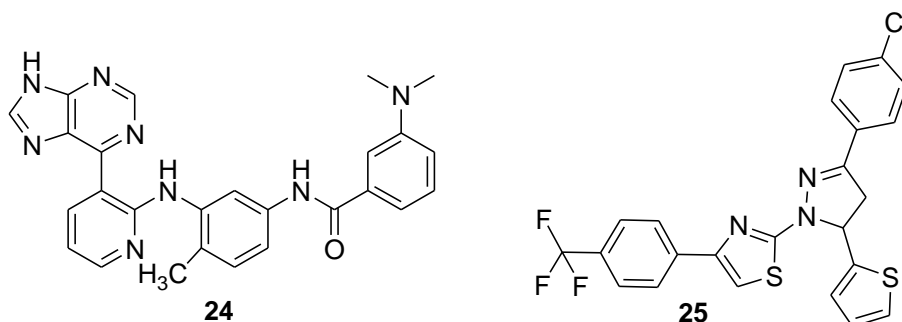
Dabrafenib is the 2nd selective B-Raf^{V600E} kinase inhibitor approved in May 2013 by the US FDA. On January 2014 FDA approved a combination of Dabrafenib with Trametinib (MEK Inhibitor) in the treatment of melanoma cancer and in Europe (April 2017) approved this combination therapy in the treatment of non-small-cell lung cancer (NSCLC).²⁷



2.1 B-Raf Small Molecule Inhibitors

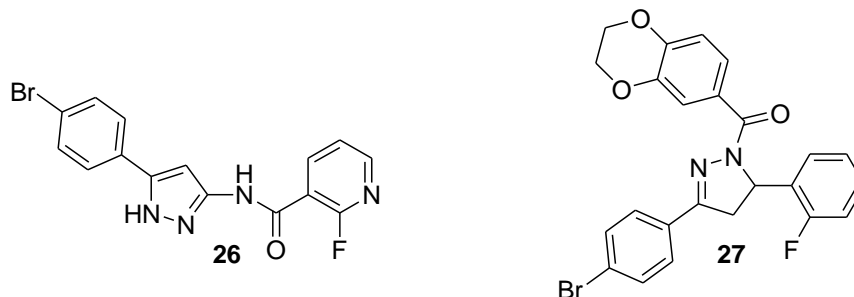
Many researchers have worked in the field of cancer progression and have reported molecules as B-Raf inhibitors for the treatment of different types of cancer. Following section contained B-Raf inhibitors, specifically inhibiting the mutant B-Raf (B-Raf^{V600E}). Here, we have reported results from 2002 to 2019 (till March) concerning kinase assay; anti-proliferative activity on various cancer cell lines and for few potent molecules, we have also reported results of *in-vivo* xenograft model studies.

Yang et al. designed and synthesized bis-aryl ureas and amides based 2-amino-3-purinylpyridine scaffold and evaluated for *in-vitro* B-Raf^{V600E} kinase enzyme inhibition and on A-375 cancer cell line. Among all these synthesized compounds, compound **24** showed potent inhibitory activity with IC₅₀ value of 0.790 nM in B-Raf^{V600E} kinase assay and 1.839 μM on A-375 cell line. Eventually, it also confirmed the inhibitory effect on tumor growth inhibition in A375 xenograft models with 71.53% tumor growth inhibition at the dose of 50 mg/kg.²⁷



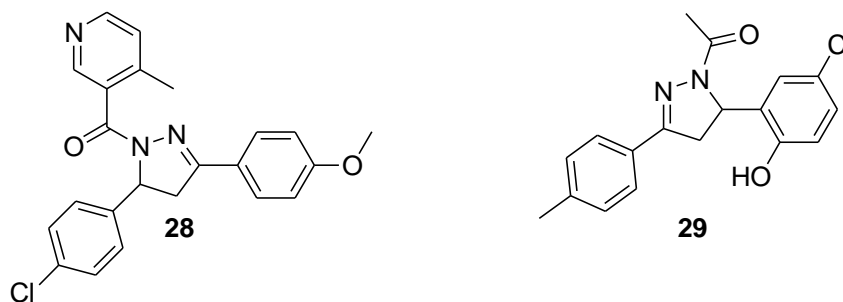
Zhao et al. synthesized novel 4,5-dihydro-1H-pyrazolothiazole derivatives and evaluated *in-vitro* for B-Raf^{V600E} kinase assay and on cancer cell lines. From the whole series of compounds, compound **25** showed the most potent kinase inhibitory activity with IC₅₀ value of 0.05 μM and inhibited growth of WM266.4 (melanoma) and MCF-7 (breast cancer) cell lines with IC₅₀ values of 0.12 μM and 0.16 μM, respectively.²⁸

Yang et al. designed and synthesized 2,3-dihydrobenzo[*b*][1,4]dioxin containing 4,5-dihydro-1H-pyrazole derivatives and screened against B-Raf^{V600E} kinase assay and on WM266.4 cancer cell line. Among all synthesized compounds, compound **26** showed the most potent kinase inhibitory activity with IC₅₀ value of 0.11 μM and inhibited growth of cancer cells with IC₅₀ value of 0.58 μM.²⁹



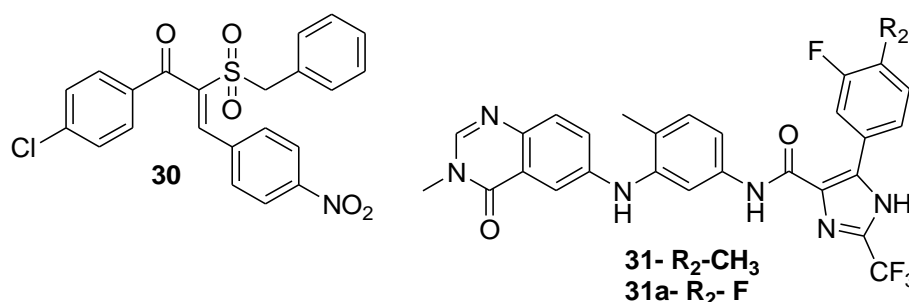
Wang et al. designed and synthesized 5-phenyl-1H-pyrazole derivatives and screened against B-Raf^{V600E} kinase assay along with B-Raf^{V600E} mutated cell lines WM266.4 and A375. For comparison, they also reported data for wild-type B-Raf (B-Raf^{WT}) cell line WM1361. Out of all synthesized compounds, compound **27** showed most potent kinase inhibitory activity with IC₅₀ value of 0.33 μM, while showed growth inhibition with IC₅₀ values of 2.63 μM and 3.16 μM on mutated B-Raf cell lines WM266.4 and A375, respectively. On B-Raf^{WT} cell line WM1361, it showed growth inhibition with IC₅₀ value of 13.25 μM.³⁰

Li et al. synthesized 4,5-dihydro-1H-pyrazole niacinamide derivatives and evaluated for B-Raf^{V600E} kinase assay and on WM266.4 cell line. From all synthesized compounds, compound **28** showed the most potent kinase inhibitory activity and cell growth inhibition on melanoma cell with IC₅₀ values of 0.20 μM and 0.89 μM, respectively.³¹



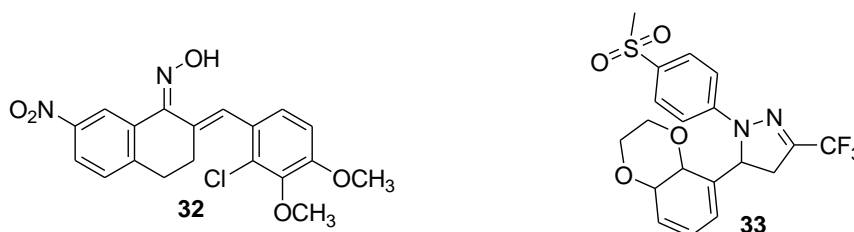
Liu et al. synthesized 4,5-dihydro-2H-pyrazole-2-hydroxyphenyl derivatives and evaluated for mutated B-Raf kinase assay and cell growth inhibition on the WM266.5 and MCF-7 cancer cell lines. Among all synthesized compounds, compound **29** showed most potent kinase inhibitory activity with IC₅₀ value of 0.22 μM, while cell growth inhibitory activity on WM266.5 and MCF-7 cell lines were observed with IC₅₀ values of 0.45 μM and 1.31 μM, respectively.³²

Li et al. designed and synthesized (*E*)- α -benzylsulfonyl chalcone derivatives and screened against B-Raf^{V600E} kinase assay, wild type cell line WM1361(B-Raf^{WT}), mutated cell line WM266.4 (B-Raf^{V600E}) and also tested against B-Raf^{V600E} cell-based ERK (Extracellular signal-regulated kinase) activity. Among all synthesized compounds, compound **30** showed most potent B-Raf^{V600E} kinase activity with the IC₅₀ value 0.17 μ M, while it showed growth inhibition on wild-type (WM1361) and mutated B-Raf (WM266.4) cell lines having IC₅₀ values 0.52 μ M and 3.56 μ M, respectively. Compound **30** also showed B-Raf^{V600E} cell-based pERK activity with IC₅₀ value of 1.23 μ M.³³



Dietrich et al. designed and synthesized 1*H*-imidazole carboxylate derivatives and evaluated against B-Raf^{V600E} kinase assay. From all these synthesized compounds, compound **31** and **31a** showed most potent kinase inhibitory activity with IC₅₀ value 0.3 nM. Compound **31** consisted of a methyl group at the R₁ position, while in compound **31a**, fluorine was present at the R₁ position.³⁴

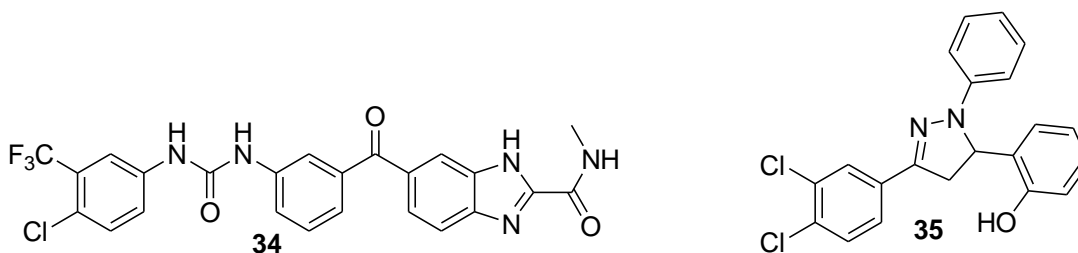
Yu et al. designed and synthesized 1-(4-(methylsulfonyl)phenyl)-3-(trifluoromethyl)-4,5-dihydro-1*H*-pyrazole derivatives and evaluated against the B-Raf^{V600E} kinase inhibitory activity and anti-proliferative activity on WM266.4 (melanoma) and Hela (Cervical) cell lines. Among all synthesized compounds, compound **32** exhibited the most potent kinase inhibitory activity with IC₅₀ value 0.12 μ M and showed anti-proliferative activity on WM266.4 and Hela cell lines with IC₅₀ values of 0.76 μ M and 25.96 μ M, respectively.³⁵



Qin et al. synthesized α,β -unsaturated carbonyl-based compounds, oxime, oxime-ether analogs and evaluated against B-Raf^{V600E} kinase assay and on various cancer cell lines.

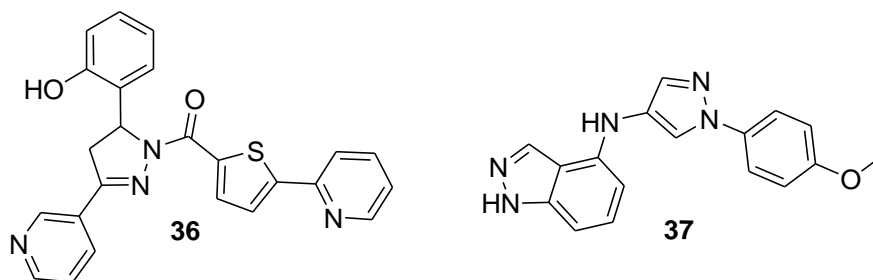
From all these synthesized compounds, α,β -unsaturated carbonyl based oxime scaffold, compound **33**, showed the most potent inhibitory activity with IC_{50} value of 0.9 μM . Compound **33** also showed good cell growth inhibition on various cancer cell lines; e.g. pancreatic cell lines Panc-1 and PaCa-2 with IC_{50} values of 0.09 μM for each; on breast cancer cell line (MCF-7) with IC_{50} value 0.07 μM ; on epithelial cell line (A-549) with IC_{50} value 0.08 μM ; on colon cancer cell line (HT-29) with IC_{50} value 0.09 μM ; on lung cancer cell line (H-460) with IC_{50} value 0.08 μM and on prostate cancer cell line (PC-3) with IC_{50} value of 0.02 μM .³⁶

Yanga et al. designed and synthesized bis-aryl ureas and bisarylamides based on 1H-benzo[d]imidazole scaffold and screened against kinase inhibitory activity, anti-proliferative activity on melanoma cell line A375, human umbilical vein endothelial cell line HUVECs and also evaluated for *in-vivo* profiling in human melanoma A375 xenograft model. Among all these compounds, compound **34** was highly active against all biological assays as well as in *in-vivo* profile. It showed kinase inhibitory activity against V600E mutant B-Raf having IC_{50} value of 57.8 nM and showed tumor growth inhibition at concentration of 3.62 μM on A375 melanoma cell line and 12.46 μM on HUVECs human umbilical vein endothelial cell line. Compound **34** also progressed to *in-vivo* profiling, which exhibited 17.99% tumor growth inhibition in human melanoma A375 xenograft model at the dose of 50mg/kg without body weight loss.³⁷



Yang et al. synthesized 2-(1,3-diaryl-4,5-dihydro-1H-pyrazole-5-yl) phenol derivatives and screened against B-Raf^{V600E} kinase assay and also screened against human melanoma cell line WM266.4. Amongst synthesized compounds, compound **35** showed potent biological activity against mutated B-Raf^{V600E} with IC_{50} value of 0.15 μM and showed growth inhibitory effect on melanoma cell line WM266.4 with the IC_{50} value of 1.75 μM .³⁸

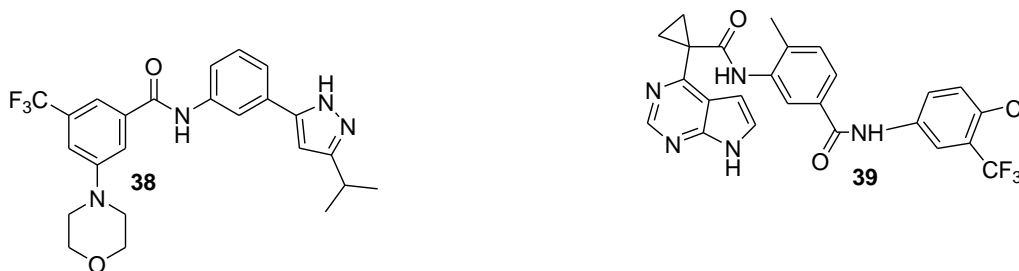
Blackburn et al. optimized and synthesized *N*-acyl and *N*-aryl pyrazolines scaffolds and evaluated for B-Raf^{V600E} mediated kinase assay and for anti-proliferative activity on melanoma cell line A375. Among all these compounds, compound **36** showed potent inhibitory activity on kinase assay and growth inhibition on A375 cell line with IC₅₀ values of 19 nM and 180 nM, respectively.³⁹



Wang et al. designed and synthesized 4-phenylamino-1*H*-indazoles derivatives and evaluated against mutated B-Raf^{V600E} and wild-type B-Raf kinase assay, growth inhibition on melanoma cell lines includes A375 (B-Raf^{V600E}), WM266.4 (B-Raf^{V600E}) and assessed for *in-vivo* xenograft model of A375 human melanoma cells in mice. From all synthesized compounds, compound **37** showed potent inhibitory activity against all biological evaluations. Compound **37** showed kinase selectivity on B-Raf^{V600E} and B-Raf^{WT} with IC₅₀ values of 0.04 μM and 0.77 μM, respectively. It also showed growth inhibition on A375 and WM266.4 with IC₅₀ values of 0.34 μM and 0.38 μM, respectively. The efficacy and safety of compound **37** were also proved by A375 xenograft model, and in this *in-vivo* study, three different doses of compound **37** (2.5, 5, 10 mg/kg) was injected to mice and measured the average weight of tumor as compared with the standard. This *in-vivo* study showed that 10mg/kg dose significantly decreased the weight of the tumor (around 0.22 gm), while 5mg/kg dose exhibited equivalent antitumor efficacy (weight of the tumor around was 0.38 gm). No significant effect was observed at the dose of 2.5mg/kg.⁴⁰

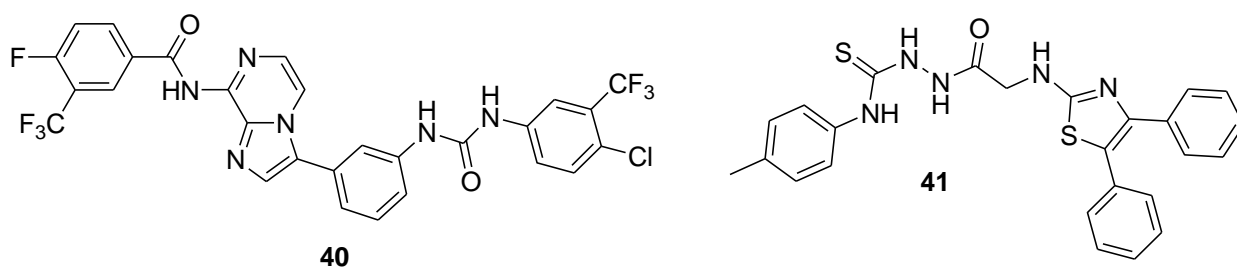
Wang et al. designed and synthesized pyrrolo[2,3 *d*]pyrimidine derivatives and screened for inhibitory activity in B-Raf kinase assay and on various cancerous cell lines. Among all these synthesized compounds, compound **38** showed potent kinase inhibitory activity on B-Raf^{WT} and B-Raf^{V600E} with IC₅₀ values of 9.4 nM and 3.5 nM, respectively. Compound **38** was also screened against various cancer cell lines (with IC₅₀ values), like

A375 (8.6 μM), SK-MEL-2 (3.3 μM), HT-29 (9.2 μM), MV4-11 (3.2 μM), HepG2 (4.1 μM), and SW579 (3.0 μM).⁴¹



Jung et al. designed and synthesized N-(3-(3-alkyl-1*H*-pyrazol-5-yl)phenyl)-arylamide derivatives and screened against kinase activity and anti-proliferative activity. Among all this compound, compound **39** showed potent kinase inhibitory activity on B-Raf^{WT} and B-Raf^{V600E} with IC₅₀ values of 13.85 μM and 0.7 μM , respectively and also showed good cell growth proliferation on A375 melanoma cell line with IC₅₀ value of 0.43 μM .⁴²

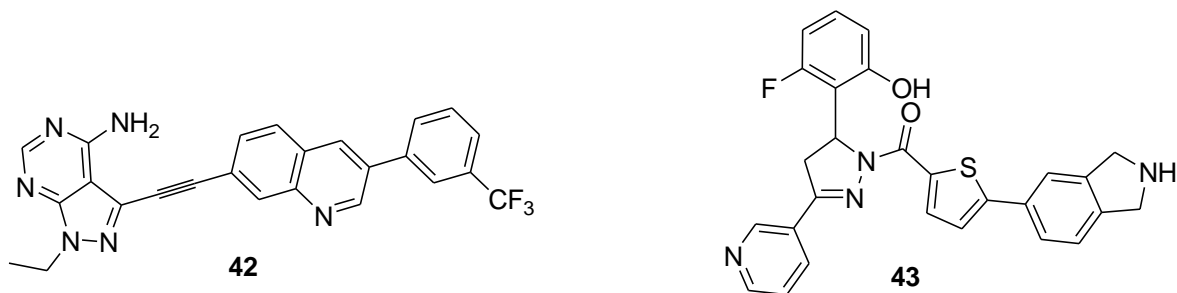
Garamvolgyi et al. synthesized novel imidazo[1,2-*a*]pyridine and imidazo[1,2-*a*]pyrazine derivatives and evaluated against B-Raf^{V600E} activity and cell growth inhibition on the melanoma cell line (A375). Among all these compounds, compound **40** showed potent kinase activity on B-Raf^{V600E} protein and anti-proliferative activity on melanoma cell line (A375) with IC₅₀ values of 5.01 μM and 0.06 μM , respectively.⁴³



Abdelazeem et al. synthesized novel diphenylthiazole derivatives and evaluated against kinase activity on B-Raf^{V600E} kinase activity. Compound **41** showed potent kinase activity with IC₅₀ value of 1.3 μM .⁴⁴

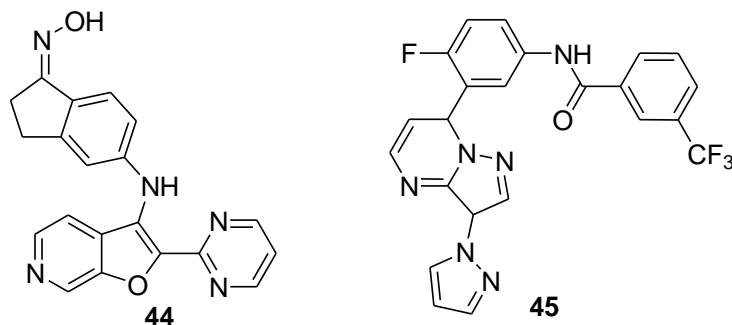
Assadieskandar et al. synthesized pyrazolo[2,3-*d*]pyrimidine derivatives and evaluated for kinase inhibitory and anti-proliferative activity. Among all these synthesized compounds,

compound **42** showed potent kinase inhibition on B-Raf^{V600E} kinase with IC₅₀ value of 13 nM and also screened against lymphoma cell line (Ba/F₃) with IC₅₀ value of 1107 μM.⁴⁵



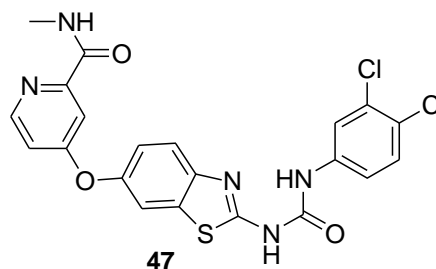
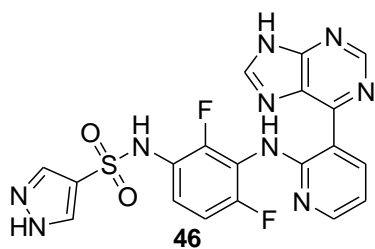
Duffey et al. synthesized pyrazoline derivative and evaluated against B-Raf^{V600E} kinase inhibitory activity. Among all these synthesized compounds, compound **43** showed potent kinase activity on B-Raf^{V600E} with IC₅₀ value of 2 nM.⁴⁶

Buckmelter et al. synthesized furo[2,3-*c*]pyridine derivatives and screened against B-Raf^{V600E} kinase activity. Among all these synthesized compounds, compound **44** showed potent kinase inhibitory activity on B-Raf^{V600E} with IC₅₀ value of 0.2 nM.⁴⁷



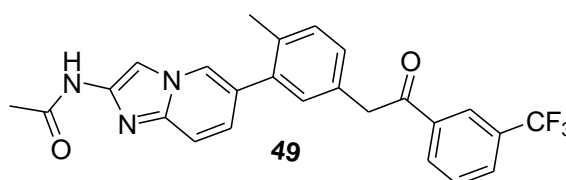
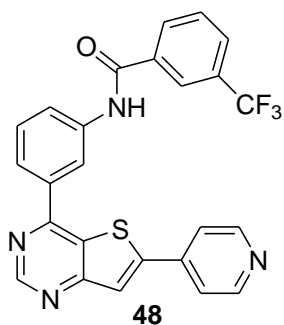
Berger et al. synthesized pyrazolopyrimidine derivatives and evaluated for kinase activity and anti-proliferative activity. Among all these synthesized compounds, compound **45** showed good kinase activity on B-Raf^{V600E} with IC₅₀ value of 0.018 μM and also showed good cell growth inhibition on melanoma cell line (WM266-4) and colon cancer cell line (HT-29) with IC₅₀ values of 6.6 μM and 2.8 μM, respectively.⁴⁸

Liu et al. synthesized purinylpyridinylamino derivatives and evaluated for kinase assay (B-Raf^{WT} and B-Raf^{V600E}) and against cancer cell proliferation on melanoma cell line A-375. Compound **46** showed potent activity in B-Raf^{V600E} kinase assay with IC₅₀ value of 0.2 nM and subsequently, showed IC₅₀ value of 1 nM in wild-type B-Raf kinase assay. It also showed growth inhibition on A375 melanoma cell line with IC₅₀ value of 6 nM.⁴⁹



El-Damasy et al. synthesized benzothiazole derivatives and evaluated for kinase activity and anti-proliferative activity on cancer cell lines panel. Among all these synthesized compounds, compound **47** showed potent kinase activity on B-Raf^{V600E} with IC₅₀ value 0.095 μM. Compound **47** also showed cell growth inhibition on various cancer cell lines panel (with IC₅₀ value in μM) which included leukaemia cell lines (3.66-6.47 μM), non-small cell lung cancer cell lines (1.89-4.09 μM), colon cancer cell lines (1.88-5.05 μM), CNS cancer cell lines (1.53-2.00 μM), melanoma cancer cell lines (1.5-2.6 μM), ovarian cancer cell lines (2.0-2.5 μM), renal cancer cell lines (1.84-4.0 μM), prostate cancer cell lines (1.95-2.5 μM) and breast cancer cell lines (2.0-5 μM).⁵⁰

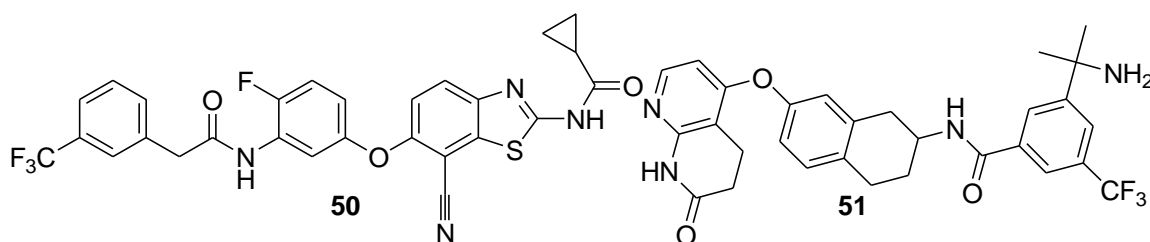
Gopalsamy et al. synthesized thieno[3,2-*d*]pyrimidine derivatives and evaluated against kinase activity on B-Raf^{V600E}. Among all these synthesized compounds, compound **48** showed potent kinase inhibition on B-Raf^{V600E} activity with IC₅₀ value of 0.032 μM.⁵¹



Smith et al. synthesized imidazo[1,2-*a*]pyridin-6-yl-benzamide analogs and evaluated against B-Raf^{V600E} kinase assay and growth inhibition on A375 melanoma cell line. From synthesized compounds, compound **49** showed the most potent kinase inhibitory activity with IC₅₀ of 0.2 nM and EC₅₀ value of 8.6 nM on A375 melanoma cell line.⁵²

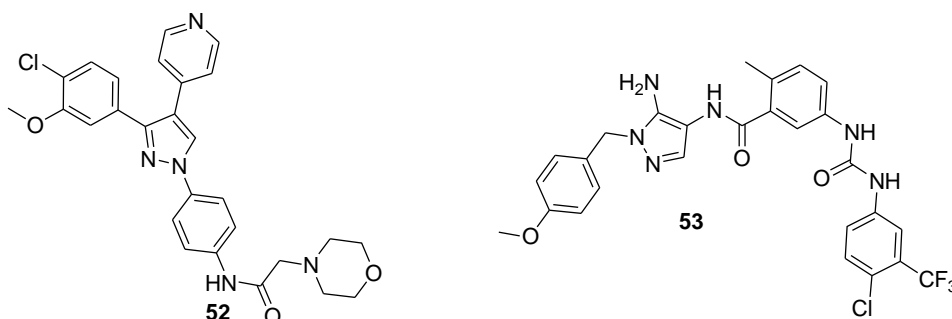
Okaniwa et al. designed and synthesized C-7-substituted 1,3-benzothiazole derivatives and evaluated against kinase assay, anti-proliferative assay and *in-vivo* xenograft model on mice. Among all synthesized compounds, compound **50** showed potent activity against

mutated B-Raf^{V600E} and wild-type kinase assay with IC₅₀ values of 2.4 nM and 8.3 nM, respectively. Compound **50** also showed cell growth inhibitory activity on A375 (B-Raf^{V600E}) and HMVII (B-Raf^{G469V}) with IC₅₀ values of 66 nM and 200 nM, respectively. During *in-vivo* studies in rat, in human melanoma A375 xenograft model, tumor growth inhibition by compound **50** was observed with 51.7 % at the dose of 25mg/kg. In human melanoma HMVII xenograft model evaluated in rats, the % tumor regression showed by compound **50** were 52%, 26%, and 0% at doses of 3.9mg/kg, 9.7mg/kg and 24.1mg/kg, respectively.⁵³



Gould et al. designed and synthesized tetrahydronaphthalene derivatives and evaluated against kinase binding selectivity. Among all these synthesized compounds, compound **51** showed potent kinase selectivity on B-Raf^{WT} and B-Raf^{V600E} with IC₅₀ values of 4.2 and 2.1 nM, respectively.⁵⁴

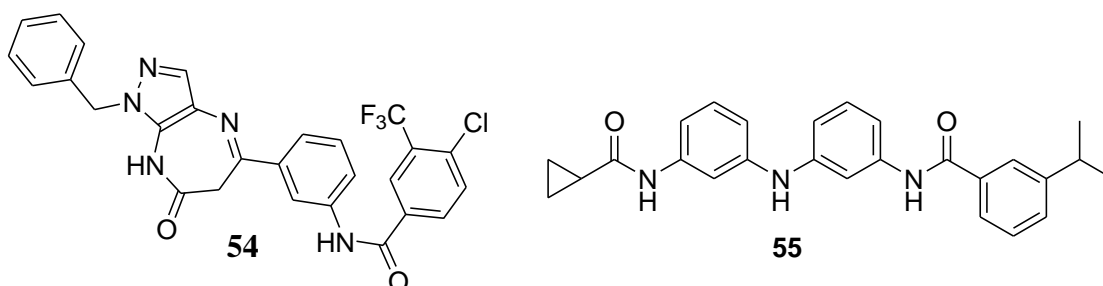
Khan et al. synthesized triarypyrazole derivatives and screened for kinase selectivity and anti-proliferative activity. Among all these synthesized compounds, compound **52** showed potent kinase selectivity against B-Raf^{WT} and B-Raf^{V600E} with IC₅₀ values of 536 and 2.98 nM, respectively and also showed good anti-proliferative activity on A375 and SK-MEL-28 melanoma cell line with IC₅₀ values of 1.82 μM and 2.21 μM, respectively.⁵⁵



Kim et al. synthesized *1H*-pyrazole derivatives and screened against kinase binding activity and anti-proliferative activity. Among all these synthesized compounds,

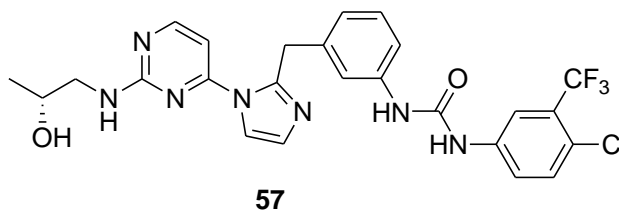
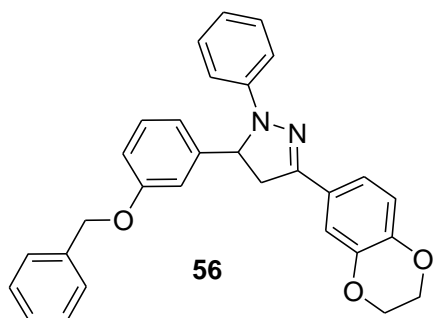
compound **53** showed potent kinase affinity on B-Raf^{V600E} with IC₅₀ value of 264 nM and also showed potent anti-proliferative activity on A375 melanoma cell line with IC₅₀ value of 0.7 μM.⁵⁶

Kim et al. synthesized phenylpyrazolodiazepin derivatives and evaluated against kinase activity and anti-proliferative activity. Among all these synthesized compounds, compound **54** showed potent kinase inhibitory activity on B-Raf^{V600E} with IC₅₀ value of 655.2 nM and also showed anti-proliferative activity against melanoma cell line (A375) with IC₅₀ value of 0.43 μM.⁵⁷



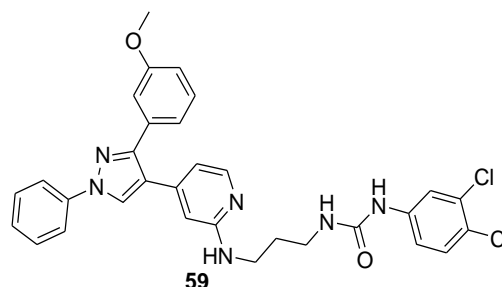
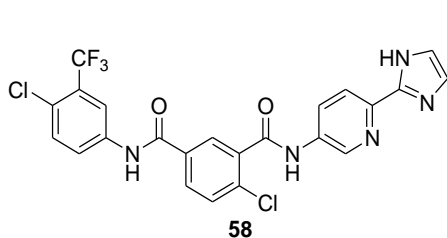
Li et al. designed and synthesized N-(4-aminopyridine-2-yl)amide derivatives and screened for kinase inhibitory activity and also for anti-proliferative activity. Among all synthesized compounds, compound **55** showed the most potent inhibitory activity on mutated B-Raf^{V600E} with IC₅₀ value of 0.013 μM and also showed inhibition of wild-type B-Raf^{WT} with the IC₅₀ value of 0.148 μM. Compound **55** also showed cell growth inhibition on colon cancer cell lines; Colo205, HT29, and HCT116, with IC₅₀ values of 0.444 μM, 0.462 μM, and 1.055 μM, respectively.⁵⁸

Yang et al. designed and synthesized dioxin-containing triaryl pyrazoline derivatives and evaluated on kinase inhibitory activity on mutated B-Raf^{V600E}, B-Raf^{WT} and also screened for anti-proliferative activity on WM266.4 cell line. Among all synthesized compounds, compound **56** showed potent kinase inhibitory activity on B-Raf^{V600E} and B-Raf^{WT} with IC₅₀ values of 0.04 μM and 1.06 μM, respectively. It also showed IC₅₀ value of 0.87 μM on melanoma cell line (WM266.4).⁵⁹



Kim et al. designed and synthesized benzyl 2-(1*H*-imidazole-1-yl) pyrimidine analogs and evaluated on kinase inhibitory activity and for anti-proliferative activity on melanoma cell line (A375) and lymphoma cell line (U937). From all synthesized compounds, compound **57** showed most potent kinase inhibitory activity on mutated B-Raf^{V600E} and on B-Raf^{WT} with IC₅₀ values of 38.3 μM and 186 μM, respectively. It showed anti-proliferative activity on A375 and U937 with IC₅₀ values of 26.2 μM, and 15.3 μM, respectively.⁶⁰

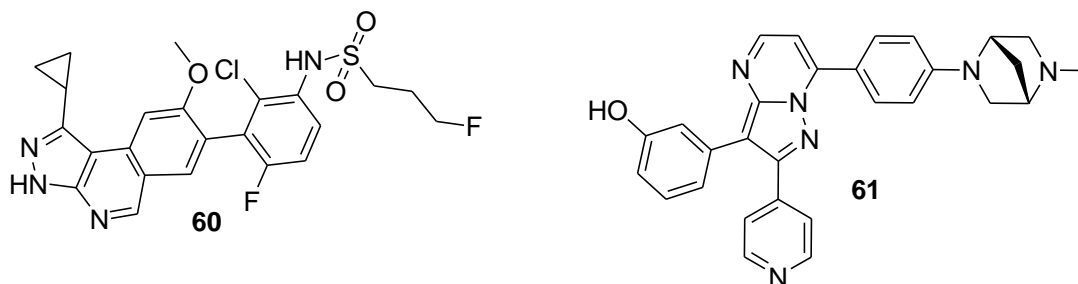
Jiao et al. designed and synthesized series of 2-(1*H*-imidazole-2-yl) pyridine and screened for B-Raf kinase inhibitory activity. Compound **58** showed the most potent kinase inhibitory activity on B-Raf with IC₅₀ value of 0.531 μM along with growth inhibition on melanoma cell line (A375), liver cancer cell line (HepG2), breast cancer cell line (MDA-MB-453) with IC₅₀ values of 2.93 μM, 3.21 μM, and 7.96 μM, respectively. It was further evaluated for *in-vivo* efficacy using xenograft model on mice with suppression of growth by 42.50% at the dose of 50mg/kg.⁶¹



Gamal El-Din et al. designed and synthesized triarylpyrazole derivatives and were screened for B-Raf kinase inhibitory activity and evaluated against panel of cell lines. Compound **59** showed potent inhibitory activity on mutated B-Raf^{V600E} with IC₅₀ value of

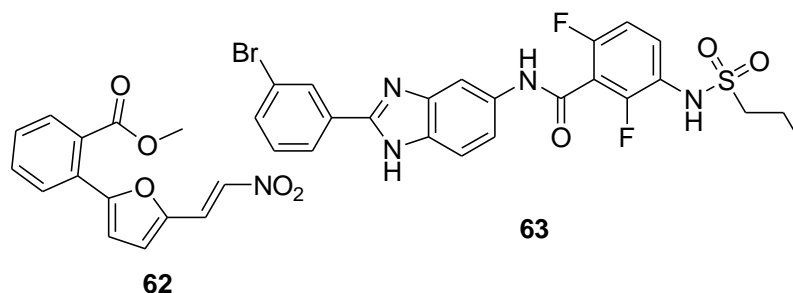
0.77 μM and also showed tumor growth inhibition on various cancer cell lines panel which included SK-MEL-5 (melanoma), K-562 (Leukemia), HOP-92 (NSCLC), Colo205 (Colon), HCT-15 (colon), SNB-75 (CNS), NCI/ADR-RES (Ovarian), RXF-393 (renal), PC-3 (prostate), MDA-MB-468 (breast) with the IC_{50} values of 1.75 μM , 2.38 μM , 2.32 μM , 1.87 μM , 2.40 μM , 2.52 μM , 2.19 μM , 1.80 μM , 3.96 μM and 1.92 μM , respectively.⁶²

Lu et al. designed and synthesized biaryl scaffold featured pyrazolo[3,4-*c*]isoquinoline derivatives and evaluated for kinase inhibitory activity, growth inhibition on melanoma cell line and also assessed for *in-vivo* efficacy. Compound **60** showed most potent B-Raf^{V600E} inhibitory activity with IC_{50} value of 7 nM and also showed good tumor growth inhibition on melanoma cell line A375 with IC_{50} value of 13 nM. Compound **60** was further evaluated for *in-vivo* efficacy using xenograft model and showed partial tumor growth inhibition of 76 % at a dose of 20mg/kg and complete tumor regression of around 95% at a dose of 60mg/kg.⁶³



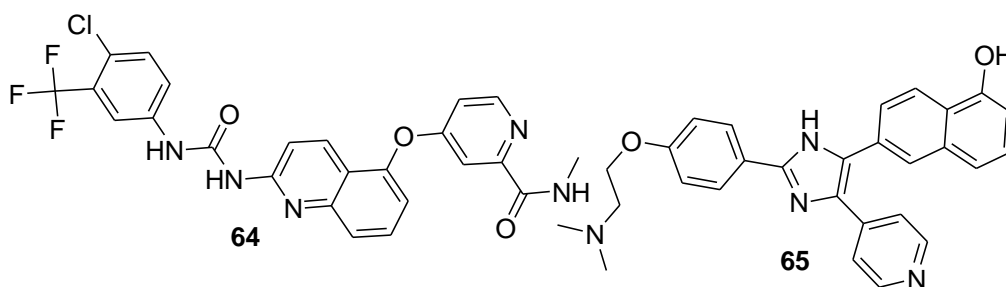
Wang et al. designed and synthesized series of pyrazolo[1,5-*a*]pyrimidine analogs and evaluated against mutated B-Raf kinase inhibitory assay and also perform the antiproliferative assay. Among all analogs, compound **61** showed the most potent B-Raf^{V600E} activity with IC_{50} value of 0.38 nM and showed cell growth inhibition on A375 melanoma cell line with IC_{50} value of 0.77 μM .⁶⁴

Kong et al. synthesized furan derivatives and evaluate against kinase selectivity. Among all these compounds, compound **62** showed potent kinase activity on B-Raf^{WT} and B-Raf^{V600E} protein with IC_{50} values of 1.38 μM and 1.96 μM , respectively.⁶⁵



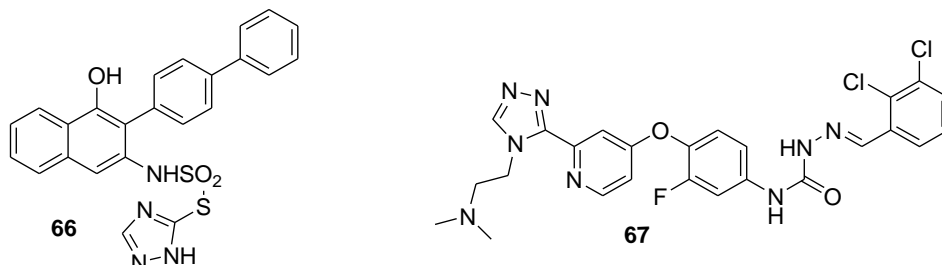
Newhouse et al. synthesized Imidazo[4,5-b]pyridine derivatives and screened against kinase binding affinity. Among all these compounds, compound **63** showed potent kinase inhibition on B-Raf^{V600E} with IC₅₀ value 0.76 nM.⁶⁶

El-damasy et al. designed and synthesized picolinamide based 2-amino and ureido quinoline derivatives and evaluated against kinase inhibitory activity and performed anti-proliferative activity on cancer cell lines panel. Among all synthesized compounds, compound **64** showed most potent kinase inhibitory activity on mutated B-Raf^{V600E} with IC₅₀ value of 361 nM and also showed 87.8% enzyme inhibition. Anti-proliferative activity was carried on various cancer cell lines panel (with IC₅₀ values in μM); e.g. non-small cell lung cancer cell lines (2.5-20.5 μM), colon cancer cell line (HCT-116 - 2.73 μM), CNS cancer cell lines (3.0-89.0 μM), melanoma cancer cell lines (1.5-3.0 μM), ovarian cancer cell lines (3.0-5.0 μM), renal cancer cell lines (2.70-13.6 μM), prostate cancer cell lines (DU-145 2.39 μM), and breast cancer cell lines (1.5-7.36 μM).⁶⁷



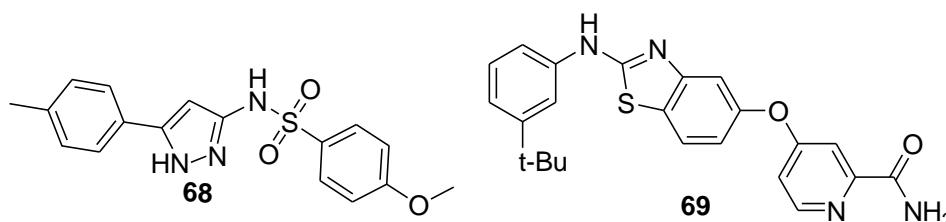
Niculescu-Duvaz et al. synthesized imidazole and benzothiofene derivatives and evaluated for kinase potency and anti-proliferative activity. Among all these synthesized compounds, compound **65** showed most potent kinase selectivity on B-Raf^{V600E} with IC₅₀ value of 0.009 μM and also showed good cell growth proliferation on melanoma cell line WM266.4 with IC₅₀ value of 0.22 μM.⁶⁸

Qin et al. synthesized novel naphthol derivatives and evaluated for kinase binding affinity on B-Raf protein. Among all these synthesized compounds, compound **66** showed potent kinase selectivity on B-Raf^{WT} and B-Raf^{V600E} with IC₅₀ values of 0.22 nM and 0.18 nM, respectively.⁶⁹



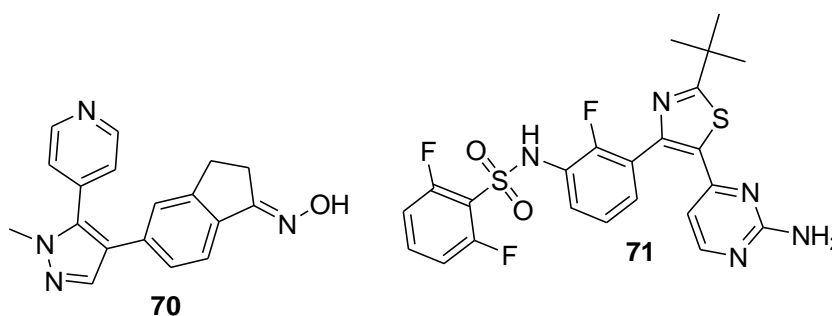
Qin et al. synthesized novel 2-(4-(2-(dimethylamino)ethyl)-4H-1,2,4-triazol-3-yl)pyridines derivatives and evaluated for kinase potency and anti-proliferative activity. Among all these synthesized compound, compound **67** showed 82.6% enzyme inhibition at 10 μ M which indicated the potent kinase inhibition activity. Compound **67** also showed cell growth inhibition on various types of cancerous cell lines which included MKN-45 (gastric cancer), H460 (lung cancer), HT-29 (colon cancer), A549 (NSCLC) with IC₅₀ values of 0.051 μ M, 0.072 μ M, 0.13 μ M and 1.09 μ M, respectively.⁷⁰

Gong et al. synthesized series of *N*-(5-phenyl-1*H*-pyrazole-3-yl)benzenesulfonamide derivatives and screened against kinase inhibitory activity on mutated B-Raf^{V600E} and also evaluated for anti-proliferative activity on mutated B-Raf^{V600E} contained cell lines, A375, and WM266.4. It was also tested against WM1361 cell line comprised wild-type B-Raf enzyme. Compound **68** showed the most potent kinase inhibitory activity on mutated B-Raf with the IC₅₀ value of 0.18 μ M and cell growth inhibition on B-Raf^{WT} enzyme contained WM1361 cell line with IC₅₀ value of 10.12 μ M. Besides, it also inhibited A375 and WM266.4 melanoma cell lines with IC₅₀ values of 2.04 μ M and 1.58 μ M, respectively.⁷¹



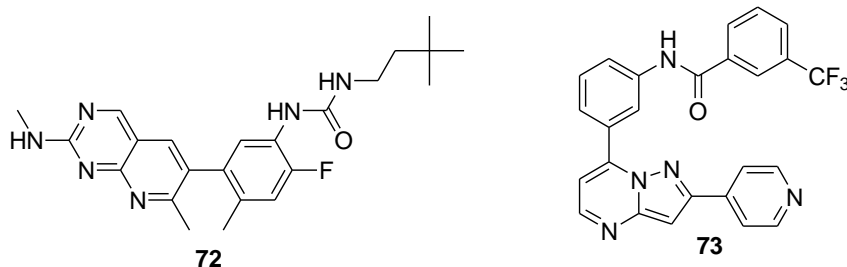
Ramurthy et al. synthesized 5,6-fused heterocyclic derivatives and screened against kinase potency. Among all these synthesized compounds, compound **69** showed potent kinase potency on B-Raf^{V600E} enzyme with IC₅₀ value of 0.002 μM.⁷²

Hansen et al. synthesized a series of the pyrazole-based moiety and evaluated against kinase inhibitory activity. From all these compounds, compound **70** showed the most potent B-Raf^{V600E} kinase inhibitory activity with IC₅₀ value of 0.02 nM.⁷³



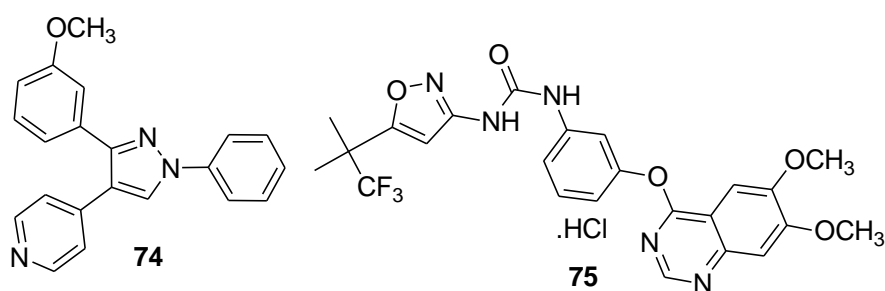
Rheault et al. synthesized pyrimidine derivatives and evaluated for kinase selectivity and anti-proliferative activity. Among all these synthesized compounds, compounds **71** showed potent kinase activity on B-Raf^{V600E} enzyme with IC₅₀ value of 0.7 nM and also showed good cell growth inhibition on cancer cell lines like SK-MEL-28, A375, and Colo205 with IC₅₀ values of 3 nM, 8 nM, and 7 nM, respectively.⁷⁴

Henry et al. designed and synthesized 1-(3,3-dimethylbutyl)-3-(2-fluoro-4-methyl-5-(7-methyl-2-(methylamino)pyrido[2,3-*d*]pyrimidin-6-yl)phenyl)urea derivatives and screened against kinase inhibitory assay. It was also evaluated for *in-vitro* and *in-vivo* activity to check the safety and efficacy of compounds. Among all synthesized compounds, compound **72** showed the highest kinase inhibitory activity on both B-Raf isoforms, B-Raf^{WT} and B-Raf^{V600E} with IC₅₀ values of 0.058 μM and 0.015 μM, respectively. This compound also showed good anti-proliferative activity on A375 melanoma and HCT116 colon cell lines with IC₅₀ values of 0.0092 μM and 0.22 μM, respectively. Compound **72** was also evaluated in rats for A375 xenograft model and showed 50% tumor inhibition at 4.36 mg/kg.⁷⁵



Gopalsamy et al. synthesized pyrazolo[1,5-*a*]pyrimidine derivatives, optimized and evaluated against kinase inhibitor activity on B-Raf and also screened against various cancer cell lines. Among all these compounds, compound **73** showed the most potent kinase inhibitory activity on B-Raf enzyme with IC_{50} value of 0.032 μM and showed cell growth inhibitory activity on A375 (melanoma), LoVo (colon), HT-29 (colon), BXPC3 (pancreatic) and WM-266-4 (melanoma) with IC_{50} values of 0.28 μM , 0.4 μM , 0.35 μM , 2.6 μM , 3.1 μM and 3.5 μM , respectively.⁷⁶

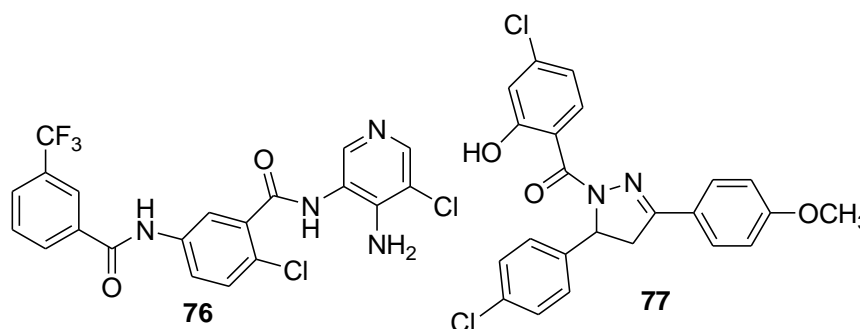
El-Gamal et al. synthesized 1,3,4-triarylpyrazole derivatives and screened against kinase binding affinity and anti-proliferative activity. Among all these synthesized compounds, compound **74** showed potent kinase affinity for B-Raf^{V600E} enzyme with IC_{50} value 1.44 μM and its IC_{50} values against leukaemia cancer cell lines (RPMI-8226 and K-562) and breast cancer cell line (MDA-MB-468) were 1.71 μM , 3.42 μM , and 6.70 μM , respectively.⁷⁷



Rowbottom et al. synthesized quinazoline-4-yl-oxy derivatives and screened for *in-vitro* and *in-vivo* pharmacological activities. Among all synthesized compounds, compound **75** showed potent kinase selectivity on B-Raf^{WT}, and B-Raf^{V600E} with K_d values of 36 and 14 nM, respectively. Compound **75** was screened across a panel of cancer cell lines expressing B-Raf^{V600E} which includes, A375 (EC_{50} 78 nM), Colo-205 (EC_{50} 36 nM), Colo-679 (EC_{50} 211 nM), SK-MEL-28 (EC_{50} 454 nM) and HT-144 (EC_{50} 228 nM). It was

also screened across a panel of cancer cell lines expressing B-Raf^{WT} includes HCT116 (EC₅₀ 669 nM), Hs578T (EC₅₀ 2736 nM), LNCap (EC₅₀ 6631 nM), DU145 (EC₅₀ 2911 nM) and PC-3 (EC₅₀ 6257 nM). Eventually, compound **75** was also screened for *in-vivo* antitumor efficacy and tolerability in B-Raf^{V600E} driven human carcinoma xenograft mouse model on Colo-205 and A375. The results showed that the dose of 30 mg/kg led to a 50 and 75% inhibition of normalized pMEK in tumor lysates at 2 and 6 h time points, respectively.⁷⁸

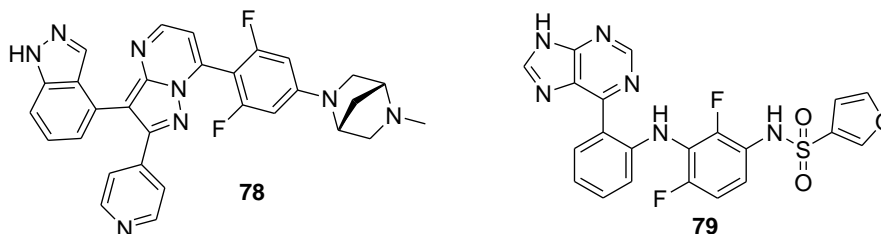
Lyne et al. synthesized amidoheteroaryls derivatives and evaluated for kinase inhibitory activity. Among all synthesized compounds, compound **76** showed good B-Raf inhibitory activity with IC₅₀ value of 0.027 μM. Compound **76** was also evaluated for *in-vivo* activity on A375 cell induced cancer in mice by oral dosage form with dose of 30mg/kg, 40mg/kg and 83mg/kg and showed % growth inhibition of 50%, 64%, and 71%, respectively.⁷⁹



Li et al. synthesized 3,5-diarylpyrazoline derivatives and evaluated against kinase inhibitory activity and anti-proliferative activity on WM266.4 melanoma cell line. From all synthesized compounds; compound **77** showed most potent B-Raf^{V600E} kinase inhibitory activity with IC₅₀ value of 0.16 μM. It also showed anti-proliferative activity on melanoma cell line WM266.4 (B-Raf^{V600E}) and WM1361 (B-Raf^{V600E}) with IC₅₀ values of 0.24 μM and 12.1 μM, respectively.⁸⁰

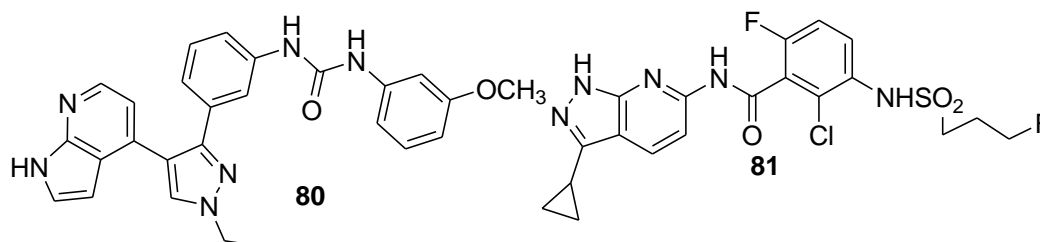
Wang et al. synthesized indazolylpyrazolopyrimidine derivatives and evaluated against kinase inhibitory activity, *in-vitro* and *in-vivo* activities. From all these synthesized compounds, compound **78** showed potent kinase inhibitory activity against B-Raf^{V600E} with IC₅₀ value 0.23 nM and also showed good anti-proliferative activity on A375 melanoma cell line with IC₅₀ value of 0.044 μM. This compound was also screened for

in-vivo testing in xenograft model of melanoma cell line A375 and showed 39% tumor growth inhibition at a dose of 7.5 mg/kg once a day.⁸¹



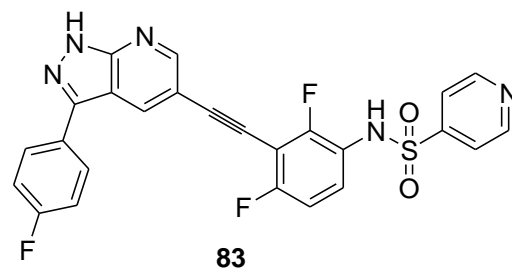
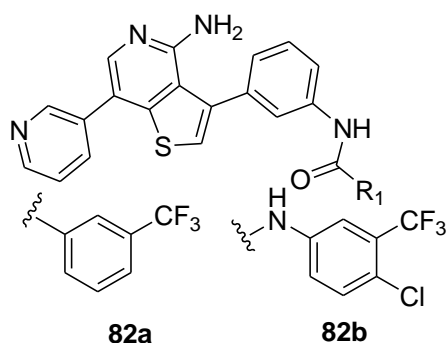
Kim et al. synthesized N-(3-(3-9H-purine-6-yl)pyridine-2-acylamino)-2,4-difluorophenyl) furan-3-sulfonamide derivatives and evaluated against kinase inhibitory activity and anti-proliferative activity. Among all these synthesized compounds, compound **79** showed most potent kinase inhibitory activity on B-Rfa^{V600E} and B-Raf^{WT} with IC₅₀ values of 2 nM and 2.2 nM, respectively. It also showed significant antiproliferative activity on melanoma cell lines.⁸²

Tang et al. synthesized 7-azaindole derivatives and evaluated against kinase binding affinity on B-Raf enzyme. Among all these synthesized compounds, compound **80** showed potent kinase binding affinity on B-Raf^{V600E} protein with IC₅₀ value of 2.1 nM.⁸³



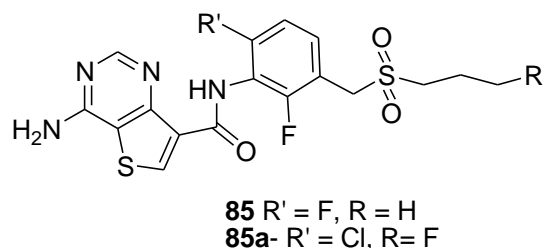
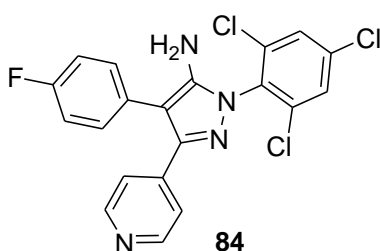
Wenglowsky et al. synthesized pyrazolopyridine derivatives and screened for kinase binding affinity. Among all these synthesized compounds, compound **81** showed potent kinase affinity on B-Raf^{V600E} with IC₅₀ value of 0.6 nM.⁸⁴

Tang et al. synthesized 4-aminothienopyridine derivatives and screened against cell-free assay and cell-based ELISA assay on B-Raf enzyme. Among all these synthesized compounds, compound **82a** and **82b** showed excellent potency on cell-free assay (IC₅₀ values of 5.1 and 16.6 nM, respectively) and cell-based assay (IC₅₀ values of 0.2 μM for both compounds), respectively.⁸⁵



Li et al. synthesized N-(3-ethynyl-2,4-difluorophenyl)sulfonamide derivatives and screened for *in-vitro* and *in-vivo* activity. Among all synthesized compounds, compound **83** showed good kinase inhibitory activity on B-Raf^{V600E} with IC₅₀ of 11 nM. It also showed anti-proliferative activity on HT29 (IC₅₀ = 0.384 μM), SK-MEL-1 (IC₅₀ = 0.448 μM), SK-MEL-28 (IC₅₀ = 0.257 μM), NZM20 (IC₅₀ = 0.023 μM), NZM07 (IC₅₀ = 0.024 μM) and A375 (IC₅₀ = 0.101 μM). This compound also showed 54% tumor growth inhibition at a dose of 25mg/kg in *in-vivo* activity on xenograft model.⁸⁶

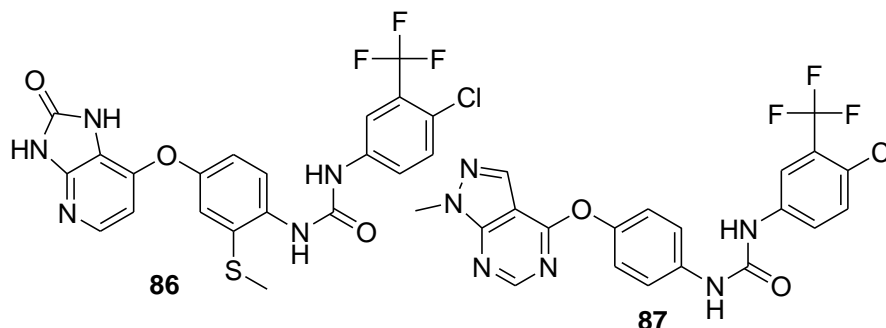
Thaher et al. synthesized novel pyrazole derivatives and screened against kinase selectivity and kinase affinity. Among all these synthesized compounds, compound **84** showed potent kinase selectivity as well as good binding affinity on B-Raf^{WT} and B-Raf^{V600E} enzyme with IC₅₀ values of 0.27 μM and 0.592 μM, respectively.⁸⁷



Mathieu et al. synthesized aminopyrimidine based scaffolds and evaluated for *in-vitro* and *in-vivo* activity. Compounds **85** & **85a** showed good kinase inhibitory activity on B-Raf^{V600E} with IC₅₀ values of 0.11 and 0.18 nM, respectively. These two compounds showed anti-proliferative activity on malma-3M cell lines with IC₅₀ values of 2.5 and 4.6 nM, respectively. Compounds **85** and **85a** also showed efficacy on xenograft model.⁸⁸

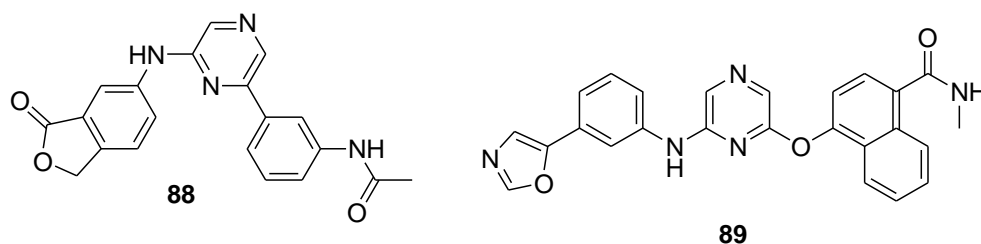
Menard et al. synthesized *1H*-imidazo[4,5-*b*]pyridine-2(3*H*)-one derivatives and screened for kinase inhibitory and anti-proliferative activity. Among all these synthesized

compounds, compound **86** showed most potent kinase inhibitory activity on B-Raf^{V600E} with IC₅₀ value of 1 nM and showed good cell growth inhibition on WM266.5 melanoma cell line with IC₅₀ value of 0.61 μM.⁸⁹



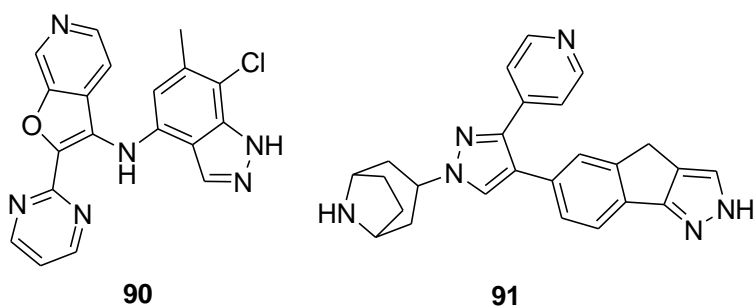
Fu et al. designed and synthesized *1H*-pyrazolo[3,4-*d*]pyrimidine derivatives and evaluated for kinase inhibitory and antiproliferative activity. From all these compounds, compound **87** showed potent kinase inhibitory activity on B-Raf^{V600E} and B-Raf^{WT} with IC₅₀ values of 23.6 nM and 51.5 nM, respectively. It also showed anti-proliferative activity on A375 (melanoma) cell line, HT-29 (colon) cell line, PC-3 (prostate) cell line, A549 (lung) cell line with IC₅₀ value of 12.21 μM, 14.72 μM, 23.41 μM and 12.49 μM, respectively. Compound **87** was also proved non-toxic for normal cells by *in-vitro* toxicity study on MDCK cell line.⁹⁰

Niculescu-Duvaz et al. optimized and synthesized disubstituted pyrazine based derivatives and evaluated for kinase inhibitory and anti-proliferative activity. From synthesized series of compounds, compound **88** showed most potent kinase inhibitory activity on B-Raf^{V600E} with IC₅₀ value of 0.74 μM and showed anti-proliferative activity with SRB based assay on WM266.4 melanoma cell lines with IC₅₀ value of 0.46 μM.⁹¹



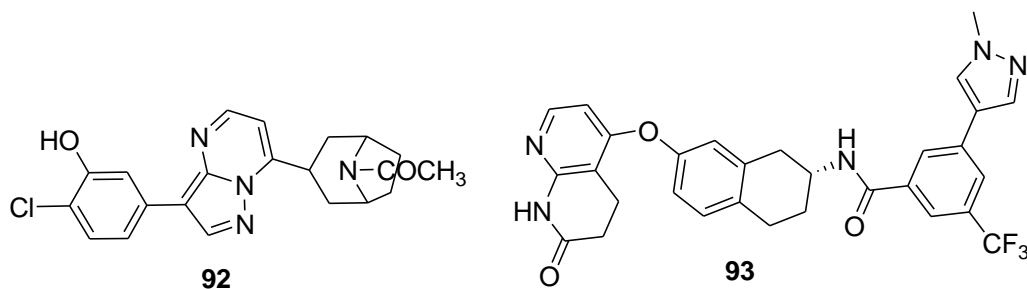
Niculescu-Duvaz et al. synthesized 2,6-disubstituted pyrazine derivatives and evaluated for kinase inhibitory activity. Among all these compounds, compound **89** showed most potent kinase inhibitory activity on B-Raf^{V600E} activity with IC₅₀ value of .31 μM.⁹²

Ren et al. synthesized and optimized furopyrimidine based scaffolds and evaluated on kinase inhibitory activity. From these synthesized compounds, compound **90** showed potent B-Raf^{V600E} activity with IC₅₀ value of 0.3 nM.⁹²



Newhouse et al. synthesized non-oxime pyrazole derivatives and screened for kinase inhibitory activity. Compound **91** showed most potent kinase inhibition on B-Raf with IC₅₀ value of 0.57 nM.⁹⁴

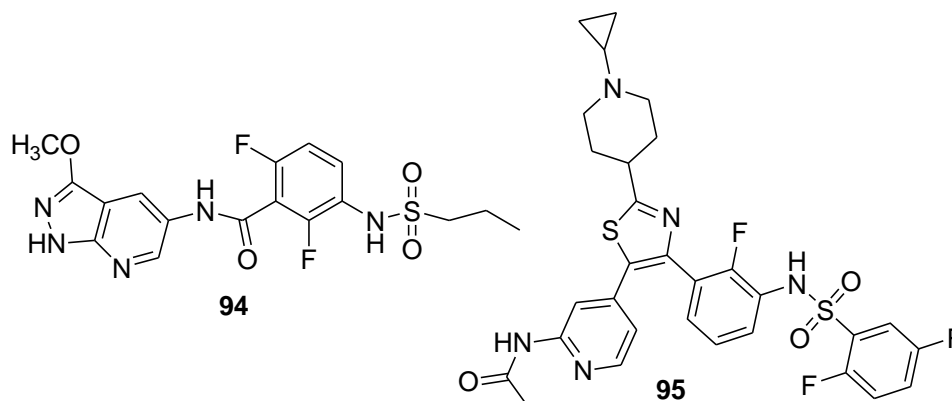
Di Grandi et al. synthesized pyrazolopyrimidine derivatives and evaluated for kinase inhibitory and anti-proliferative activity. Among all these synthesized compounds, compound **92** showed most potent kinase inhibitory activity on B-Raf with IC₅₀ value of 0.0003 μM and also showed cell growth inhibition on A375 and WM266.4 melanoma cell lines with IC₅₀ values of 0.9 μM and 0.26 μM, respectively.⁹⁵



Huang et al. synthesized tetrahydronaphthalene derivatives and evaluated for *in-vitro* and *in-vivo* activities. From all these synthesized compounds, compound **93** showed most potent kinase inhibitory activity on B-Raf^{V600E} with IC₅₀ value of 2.1 nM and also showed

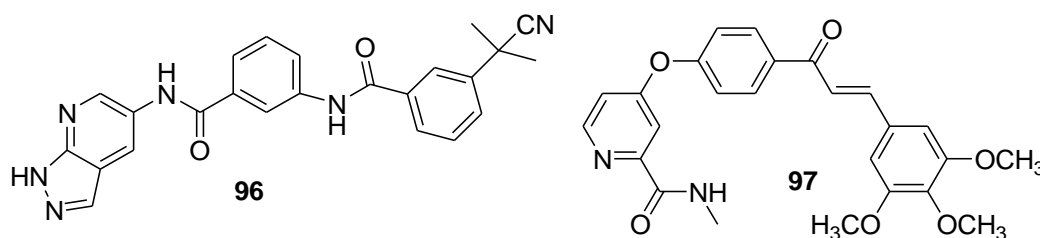
cell growth inhibition on A375 melanoma cell line with IC_{50} value of 34 nM. Compound **93** showed good pharmacodynamics and anti-tumor activity *in-vivo* and showed strong inhibition at a dose of 33 mg/kg by oral route on A375 xenograft model.⁹⁶

Ren et al. synthesized pyrazolo[1,5-*a*]pyrimidine derivatives and evaluated against kinase inhibitory activity. From all these compound; compound **94** showed most potent kinase inhibition on B-Raf with IC_{50} value of 5 nM.⁹⁷



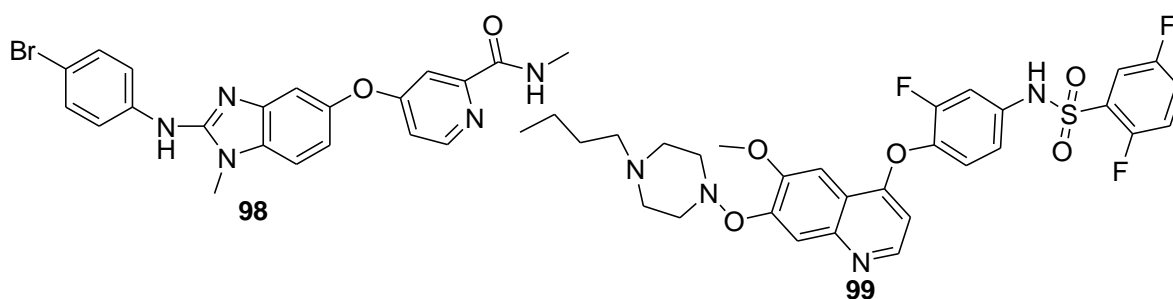
Pulici et al. synthesized diarylthiazole derivatives and evaluated for *in-vitro* and *in-vivo* activity. Among all these synthesized compounds, compound **95** showed potent kinase inhibitory activity on B-Raf^{V600E} and B-Raf^{WT} with IC_{50} values of 3.7 nM and 4.8 nM, respectively. It also showed good cell growth inhibition on various cancer cell lines with IC_{50} value includes; A375 (0.003 μM), WM115 (0.148 μM), COLO205 (0.005 μM), SW1417 (0.208 μM) and RKO (2.275 μM). *In-vivo* screening of Compound **95** demonstrated the efficacy of the compound and showed complete tumor inhibition up to 6h after a single dose of 30 mg/kg.⁹⁸

Wenglowky et al. synthesized a series of pyrazolopyrimidine derivatives and evaluated for kinase inhibitory activity. Compound **96** from designed series showed potent kinase inhibition on B-Raf with IC_{50} value of 0.9 nM.⁹⁹



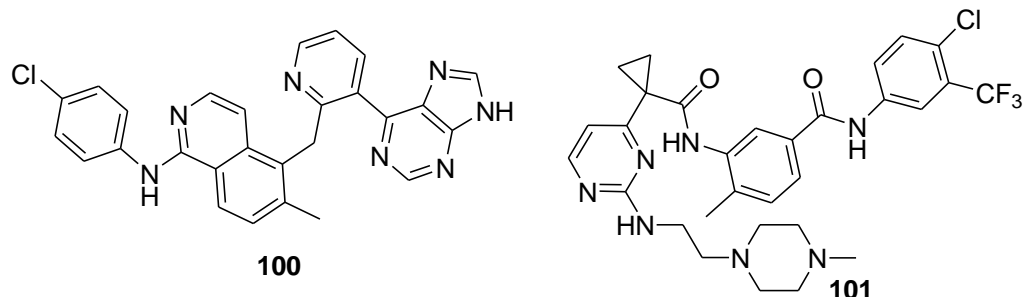
Wang et al. synthesized Sorafenib analogs and evaluated for kinase inhibition and anti-proliferative activity. Among all these synthesized compounds, compound **97** showed potent B-Raf kinase inhibition on mutated B-Raf^{V600E} enzyme with IC₅₀ value of 1.8 μM. It also showed good cell growth proliferation on A549, HepG2, MCF-7, and PC-3 cell lines with IC₅₀ values of 9.50 μM, 2.87 μM, 10.37 μM and 3.40 μM, respectively.¹⁰⁰

Ramurthy et al. designed and synthesized benzimidazole derivatives and evaluated for kinase inhibitory and anti-proliferative activity. Among all these synthesized compounds, compound **98** showed potent inhibitory activity on B-Raf^{V600E} with IC₅₀ value of 0.002 μM and showed good cell growth inhibition on melanoma cell line SK-MEL-28 with IC₅₀ value of 4.6 μM.¹⁰¹



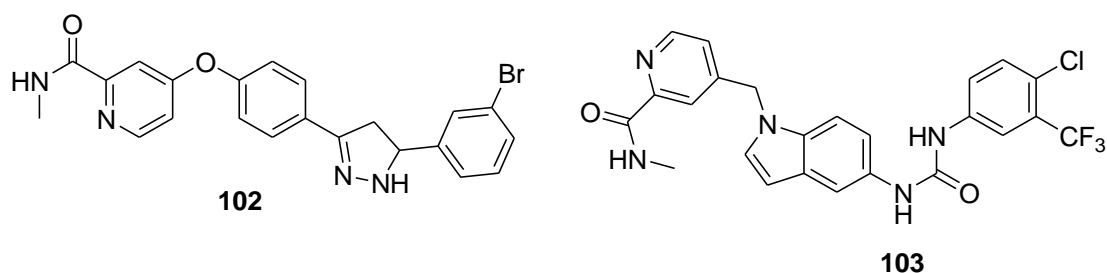
Baska et al. synthesized quinoline-based derivatives and evaluated for kinase inhibitory activity. From all these synthesized compounds, compound **99** showed most potent kinase inhibitory activity on B-Raf^{WT} and B-Raf^{V600E} with IC₅₀ values of 0.1 μM and 0.091 μM, respectively.¹⁰²

Smith et al. synthesized aminoisoquinoline derivatives and evaluated for *in-vitro* and *in-vivo* activity. From all these synthesized compounds, compound **100** showed good kinase inhibitory activity on B-Raf^{V600E} with IC₅₀ value of 1.6 nM and showed cell growth inhibition on melanoma cell line A375 with IC₅₀ value of 1.8 nM. Compound **100** also showed *in-vivo* activity to check the efficacy of the compound on the xenograft model with 85% tumor inhibition at 5mg/kg.¹⁰³



Wang et al. synthesized pyrimidine derivatives and screened for kinase selectivity and anti-proliferative activity on various cancer cell lines. Among all these synthesized compounds, compound **101** showed potent kinase selectivity on B-Raf^{WT} and B-Raf^{V600E} with IC₅₀ value of 19.7 nM and 12.6 nM, respectively. Compound **101** also showed good cell growth inhibition on various cancer cell lines with IC₅₀ value like A375 (1.07 μM), COLO-205 (1.92 μM), SK-MEL-2 (0.58 μM) and HepG2 (2.46 μM).¹⁰⁴

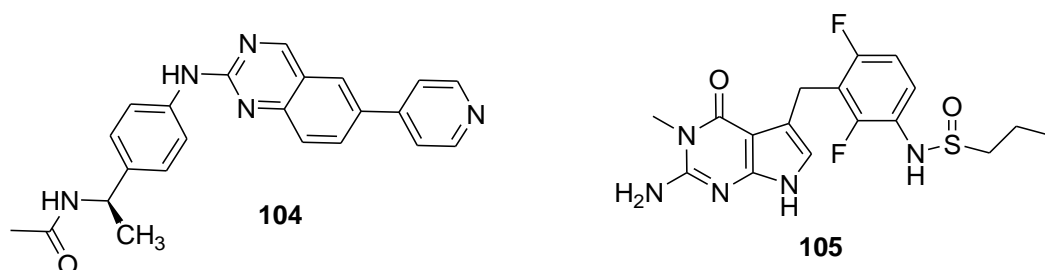
Wang et al. synthesized novel Sorafenib derivatives and screened for kinase activity and anti-proliferative activity. Among all these synthesized compounds, compound **102** showed potent kinase activity on B-Raf^{V600E} with IC₅₀ value of 3.4 μM and also showed good cell growth inhibition on various cancer cell lines with IC₅₀ values, e.g. A549 (2.84 μM), HepG2 (1.85 μM), MCF-7 (1.96 μM), and PC-3 (3.54 μM).¹⁰⁵



Wua et al. synthesized indole derivatives and screened for kinase binding activity and anti-proliferative activity. Among all synthesized compounds, compound **103** showed potent kinase activity on B-Raf^{V600E} with IC₅₀ value of 0.51 μM and also showed good cell growth inhibition on various cancer cell lines, HepG2, MDA-MB-453, and SW480 with IC₅₀ values of 6.63 μM, 21.9 μM and 13.5 μM, respectively.¹⁰⁶

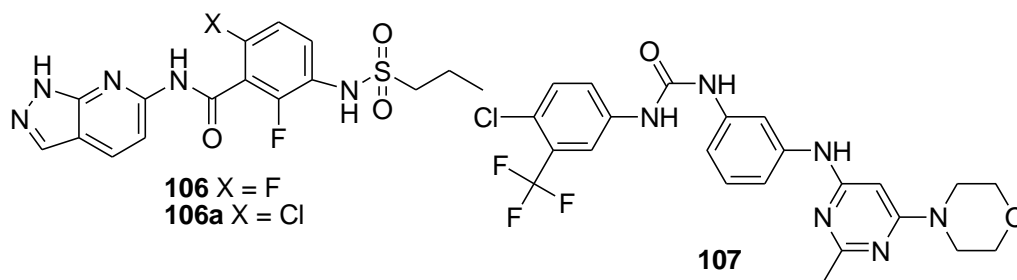
Vasbinder et al. discovered, optimized and synthesized quinazoline-based derivatives and screened for *in-vitro* and *in-vivo* activity. From the series of compounds, compound **104** showed most potent kinase inhibitory activity on B-Raf^{V600E} with IC₅₀ value of 19 nM and

also showed good cell growth inhibition on A375 melanoma cell line with IC_{50} value of 35 nM. Compound **104** was further evaluated for *in-vivo* efficacy in an A375 mutated B-Raf xenograft model and showed significant tumor growth inhibition at a dose of 25 mg/kg for 11 days.¹⁰⁷



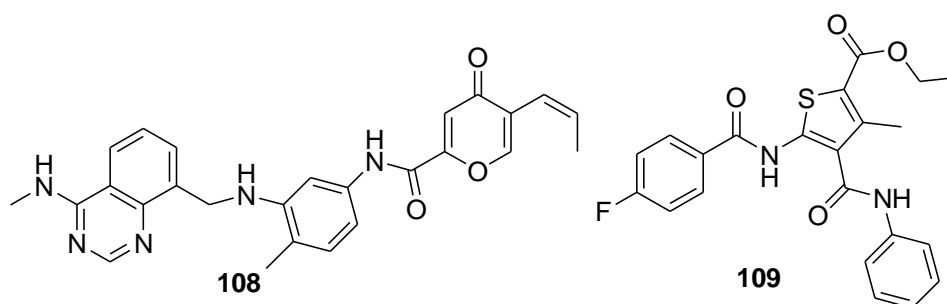
Wang et al. synthesized novel deazapurine derivatives and screened for kinase inhibitory and anti-proliferative activity. From all these synthesized compounds, compound **105** showed potent kinase inhibitory activity on B-Raf^{V600E} and B-Raf^{WT} with IC_{50} values of 0.05 μ M and 0.44 μ M, respectively and also showed good anti-proliferative activity on A375, HT-29, and COLO205 cancer cell lines with IC_{50} values of 0.80, 0.55 and 1.64 μ M, respectively.¹⁰⁸

Wenglowsky et al. designed and synthesized pyrazolopyridine derivatives and evaluated for kinase inhibitory activity, *in-vitro* and *in-vivo* activities. All these synthesized compounds, compound **106** and **106a**, showed good kinase inhibitory activity on B-Raf^{V600E} with IC_{50} values of 4.8 and 1.7 nM respectively. These two compounds also showed good cell growth inhibition on Malme-3M and A375 with IC_{50} for compound **106** (19 nM and 20 nM, respectively) and compound **106a** (150 nM and 240 nM, respectively). These two compounds also evaluated for *in-vivo* testing to check the efficacy of both the compounds on xenograft model. It was observed that compound **106** showed 76% growth inhibition at dose of 20mg/kg for 20 days, while compound **106a** showed 95% growth inhibition at dose of 11mg/kg for 17 days.¹⁰⁹



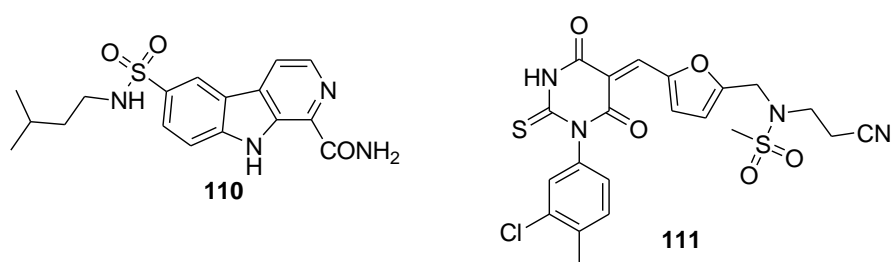
Zhang et al. synthesized 4-phenylaminopyrimidine urea derivatives and evaluated for *in-vitro* and *in-vivo* activity. Among all these synthesized compounds, compound **107** showed potent kinase inhibitory activity on B-Raf^{WT} and B-Raf^{V600E} with IC₅₀ values of 271 nM and 142 nM, respectively. This compound was also screened for *in-vivo* activity on xenograft model, and significant cell growth inhibition was observed on A549 cell line with a dose of 25 mg/kg.¹¹⁰

Lee et al. synthesized aminoquinazoline derivatives and evaluated for kinase inhibitory and anti-proliferative activity. From all these synthesized compounds, compound **108** showed good kinase inhibitory activity on B-Raf^{V600E} with IC₅₀ value of 19.5 μM and also showed cell growth inhibition on A375 and HS27 cell lines with IC₅₀ values of 0.006, and 0.230 μM, respectively.¹¹¹



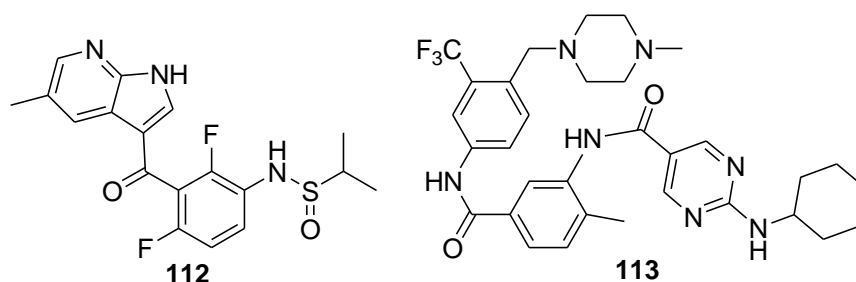
Xie et al. synthesized N-(thiophene-2-yl)benzamide derivatives and screened for kinase selectivity on B-Raf^{V600E} protein. Among all these synthesized compounds, compound **109** showed potent B-Raf^{V600E} activity with IC₅₀ value of 0.67 μM.¹¹²

Xin et al. synthesized β-carboline derivatives and evaluated against kinase binding affinity. Among all, compound **110** showed potent kinase inhibition on B-Raf^{V600E} with IC₅₀ value of 1.62 μM.¹¹³



Xu et al. performed ligand based drug design approaches against the ZINC database and evaluated against B-Raf kinase activity (V600E). Among all virtual compounds, compound **111** showed potent kinase activity on B-Raf^{V600E} enzyme with IC₅₀ value of 0.31 μM.¹¹⁴

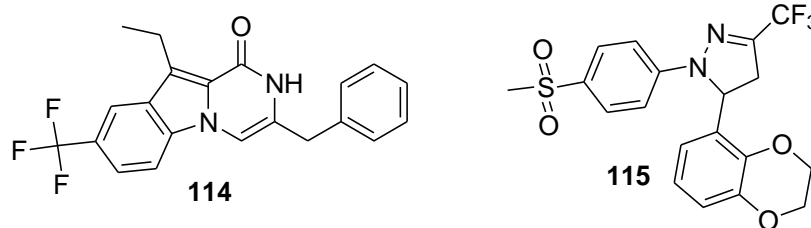
Yao et al. synthesized Vemurafenib analogs and evaluated for B-Raf kinase selectivity. Among all these compounds, compound **112** showed potent kinase selectivity on B-Raf^{WT}, and B-Raf^{V600E} with IC₅₀ values of 200 and 54 nM, respectively.¹¹⁵



Cheng et al. synthesized *1H*-pyrazolo[3,4-*b*]pyridine-5-carboxamide derivatives and evaluated for kinase inhibitory and anti-proliferative activity. From all these synthesized compounds, compound **113** showed most potent kinase inhibition on B-Raf^{V600E} with IC₅₀ value of 37 nM and also showed good cell growth inhibitory activity on melanoma cell line SK-MEL-28 with IC₅₀ value of 2.38 μM.¹¹⁶

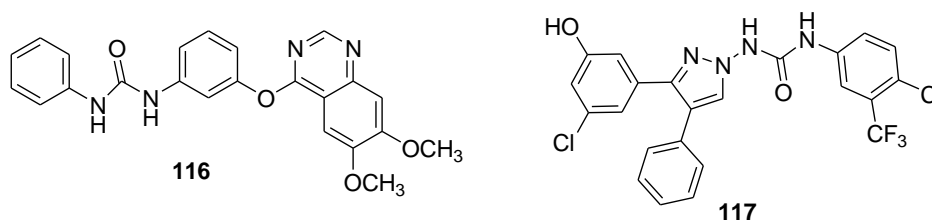
Youssif et al. synthesized novel indole-2-carboxamides and pyrazino[1,2-*a*]indol-1(2*H*)-one derivatives and evaluated for kinase activity and anti-proliferative activity on various cancer cell lines. Among all these synthesized compounds, compound **114** showed potent kinase inhibition on B-Raf^{V600E} activity with IC₅₀ value of 0.1 μM. Compound also showed good cell growth inhibition on various cancer cell lines includes PC-3 (prostate

cancer), A-549 (epithelial cancer), MCF-7 (breast cancer) and HT-29 (colon cancer) with IC_{50} values of 1.0 μM , 1.4 μM , 0.9 μM and 0.9 μM , respectively.¹¹⁷



Yu et al. synthesized pyrazoline derivatives and evaluated for kinase activity and anti-proliferative activity on cancer cell lines. Among all these synthesized compounds, compound **115** showed potent kinase inhibition on B-Raf^{V600E} activity with IC_{50} value of 0.12 μM . Compound also showed good cell growth inhibition on HeLa, and WM266.4 cell line with IC_{50} values of 25.96 μM and 0.76 μM , respectively.¹¹⁸

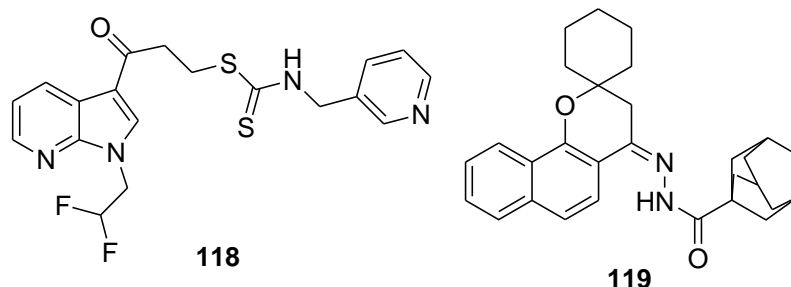
Holladay et al. synthesized 4-quinazolinyl-oxy-diaryl ureas derivatives and screened for its binding affinity and anti-proliferative activity. From all these synthesized compounds, compounds **116** showed a good binding affinity towards B-Raf^{V600E} with K_d value 370 nM and also evaluated for anti-proliferative activity on A375 melanoma cell line with IC_{50} value of 15 μM .¹¹⁹



Tarazi et al. synthesized triarylpyrazole containing amide or urea derivatives and evaluated for kinase potency. Among all these synthesized compounds, compound **117** showed selectivity and potency against B-Raf^{V600E} with IC_{50} value of 7 nM.¹²⁰

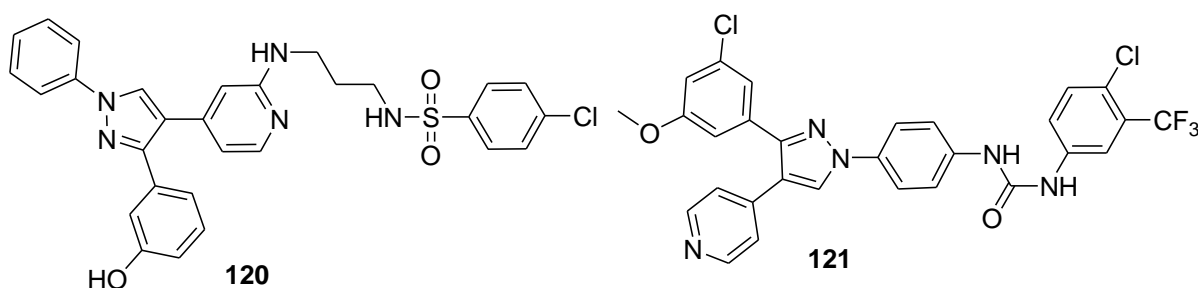
Liu et al. synthesized novel 7-azaindole derivatives and evaluated for *in-vitro* and *in-vivo* activity. From all these synthesized compounds, compound **118** showed a good B-Raf^{V600E} kinase potency and observed 41% inhibition at 10 μM and also showed good cell growth inhibition on A375 melanoma cell line with IC_{50} value 0.28 μM . Compound **118** also evaluated against *in-vivo* efficacy in A375 mutated B-Raf xenograft model and

showed significant tumor growth inhibition at a dose of 50 mg/kg for 14 consecutive days.¹²¹



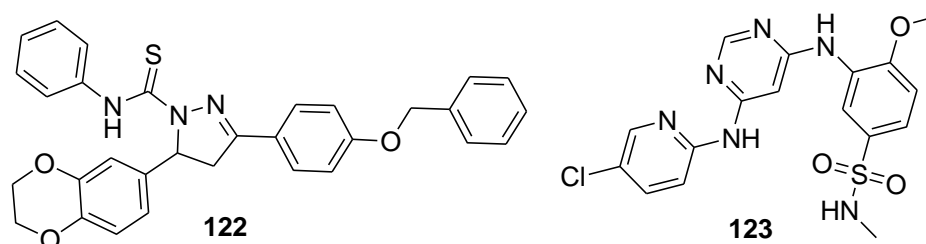
Abdelatef et al. design and synthesized novel spirobenzo[*h*]chromene and spirochromane derivatives and evaluated for kinase potency. Among all these compounds, compound **119** showed good kinase selectivity on B-Raf^{V600E} with IC₅₀ value of 2.6 μM.¹²²

Abdel-Maksoud et al. synthesized 1,3,4-triarylpyrazole derivatives and screened against kinase inhibitory activity and anti-proliferative activity. Among all these compounds, compound **120** inhibited B-Raf^{V600E} with IC₅₀ value of 1.16 μM and also showed IC₅₀ value of 4.87 μM on B-Raf^{WT}. Compound **120** also showed good cell growth inhibition on SK-MEL-5 melanoma cell line with IC₅₀ value of 1.27 μM.¹²³



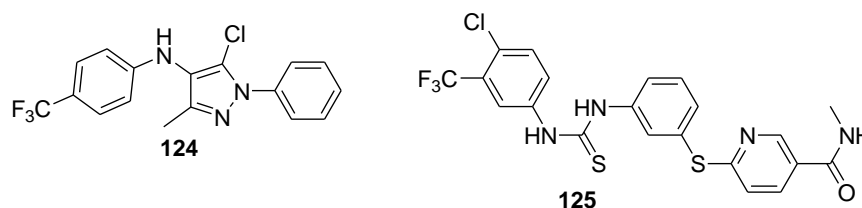
El-Gamal et al. synthesized pyrazole derivatives and evaluated for *in-vitro* kinase activity and anti-proliferative activity. Among all these synthesized compounds, compound **121** showed kinase potency on B-Raf^{V600E} with IC₅₀ value 0.39 μM. Compound **121** also screened against cell growth inhibition on various melanoma cancer cell lines with IC₅₀ value which included MALME-3M (0.53 μM), M14 (0.44 μM), MDA-MB-435 (0.43 μM), SK-MEL-2 (0.66 μM), SK-MEL-28 (0.90 μM), SK-MEL-5 (1.14 μM), UACC-257 (0.41 μM), and UACC-62 (0.36 μM).¹²⁴

Li et al. synthesized novel triarylpyrazoline derivatives and screened against kinase inhibitory activity and anti-proliferative activity. Among all these synthesized compounds, compound **122** showed B-Raf^{V600E} and B-Raf^{WT} kinase inhibition with IC₅₀ values of 0.01 μM and 5.23 μM, respectively. Compound **122** also showed cell growth inhibition on melanoma cell lines like A375, WM2664, and WM1361 with IC₅₀ values of 0.35 μM, 0.42 μM, and 8.23 μM, respectively.¹²⁵



Philp et al. synthesized 4,6-diaminopyrimidine derivatives and evaluated against kinase selectivity. Among all these synthesized compounds, compound **123** showed potent B-Raf^{V600E} activity with IC₅₀ value of 20 nM.¹²⁶

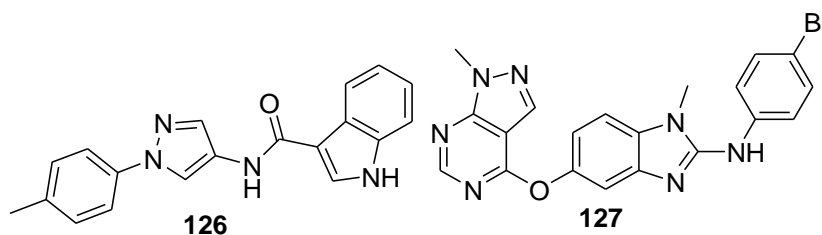
Ruan et al. synthesized novel 1*H*-pyrazol derivatives and evaluated against kinase selectivity and anti-proliferative activity. Among all synthesized compounds, compound **124** showed potent B-Raf^{V600E} kinase activity with IC₅₀ value 0.066 μM and also showed good cell growth inhibition on A375 melanoma cell line with IC₅₀ value 0.81 μM.¹²⁷



Sun et al. synthesized nicotinamide derivatives and screened against kinase binding affinity. Among all these compounds, **125** showed potent kinase selectivity on B-Raf^{WT} and B-Raf^{V600E} with IC₅₀ values of 17 and 16 nM, respectively.¹²⁸

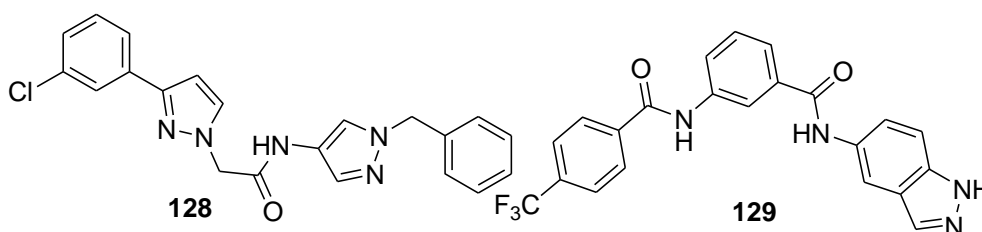
Wang et al. synthesized pyrazole derivatives and evaluated for selective kinase activity and anti-proliferative activity. Among all these synthesized compounds, compound **126** showed potent kinase inhibition on B-Raf^{V600E} with IC₅₀ value of 0.1 μM and effectiveness on B-Raf^{WT} with IC₅₀ value of 0.92 μM. Compound also showed cell

growth inhibition on A375 and WM-1361 melanoma cell lines with IC_{50} values of 0.93 μ M and 10.02 μ M, respectively.¹²⁹



Wang et al. synthesized pyrazolo[3,4-*d*]pyrimidine derivatives and evaluated against kinase inhibitory activity and anti-proliferative activity. Among all these synthesized compounds, compound **127** showed potent B-Raf^{V600E} kinase inhibition with IC_{50} value of 40.9 nM and also showed good cell growth inhibition on A375 melanoma cell line with IC_{50} value of 30.25 μ M.¹³⁰

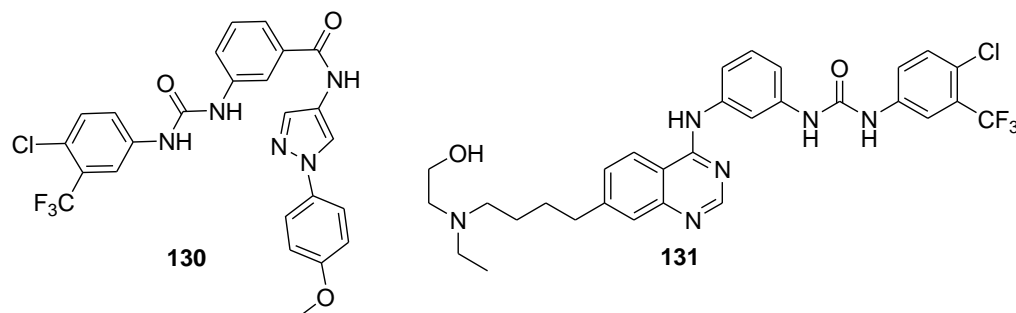
Wang et al. synthesized pyrazole derivatives and tested against kinase and cell proliferative activity. Among all, compound **128** showed potent kinase inhibition on B-Raf^{V600E} with IC_{50} value of 0.10 μ M and good cell growth proliferation on A375 melanoma cell line with IC_{50} value of 0.96 μ M.¹³¹



Wang et al. design and synthesized different indole and indazole derivatives and screened for binding affinity on kinase and cell growth proliferative activity. Among all these synthesized compounds, compound **129** showed potent B-Raf^{V600E} kinase activity with IC_{50} value of 0.18 μ M and also showed good cell growth inhibition on A375 and WM-1361 melanoma cell lines with IC_{50} values of 1.97 μ M and 12.75 μ M, respectively.¹³²

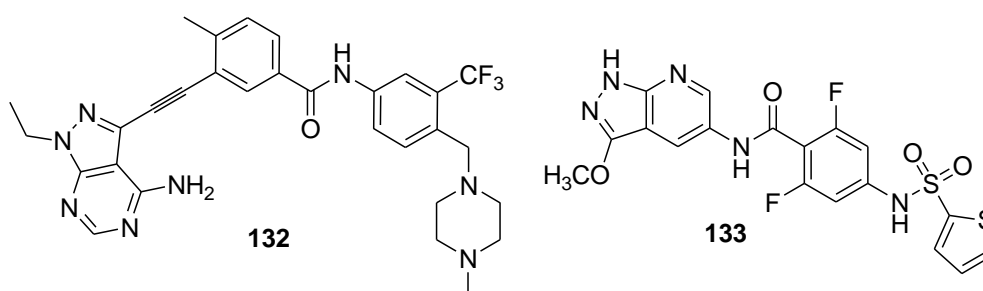
Wang et al. synthesized pyrazole derivatives and evaluated against selective kinase activity and anti-proliferative activity. Among all these synthesized compounds, compound **130** showed potent kinase inhibition on B-Raf^{V600E} with IC_{50} value of 0.035 μ M and effectiveness on B-Raf^{WT} with IC_{50} value of 0.22 μ M. Compound also showed

cell growth inhibition on A375 and WM-1361 melanoma cell lines with IC_{50} values of 0.39 μM and 7.12 μM , respectively.¹³³



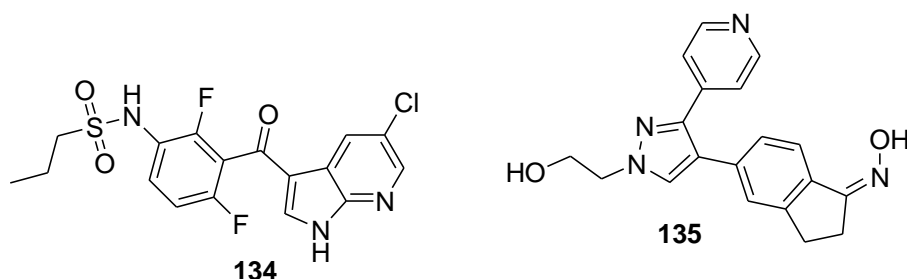
Zhang et al. synthesized 4-aminoquinazoline derivatives and evaluated for kinase selectivity. Among all these synthesized compounds, compound **131** showed potent kinase selectivity on B-Raf^{WT}, and B-Raf^{V600E} with IC_{50} value of 22 and 13 nM, respectively.¹³⁴

Zhang et al. synthesized *1H*-pyrazolo[3,4-*d*]pyrimidin derivatives and evaluated for *in-vitro* and *in-vitro* study. Among all these synthesized compounds, compound **132** showed potent selective kinase affinity on B-Raf^{WT}, and B-Raf^{V600E} enzyme with IC_{50} values of 0.092 μM and 0.015 μM , respectively. Compound **132** also showed good cell growth inhibition on various cancer cell lines panel with wide range of IC_{50} values, like breast cancer cell line panel (IC_{50} range 0.005-7.25 μM), lymphadenoma cancer cell line panel (IC_{50} range 2.16-10 μM), myeloma cell line (IC_{50} value of 0.872 μM), leukemia cell line (IC_{50} value of 5.11 μM), glioblastoma cell line (IC_{50} value of 0.742 μM), hepatocarcinoma (IC_{50} value of 8.672 μM), cervical cancer cell line (IC_{50} value of 5.410 μM), lung cancer cell line (IC_{50} value of 1.665 μM), melanoma cancer cell line (IC_{50} value of 1.908 μM), and pancreatic cancer cell line (IC_{50} value of 6.556 μM). Eventually, compound **132** showed good *in-vivo* study results on MDA-MB-231 induced xenograft model on mice. Three different doses of compound **132** with 7.5, 15, and 30 $\text{mg kg}^{-1} \text{d}^{-1}$ once a day were given orally, for 18 days. Results showed that at the dose of 30 $\text{mg kg}^{-1} \text{d}^{-1}$, the tumor growth regression was completely stopped without any obvious toxicity.¹³⁵



Wenglowsky et al. synthesized pyrazolopyridine derivatives and screened for kinase binding affinity. Among all these synthesized compounds, compound **133** showed potent kinase affinity on B-Raf^{V600E} with IC₅₀ value of 0.2 nM.¹³⁶

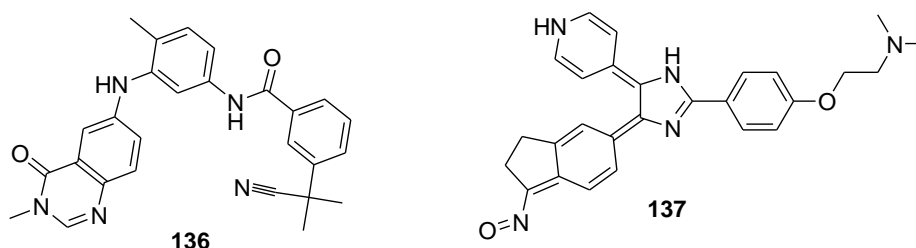
Compound PLX-4720 **134** was potent and selective azaindole derivative which inhibited B-Raf^{V600E} with IC₅₀ value of 13 nM and showed IC₅₀ value of 160 nM on B-Raf^{WT} kinase inhibitory assay. It showed 10-fold selectivity for B-Raf^{V600E} than B-Raf^{WT}. It showed tumor cell growth inhibition on various cell lines containing B-Raf^{V600E} enzyme such as COLO205 (IC₅₀ = 0.31 μM), A375 (IC₅₀ = 0.50 μM), WM2664 (IC₅₀ = 1.5 μM) and COLO829 (IC₅₀ = 1.7 μM). Subsequently, at 1 μM concentration, it showed the induction of cell cycle arrest, and apoptosis was obtained in B-Raf^{V600E} cells, but there was no prominent cell cycle arrest in B-Raf^{WT}. In preclinical stages, compound **134** was administered to mice with the dose of 20 mg/kg/day via the oral route which resulted in significant tumor growth delay. Regressions in B-Raf^{V600E} dependent COLO205 tumor xenograft was observed without any serious adverse effect even at the dose of 1g/kg. It also showed more than 90% tumor growth inhibition at 30 mg/kg/day on 8505c xenograft model.¹³⁷



Compound GDC-0879 **135** was pyrazole-pyridine derivative and selective B-Raf inhibitor with having IC₅₀ 0.1 nM in A375 melanoma cell line. It also inhibited cellular pERK with IC₅₀ value of 63 nM. It showed tumor cell growth inhibitions on melanoma

cell line A375 bearing B-Raf^{V600E} mutant with IC₅₀ value of 59 nM for pMEK1 inhibition. This compound potently inhibited B-Raf^{V600E} in Malme3M cells with IC₅₀ value of 0.75 μM.¹³⁸

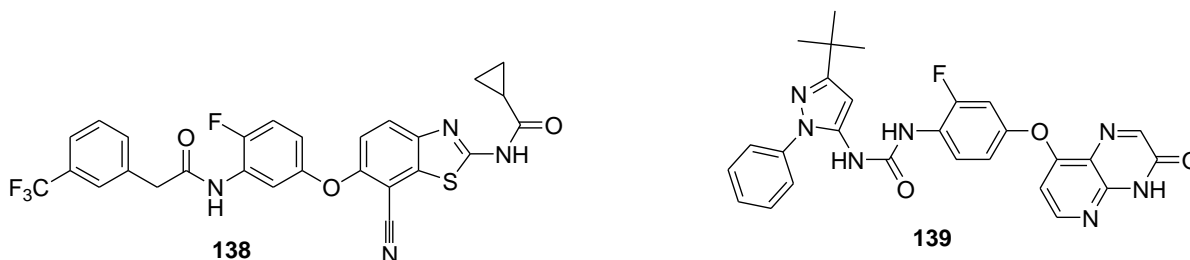
Compound AZ628 **136** was quinazolinone derivatives and showed potent kinase inhibitory activity on B-Raf^{WT} and B-Raf^{V600E} with IC₅₀ values of 105 nM and 34 nM, respectively. Compound **136** also showed good tumor cell growth inhibition on melanoma cell line with IC₅₀ value of 10 μM, as compared with 0.1 μM for the M14 parental cell line.^{139,140}



Compound SB590885 **137** was imidazole-based derivative and evaluated for kinase inhibitory activity and screened for anti-proliferative activity. Compound **137** showed potent B-Raf^{V600E} with IC₅₀ value 0.3 nM. Compound **137** showed good anti-proliferative activity on A375, MALME-3M and SK-MEL-28 melanoma cell lines with the IC₅₀ values 0.37 μM, 0.15 μM and 0.12 μM, respectively. In preclinical stages, compound **137** showed good *in-vivo* activity in mice with induction of cancer by A375 melanoma cell line and showed inhibition of tumor growth by around 80% at the dose of 50mg/kg when given by IV route.^{141,142}

Compound TAK-632 **138** was 1,3 benzothiazole derivative which showed good kinase inhibitory activity on B-Raf^{WT} and B-Raf^{V600E} with IC₅₀ values of 8.3 nM and 2.4 nM, respectively. Compound **138** also showed good anti-proliferative activity on various melanoma cell lines like A375 (B-Raf^{V600E}), HT-144 (B-Raf^{V600E}), MALME-3M (B-Raf^{V600E}), CHL-1(B-Raf^{WT}), HMCB (B-Raf^{WT}), SK-MEL-2 (B-Raf^{WT}), HMVII (B-Raf^{G469V}) with IC₅₀ values of 160 nM, 110 nM, 50 nM, 2.07 μM, 350 nM, 60 nM and 200 nM, respectively. In preclinical stages, compound **138** showed the decreased in tumor growth in human melanoma A375 cells bearing in F344 nude rats. At a dose of 9.7 mg/kg

and 24.1 mg/kg, it showed significant tumor growth inhibition with %T/C by -2.1 and -12.1, respectively.¹⁴³



Compound CCT196969 **139** was dihydropyridopyrazine derivative and showed good kinase inhibitory activity on wild-type as well as mutated B-Raf with IC₅₀ values of 0.1 μM and 0.04 μM, respectively. It was active against melanoma cell line (A375) with IC₅₀ value of 12 μM. In preclinical studies, compound **139** showed exceptionally well tolerated at the doses and did not produce any significant side effect at the dose of 10 mg/kg/day (data not shown). Compound **139** accomplished plasma disclosure of 40 μM in nude mice.¹⁴⁴

2.2 Clinical Trial Data

All drugs, regardless of disease, have to be extensively and carefully tested before the FDA approves them for regular use in humans. Clinical trial data give an idea about the effectiveness, safety, and efficacy of small molecules on the human subjects in the treatment of the disease and/or disorders. During clinical trial studies, small molecules passed through the four different phases of the clinical trials concerning the particular disease.

Clinical trials for cancer are quite different as compared to other clinical trials. Generally in the oncogenic clinical trials, study is carried out in combination of one or more chemotherapeutic drugs due to the problem of resistance. B-Raf kinase has investigating potential, specifically for the treatment of melanoma, thyroid, colorectal and ovarian cancer, along with other types of the tumor. Currently, there are two selective B-Raf inhibitors available in the market viz. Vemurafenib and Dabrafenib. These two drugs are generally not used alone for the treatment of cancer but used with a combination of other MEK inhibitors.

Here, we have compiled preliminary data of all four phases of clinical trials for small molecules active on B-Raf; B-Raf macromolecule inhibitors (vaccines/monoclonal antibody) and combination of B-Raf inhibitors at different clinical trial stages. All data are accounted in **Table 7** showed clinical trial studies of drug/molecule or combination of two molecules and their status as active but not recruiting. **Table 8** provided information about clinical trial studies of drug/molecule or combination of two or more molecules as inhibitors of B-Raf^{V600E} mutation with their date of completion.¹⁴⁵

Table 7. Clinical Trial Studies of Drug/Molecule or Combination of Two Molecules and Their Status; Active But Not Recruiting

Drug	Combination	Clinical trial NCT No.	Description	Starting Date	Sponsors
Phase- IV					
Nivolumab	-	NCT02626065	Immune Modulation Study in Patients With Metastatic Melanoma Treated With Anti-PD1 Monoclonal Antibodies	April 2015	Hospices Civils de Lyon
ZelboRaf (Vemurafenib)	-	NCT01898585	An Open-Label Study of ZelboRaf (Vemurafenib) in Patients With B-Raf ^{V600} Mutation Positive Metastatic Melanoma	October 2013	Hoffmann-La Roche
Vemurafenib	-	NCT01739764	An Extension (Rollover) Study of Vemurafenib in Participants With BRAF V600 Mutation-Positive Malignancies Previously Enrolled in an Antecedent Vemurafenib Protocol	February 2013	Hoffmann-La Roche
Phase-III					
Vemurafenib	Placebo	NCT01667419	A Study of Vemurafenib Adjuvant Therapy in Participants With Surgically Resected Cutaneous BRAF-Mutant Melanoma	September 2012	Hoffmann-La Roche
Dabrafenib	1) Dabrafenib + Trametinib 2) Trametinib	NCT01584648	A Study Comparing Trametinib and Dabrafenib Combination Therapy to Dabrafenib Monotherapy in Subjects With BRAF-mutant Melanoma	May 2012	Novartis
Dabrafenib	Trametinib	NCT01682083	Dabrafenib With Trametinib in the Adjuvant Treatment of High-risk BRAF V600 Mutation-positive Melanoma (COMBI-AD). (COMBI-	January 2013	Novartis

Encorafenib Binimetinib Cetuximab Irinotecan Folinic Acid 5-Fluorouracil	-	NCT02928224	AD) Study of Encorafenib + Cetuximab Plus or Minus Binimetinib vs. Irinotecan/Cetuximab or Infusional 5-Fluorouracil (5-FU)/Folinic Acid (FA)/Irinotecan (FOLFIRI)/Cetuximab With a Safety Lead-in of Encorafenib + Binimetinib + Cetuximab in Patients With BRAF V600E-mutant Metastatic Colorectal Cancer (BEACON CRC)	August 2016	Array BioPharma
Dabrafenib Vemurafenib	Trametinib	NCT01597908	Dabrafenib Plus Trametinib vs Vemurafenib Alone in Unresectable or Metastatic BRAF V600E/K Cutaneous Melanoma	June 2012	Novartis Pharmaceuticals
Vemurafenib	Cobimetinib (GDC-0973)	NCT01689519	A Study Comparing Vemurafenib Versus Vemurafenib Plus Cobimetinib in Participants With Metastatic Melanoma	January 2013	Hoffmann-La Roche
Vemurafenib	LGX818 MEK162	NCT01909453	Study Comparing Combination of LGX818 Plus MEK162 Versus Vemurafenib and LGX818 Monotherapy in BRAF Mutant Melanoma	September 2013	Array BioPharma

Phase-II

LGX818	MEK162 LEE011	NCT01543698	A Phase Ib/II Study of LGX818 in Combination With MEK162 in Adult Patients With BRAF Dependent Advanced Solid Tumors	May 2012	Array BioPharma
Vemurafenib	Cetuximab Irinotecan HCl	NCT02164916	S1406 Phase II Study of Irinotecan and Cetuximab With or Without Vemurafenib in BRAF Mutant Metastatic Colorectal Cancer	November 2014	Southwest Oncology Group

Vemurafenib	-	NCT01711632	BRAF Inhibitor, Vemurafenib, in Patients With Relapsed or Refractory Hairy Cell Leukemia		Memorial Sloan Kettering Cancer Center
Dabrafenib	Trametinib Panitumumab 5-fluorouracil	NCT01750918	BRAF/MEK/EGFR Inhibitor Combination Study in Colorectal Cancer (CRC)	December 2012	Novartis
Dabrafenib	Trametinib	NCT01972347	Neoadjuvant Dabrafenib + Trametinib for AJCC Stage IIIB-C BRAF ^{V600} Mutation Positive Melanoma	October 2014	Melanoma Institute Australia
Dabrafenib	Trametinib	NCT02083354	Study to Investigate the Objective Response Rate of Dabrafenib in Combination With Trametinib in Subjects With BRAF ^{V600} Mutation-Positive Melanoma	March 2014	Novartis
MEK162	-	NCT01320085	A Phase II Study of Single Agent MEK162 in Patients With Advanced Melanoma	March 2011	Array BioPharma
Dabrafenib	Trametinib	NCT02034110	Efficacy and Safety of the Combination Therapy of Dabrafenib and Trametinib in Subjects With BRAF V600E- Mutated Rare Cancers	March 2014	Novartis
-	Panitumumab Irinotecan Folinic acid 5-FU	NCT03142516	FOLFIRI + Panitumumab First-line Treatment in Elderly Patients With Unresectable Metastatic Colorectal Cancer, RAS/BRAF Wild-type and Good Performance Status (OPALO)	October 2017	Grupo Espanol Multidisciplinario del Cancer Digestivo
Dabrafenib	Trametinib	NCT01336634	Study of Selective BRAF Kinase Inhibitor Dabrafenib Monotherapy Twice Daily and in Combination With Dabrafenib Twice Daily and Trametinib Once Daily in Combination	June 2011	Novartis

			Therapy in Subjects With BRAF V600E Mutation Positive Metastatic (Stage IV) Non-small Cell Lung Cancer.		
Trametinib	-	NCT02296112	Trametinib in Treating Patients With Advanced Melanoma With BRAF Non-V600 Mutations	January 2015	Vanderbilt-Ingram Cancer Center
MEK162	-	NCT02094872	Molecularly Targeted Therapy in Treating Patients With BRAF Wild-type Melanoma That is Metastatic	May 2014	Yale University
Vemurafenib	Cobimetinib	NCT02768207	A Study to Detect V-Raf Murine Sarcoma Viral Oncogene Homolog B1 (BRAF) V600 Mutation on Cell-Free Deoxyribonucleic Acid (cfDNA) From Plasma in Participants With Advanced Melanoma	May 2016	Hoffmann-La Roche
-	LGX818 MEK162 LEE011 BGJ398 BKM120 INC280	NCT02159066	LGX818 and MEK162 in Combination With a Third Agent (BKM120, LEE011, BGJ398 or INC280) in Advanced BRAF Melanoma (LOGIC-2)	July 2014	Array BioPharma
-	Cetuximab Irinotecan	NCT02296203	Cetuximab Rechallenge in Irinotecan-pretreated mCRC, KRAS, NRAS and BRAF Wild-type Treated in 1st Line With Anti-EGFR Therapy	October 2014	Gruppo Oncologico del Nord-Ovest
Vemurafenib	Cobimetinib	NCT02768207	A Study to Detect V-Raf Murine Sarcoma Viral Oncogene Homolog B1 (BRAF) V600 Mutation on Cell-Free Deoxyribonucleic Acid (cfDNA) From Plasma in Participants With Advanced Melanoma	May 2016	Hoffmann-La Roche

-	LGX818 Cetuximab BYL719	NCT01719380	Study of LGX818 and Cetuximab or LGX818, BYL719, and Cetuximab in BRAF Mutant Metastatic Colorectal Cancer	November 2012	Array BioPharma
Dabrafenib	APR-246	NCT03391050	A Study of APR-246 in Combination With Dabrafenib in Resistant Patients With BRAF V600 Mutant Melanoma	January 2018	Aprea Therapeutics AB
Vemurafenib	Cobimetinib	NCT02537600	Vemurafenib and Cobimetinib Combination in BRAF Mutated Melanoma With Brain Metastasis (CONVERCE)	December 2015	Center Eugene Marquis
PLX8934	-	NCT02428712	A Study of PLX8394 as a Single Agent in Patients With Advanced Unresectable Solid Tumors	April 2015	Plexxikon
Dabrafenib	Trametinib	NCT01723202	Dabrafenib With or Without Trametinib in Treating Patients With Recurrent Thyroid Cancer	November 2012	Manisha Shah
AZD6244	Docetaxel	NCT01256359	Docetaxel With or Without AZD6244 in Melanoma (DOC-MEK)	October 2010	University of Oxford
-	Cetuximab Irinotecan Oxaliplatin Folinic Acid Calcium Carbonate	NCT01867697	Nordic 8 - A Phase II Trial	May 2012	Per Pfeiffer
Dasatinib	-	NCT01876212	Dendritic Cell Vaccines + Dasatinib for Metastatic Melanoma	May 2014	Walter J. Storkus
Vemurafenib	-	NCT01709292	Vemurafenib Neoadjuvant Trial in Locally Advanced Thyroid Cancer	November 2012	M.D. Anderson Cancer Center

Phase-I

Dabrafenib	Trametinib	NCT02027961	Phase 1 Safety and Tolerability of MEDI4736 in Combination With Dabrafenib and Trametinib or With Trametinib Alone	December 2013	MedImmune LLC
LGX818	MEK818	NCT01543698	A Phase Ib/II Study of LGX818 in Combination With MEK162 in Adult Patients With BRAF Dependent Advanced Solid Tumors	May 2012	Array BioPharma
Vemurafenib	XL888	NCT01657591	Study of XL888 With Vemurafenib for Patients With Unresectable BRAF Mutated Stage III/IV Melanoma	July 2012	H. Lee Moffitt Cancer Center and Research Institute
Vemurafenib	Sorafenib Crizotinib	NCT01531361	Vemurafenib With Sorafenib Tosylate or Crizotinib in Treating Patients With Advanced Malignancies With BRAF Mutations	February 2012	M.D. Anderson Cancer Center
LGX818	-	NCT01436656	A Phase I Study of Oral LGX818 in Adult Patients With Advanced or Metastatic BRAF Mutant Melanoma	September 2011	Array BioPharma
Vemurafenib	Everolimus Temsirrolimus	NCT01596140	Vemurafenib in Combination With Everolimus or Temsirolimus With Advanced Cancer	December 2012	M.D. Anderson Cancer Center
Dabrafenib	Onalespib Trametinib	NCT02097225	Onalespib, Dabrafenib, and Trametinib in Treating Patients With BRAF-Mutant Melanoma or Solid Tumors That Are Metastatic or Cannot Be Removed by Surgery	May 2014	National Cancer Institute (NCI)
Dabrafenib	Lapatinib	NCT01947023	Dabrafenib and Lapatinib Ditosylate in Treating Patients With Refractory Thyroid Cancer That Cannot Be Removed by Surgery	August 2013	National Cancer Institute (NCI)
LGX818	Cetuximab BYL719	NCT01719380	Study of LGX818 and Cetuximab or LGX818, BYL719, and Cetuximab in BRAF Mutant	November 2012	Array BioPharma

Dabrafenib	APR-246	NCT03391050	Metastatic Colorectal Cancer A Study of APR-246 in Combination With Dabrafenib in Resistant Patients With BRAF V600 Mutant Melanoma	January 2018	Aprea Therapeutics AB
Ipilimumab	Dabrafenib Trametinib Nivolumab	NCT01940809	Ipilimumab With or Without Dabrafenib, Trametinib, and/or Nivolumab in Treating Patients With Melanoma That Is Metastatic or Cannot Be Removed by Surgery	August 2013	National Cancer Institute (NCI)
Vemurafenib	Cobimetinib XL888	NCT02721459	XL888 + Vemurafenib + Cobimetinib for Unresectable BRAF Mutated Stage III/IV Melanoma	August 2016	H. Lee Moffitt Cancer Center and Research Institute
Vemurafenib	Cetuximab Irinotecan	NCT01787500	Vemurafenib, Cetuximab, and Irinotecan in Advanced Solid Cancers	February 2013	M.D. Anderson Cancer Center
Trametinib	5-FU	NCT01740648	A Phase I Trial of MEK Inhibitor Trametinib in Combination With Neoadjuvant 5-Fluorouracil Chemoradiation in the Treatment of KRAS, BRAF, and NRAS-MUTANT Rectal Cancers	November 2012	Terence Williams
Cobimetinib	-	NCT03178851	A Phase Ib Study Evaluating Cobimetinib Plus Atezolizumab in Patients With Advanced BRAF V600 Wild-Type Melanoma Who Have Progressed During or After Treatment With Anti-PD-1 Therapy and Atezolizumab Monotherapy in Patients With Previously Untreated Advanced BRAF V600 Wild-Type Melanoma	June 2017	Hoffmann-La Roche
Vemurafenib	Cobimetinib	NCT01876641	Treatment of a Resistant Disease Using	October	University of

	Decitabine		Decitabine Combined With Vemurafenib Plus Cobimetinib (ML28604)	2013	Iowa
Vemurafenib	LY3022855 Cobimetinib	NCT03101254	LY3022855 With BRAF/MEK Inhibition in Patients With Melanoma	June 2017	Dana-Farber Cancer Institute
ASN003	-	NCT02961283	Study of ASN003 in Subjects With Advanced Solid Tumors	October 2016	Asana BioSciences

Table 8. Clinical Trial Studies of Drug/Molecule or Combination of Two or More Molecules as Inhibitors of B-Raf^{V600E} Mutation with Their Year of Starting and Completion

Drug	Combination	Clinical trial NCT no.	Description	Sponsors	Year of Starting	Year of Completion
Phase-III						
GSK2118436	Dacarbazine	NCT01227889	A Study Comparing GSK2118436 to Dacarbazine (DTIC) in Previously Untreated Subjects With BRAF Mutation Positive Advanced (Stage III) or Metastatic (Stage IV) Melanoma	GlaxoSmithKline	December 2010	September 2016
Vemurafenib	Dacarbazine	NCT01006980	A Study of Vemurafenib (RO5185426) in Comparison With Dacarbazine in Previously Untreated Patients With Metastatic Melanoma (BRIM 3)	Hoffmann-La Roche	January 2010	July 2015
GSK1120212	Chemotherapy	NCT01245062	GSK1120212 vs Chemotherapy in Advanced or Metastatic BRAF ^{V600E/K} Mutation-positive Melanoma	GlaxoSmithKline	November 2010	December 2016
-	Fluorouracil Irinotecan hydrochloride Leucovorin calcium Oxaliplatin	NCT00975897	Study of Tumor Tissue Testing in Selecting Treatment for Patients With Metastatic or Locally Advanced Colorectal Cancer	Medical Research Council	July 2009	December 2012
Phase-II						
AZD6244	Dacarbazine	NCT00936221	Comparison of AZD6244 in Combination With Dacarbazine Versus (vs) Dacarbazine Alone in BRAF Mutation Positive Melanoma Patients	AstraZeneca	July 2009	November 2014
Vemurafenib	Fotemustine	NCT01983124	Vemurafenib + Fotemustine to Treat	Paola Queirolo	February	September

			Advanced Melanoma Patients With B-Raf ^{V600} Mutation Recurred While on Vemurafenib (BeyPro1)		2013	2015
GSK1120212	-	NCT01037127	Study to Determine the Effectiveness of GSK1120212 in BRAF Mutation-positive Melanoma Previously Treated With or Without a BRAF Inhibitor	GlaxoSmithKline	November 2009	January 2013
Vemurafenib	-	NCT01781026	Phase 2 Study of Neoadjuvant Vemurafenib in Melanoma Patients With Untreated Brain Metastases	Yale University	April 2013	June 2014
GSK2118436	-	NCT01266967	A Study of GSK2118436 in BRAF Mutant Metastatic Melanoma to the Brain (Break MB)	GlaxoSmithKline	February 2011	November 2012
Dabrafenib	Trametinib	NCT02281760	Dabrafenib and Trametinib in People With BRAF V600E Mutation Positive Lesions in Erdheim Chester Disease	National Human Genome Research Institute (NHGRI)	November 2014	August 2018
Dabrafenib	Trametinib	NCT01726738	LCCC 1128: Open Label Phase II Trial of the BRAF Inhibitor (Dabrafenib) and the MEK Inhibitor (Trametinib) in Unresectable Stage III and Stage IV BRAF Mutant Melanoma; Correlation of Resistance With the Kinome and Functional Mutations	UNC Lineberger Comprehensive Cancer Center	October 2012	September 2018
FOLFOXIRI	Panitumumab	NCT01358812	FOLFOXIRI Plus Panitumumab In Kras and Braf Wild-Type Metastatic Colorectal Cancer (TRIP)	Gruppo Oncologico del Nord-Ovest	March 2010	October 2011
Dabrafenib	Trametinib	NCT02296996	Dabrafenib and Trametinib for BRAF-	Universitair	October	December

			inhibitor Pretreated Patients	Ziekenhuis Brussel	2014	2017
LGX818	-	NCT01894672	BRAF Inhibitor, LGX818, Utilizing a Pulsatile Schedule in Patients With Stage IV or Unresectable Stage III Melanoma Characterized by a BRAFV600 Mutation	Memorial Sloan Kettering Cancer Center	July 2013	March 2016
Dabrafenib	Trametinib	NCT01928940	Japan Ph-I/II of GSK2118436 and GSK1120212 Combination in Subjects With BRAF ^{V600E} /K Mutation Positive Advanced Solid Tumors (Phase I Part) or Cutaneous Melanoma (Phase II Part)	GlaxoSmithKline	August 2013	July 2016
Vemurafenib	Ipilimumab	NCT01673854	Phase II Safety Study of Vemurafenib Followed by Ipilimumab in Subjects With V600 BRAF Mutated Advanced Melanoma	Bristol-Myers Squibb	September 2012	May 2015
GSK2118436	-	NCT01153763	A Study of GSK2118436 in BRAF Mutant Metastatic Melanoma	GlaxoSmithKline	August 2010	June 2016
GSK2118436	GSK1120212	NCT01619774	An Open-Label Phase II Study of the Combination of GSK2118436 and GSK1120212 in Patients With Metastatic Melanoma Which is Refractory or Resistant to BRAF Inhibitor	M.D. Anderson Cancer Center	September 2012	August 2015
Selumetinib	-	NCT00866177	MEK Inhibitor AZD6244 in Treating Patients With Stage III or Stage IV Melanoma	National Cancer Institute (NCI)	March 2009	September 2013
Bevacizumab Cetuximab	Fluorouracil/ Leucovorin /Oxaliplatin	NCT01640444	Influence of BRAF and PIK3K Status on the Efficacy of 5-Fluorouracil/Leucovorin/Oxaliplatin	Spanish Cooperative Group for the	July 2012	November 2018

	(FOLFIRI)		(FOLFIRI) Plus Bevacizumab or Cetuximab in Patients With RAS Wild-type Metastatic Colorectal Carcinoma and < 3 Circulating Tumor Cells (CTC) (VISNU-2)	Treatment of Digestive Tumours (TTD)		
GSK2118436	-	NCT01266967	A Study of GSK2118436 in BRAF Mutant Metastatic Melanoma to the Brain (Break MB)	GlaxoSmithKline	February 2011	November 2012
Dabrafenib	Trametinib	NCT02039947	Study to Evaluate Treatment of Dabrafenib Plus Trametinib in Subjects With BRAF Mutation-Positive Melanoma That Has Metastasized to the Brain	Novartis	February 2014	February 2018
GSK2118436	GSK1120212	NCT01619774	An Open-Label Phase II Study of the Combination of GSK2118436 and GSK1120212 in Patients With Metastatic Melanoma Which is Refractory or Resistant to BRAF Inhibitor	M.D. Anderson Cancer Center	September 2012	August 2015
Panitumumab	FOLFIRI	NCT01704703	Study of FOLFIRI + Panitumumab Using Ultra-selection Technology of Patients With Stage IV Colorectal Cancer Refractory to Irinotecan Without Any Mutation on KRAS, PIK3Ca, BRAF and NRAS Genes Detected With Highly Sensitive Techniques (ULTRA)	Spanish Cooperative Group for the Treatment of Digestive Tumours (TTD)	October 2012	July 2016
Selumetinib	-	NCT00888134	Selumetinib in Cancers With BRAF Mutations	National Cancer Institute (NCI)	July 2009	January 2015
Vemurafenib	Cetuximab	NCT01524978	A Study of Vemurafenib in Participants With BRAF V600 Mutation-Positive Cancers	Hoffmann-La Roche	April 2012	October 2016
-	Panitumumab Oxaliplatin	NCT01308840	Gemcitabine, Oxaliplatin and Panitumumab in Kras/B-raf Wild-Type	University of Rochester	December 2010	January 2013

	Gemcitabine		Biliary Track and Gallbladder Cancer (UGIH09067)			
Vemurafenib	-	NCT01286753	A Study of Vemurafenib (RO5185426) in Participants With Metastatic or Unresectable Papillary Thyroid Cancer Positive for the BRAF V600 Mutation	Hoffmann-La Roche	June 2011	May 2015
Vemurafenib	BKM120	NCT01512251	BKM120 Combined With Vemurafenib (PLX4032) in BRAFV600E/K Mutant Advanced Melanoma	University of California, San Francisco	June 2012	March 2017
Vemurafenib	IL-2	NCT01603212	Systemic Therapy With Interferon, Interleukin-2 and BRAF Inhibitor	M.D. Anderson Cancer Center	July 2013	July 2017
Cetuximab	BMS-908662	NCT01086267	Safety and Efficacy Study of BMS-908662 Alone or in Combination With Cetuximab in Subjects With K-RAS or B-RAF Mutation Positive Advanced or Metastatic Colorectal Cancer	Bristol-Myers Squibb	July 2010	August 2011
Selumetinib	-	NCT01116271	Study of Selumetinib (AZD6244)(ARRY-142886) in Combination With Irinotecan in Previously Treated Patients With Colorectal cancer	AstraZeneca	April 2010	July 2012
GSK2118436 GSK1120212	-	NCT01072175	Investigate Safety, Pharmacokinetics and Pharmacodynamics of GSK2118436 & GSK1120212	Novartis	March 2010	February 2018
GSK1120212	Docetaxel	NCT01362296	An Open-label Study of GSK1120212 Compared With Docetaxel in Stage IV KRAS-mutant Non-small Cell Lung Cancer	GlaxoSmithKline	September 2011	September 2013
LGX818 WNT974	-	NCT02278133	Study of WNT974 in Combination With LGX818 and Cetuximab in Patients With BRAF-mutant Metastatic Colorectal Cancer (mCRC) and Wnt Pathway	Array BioPharma	December 2014	June 2017

Vemurafenib	Lymphodepleting chemotherapy TIL infusion Interleukin-2	NCT02354690	Mutations Vemurafenib and TIL Therapy for Metastatic Melanoma	Inge Marie Svane	November 2014	December 2018
Dabrafenib	Trametinib	NCT02027961	Phase 1 Safety and Tolerability of MEDI4736 in Combination With Dabrafenib and Trametinib or With Trametinib Alone	MedImmune LLC	January 2014	May 2018
-	Oxaliplatin Capecitabine	NCT01108107	Neoadjuvant Treatment of Colon Cancer	Vejele Hospital	April 2010	March 2015
-	FOLFIRI (m) FOLFOX-6 (m) Cetuximab	NCT01276379	Study Evaluating Biomarkers in Patients With Colorectal Cancer and Native KRAS Treated With Chemotherapy + Cetuximab (POSIBA)	Grupo Espanol Multidisciplinario del Cancer Digestivo	January 2011	December 2017

Phase-I

Vemurafenib	¹⁴ C-labeled Vemurafenib	NCT02441465	Bioavailability Study of Vemurafenib in Participants With BRAF ^{V600} Mutation-Positive Malignancies	Hoffmann-La Roche	August 2015	January 9, 2017
RO5185426	-	NCT01264380	A Study of the Effect of Food on the Pharmacokinetics of Single Dose RO5185426 And the Safety And Efficacy of Continuous Administration in Patients With BRAF ^{V600E} Mutation-Positive Metastatic Melanoma	Hoffmann-La Roche	January 2011	May 2013
Dabrafenib	Trametinib, Ipilimumab	NCT01767454	Study of Dabrafenib +/- Trametinib in Combination With Ipilimumab for ^{V600E} /K Mutation Positive Metastatic or Unresectable Melanoma	GlaxoSmithKline	February 2013	September 2015

ARQ-736	-	NCT01225536	Dose Escalation Study of ARQ 736 in Adult Subjects With Advanced Solid Tumors Harboring BRAF and/or NRAS Mutations	ArQule	October 2010	March 2013
GSK2118436	-	NCT01582997	A Phase I Study to Investigate the Safety, Tolerability and Pharmacokinetic Profile of of GSK2118436 in Japanese Subjects With BRAF Mutation Positive Solid Tumors	GlaxoSmithKline	May 2012	April 2015
Vemurafenib	SAR260301	NCT01673737	A Phase I/Ib Trial for the Evaluation of SAR260301 in Monotherapy or in Combination With Vemurafenib in Patients With Various Advanced Cancer	Sanofi	August 2012	February 2015
Dabrafenib	Rabeprazole, Rifampin	NCT01954043	A Pharmacokinetics (PK) Study of the Effects Rabeprazole and Rifampin on Dabrafenib in Subjects With BRAF V600 Mutation Positive Tumors	GlaxoSmithKline	December 2013	February 2016
Dabrafenib	Rosuvastatin, Midazolam	NCT02082665	Effects of Dabrafenib on the Single Dose Pharmacokinetics (PK) of Rosuvastatin and Midazolam	GlaxoSmithKline	February 2015	August 2016
GSK2118436	-	NCT01231594	A Rollover Study to Provide Continued Treatment With GSK2118436 to Subjects With BRAF Mutation-Positive Tumors	Novartis	November 2010	April 2018
Vemurafenib	Itraconazole Rifampin	NCT02608034	A Study to Investigate the Effect of Itraconazole and Rifampin on Pharmacokinetics (PK) of Vemurafenib at Steady State	Genentech, Inc.	May 2016	September 2018
GSK2118436	-	NCT01262963	An Absorption, Distribution, Metabolism	GlaxoSmithKline	January	April 2011

			and Excretion (ADME) Study of Single Oral Dose [14C] GSK2118436 in Subjects With BRAF Mutant Solid Tumors	e	2011	
Vemurafenib	Panitumumab	NCT01791309	Vemurafenib and Panitumumab Combination Therapy in Patients With BRAF V600E Mutated Metastatic Colorectal Cancer	Memorial Sloan Kettering Cancer Center	January 2013	March 2015
GSK2118436	-	NCT01231568	An Open Label Study to Examine the Effects of a High-Fat Meal and Particle Size on the Pharmacokinetics of Orally Administered GSK2118436 in Subjects With BRAF Mutation Positive Tumor	GlaxoSmithKline	October 2010	May 2011
GSK2118436	-	NCT01340833	Determination of the Absolute Bioavailability of GSK2118436 Following a Single Oral Dose Co-Administered With an Intravenous Radiolabelled Microtracer of GSK2118436 in Subjects With BRAF Mutant Solid Tumors	GlaxoSmithKline	June 2011	September 2011
GSK2118436	-	NCT01738451	A Study to Evaluate the Effect of Repeat Oral Dosing of GSK2118436 on Cardiac Repolarization in Subjects With V600 BRAF Mutation-Positive Tumors	GlaxoSmithKline	January 2013	November 2014
GSK2118436	Warfarin Ketoconazole Gemfibrozil	NCT01340846	A Pharmacokinetics Study of the Effects of GSK2118436 on Warfarin, the Effects of Ketoconazole and Gemfibrozil on GSK2118436, and the Effects of Repeat Doses of GSK2118436 in Subjects With BRAF Mutant Solid Tumors	GlaxoSmithKline	September 2012	November 2012

Vemurafenib	Hydroxychloroquine	NCT01897116	A Phase I Trial of Vemurafenib and Hydroxychloroquine in Patients With Advanced BRAF Mutant Melanoma	Abramson Cancer Center of the University of Pennsylvania	June 2013	October 2016
Trametinib	Digoxin	NCT02138292	A Phase 1B Clinical Trial of Trametinib Plus Digoxin in Patients With Unresectable or Metastatic BRAF Wild-type Melanoma	University of Texas Southwestern Medical Center	July 2014	February 2017
Vemurafenib	-	NCT02456701	Enhancing Radioiodine Incorporation Into BRAF Mutant Thyroid Cancers With the Combination of Vemurafenib and KTN3379	Celldex Therapeutics	June 2015	October 2016
Vemurafenib	-	NCT01910181	A Study of Vemurafenib (Zelboraf) in Chinese Participants With BRAF V600 Mutation-Positive Unresectable or Metastatic Melanoma	Hoffmann-La Roche	August 2013	April 2018
Vemurafenib	-	NCT01767623	A Study of The Impact of Severe Hepatic Impairment on the Pharmacokinetics and Safety of Vemurafenib in BRAF V600 Mutation-Positive Cancer Participants	Hoffmann-La Roche	August 2013	April 2017
RO5212054	-	NCT01143753	A Study of RO5212054 (PLX3603) in Participants With BRAF V600-Mutated Advanced Solid Tumors	Hoffmann-La Roche	June 2010	July 2017
Dabrafenib	Pazopanib	NCT01713972	Dabrafenib and Pazopanib Hydrochloride in Treating Patients With Advanced Malignant Tumors	Manisha Shah	November 2012	December 2018
GSK2118436	Midazolam	NCT00880321	A Phase I Study to Investigate the Safety, Pharmacokinetics, and Pharmacodynamics	GlaxoSmithKlin e	June 2009	March 2012

Vemurafenib	Interferon Alfa-2b	NCT01943422	of GSK2118436 in Subjects With Solid Tumors Safety and Efficacy Study of Vemurafenib and High-dose Interferon Alfa-2b in Melanoma (12-107)	John Kirkwood	October 2013	December 2016
BGB-283	-	NCT02610361	Study of the Safety and Pharmacokinetics of BGB-283 in Patients With Solid Tumors	BeiGene	November 2013	October 2017
RO5185426	-	NCT01107418	A Pharmacokinetic/Pharmacodynamic Study of RO5185426 in Previously Treated Patients With Metastatic Melanoma	Hoffmann-La Roche	May 2010	February 2013
Vemurafenib	GDC-0973	NCT01271803	A Study of Vemurafenib and GDC-0973 (Cobimetinib) in Participants With BRAFV600E Mutation-Positive Metastatic Melanoma	Hoffmann-La Roche	February 2011	December 2017
TAK-733	-	NCT00948467	Study of TAK-733 in Adult Patients With Advanced Nonhematologic Malignancies	Millennium Pharmaceuticals, Inc.	December 2009	June 2013
GSK1120212	-	NCT01138085	Safety, Pharmacokinetics (PK) of AKT and MEK Combination	GlaxoSmithKline	May 2010	November 2014
GSK2141795	-	NCT01877811	Study of RXDX-105, Potent RET Inhibitor in Patients With Advanced Lung Cancer and Other Solid Tumors	Hoffmann-La Roche	June 2013	February 2019
RXDX-105	-					
BYL719	MEK162	NCT01449058	A Phase Ib Study of MEK162 Plus BYL719 in Adult Patients With Selected Advanced Solid Tumors	Array BioPharma	March 2012	August 2017

Aim

The aim of this research work is to design and synthesize novel B-Raf inhibitors in the treatment of Skin Cancer.

Objective

1. To carry out literature survey of various computational approaches used for designing of B-Raf inhibitors and their synthetic procedures.
2. To generate ligand based pharmacophore model from structurally diverse B-Raf inhibitor using DISCOtech refined with GASP module of Sybyl X followed by pharmacophore validation and virtual screening.
3. To perform various 3D-QSAR techniques includes CoMFA, CoMSIA, HQSAR, and Topomer CoMFA.
4. To design molecules novel B-Raf inhibitors by using knowledge-based drug design followed by molecular docking and *in-silico* ADMET of design molecules.
5. To design synthetic scheme, synthesis, purification, physical and, spectral characterization of novel molecules.
6. To carry out *in-vitro* screening of all synthesized compounds.
7. To carry out *in-vivo* screening of potent molecules.

4.1 Introduction to Computer-aided drug design

Design and discovery of new lead or drug like molecule is a costly and laborious process. To overcome this problem computer-aided drug design (CADD) was typically designated. The different CADD tools cover broad range of application in the design of novel drug like molecules. The aim of the use of CADD is to speed up drug design process with low cost. High-throughput screening (HTS) is automatic or semi-automatic CADD tool for testing of thousands of compounds with a suitable bioassay. These are *in-silico* techniques which helps out to filtering of libraries of compounds using computational methods to rank out most active molecules for a given target.¹⁴⁶

The ultimate goal is to design and develop highly potent compound, and has good target specific activity. This can be accomplished with the help of classical medicinal chemistry approaches, where the novel molecule could be design based on the structural activity relationship (SAR) or based on the available marketed molecules. However, computational methods can used to create novel molecule based on the different heterocyclic scaffolds and statistical algorithm.

All CADD methods follow different chemo-informatics tools, which include the application of data storage, data handling, different retrieval methods for chemical structure, and ADME prediction. These tools also covers the calculation of physicochemical properties or molecular descriptors based on the molecular structure which could be useful for shorting out of the compounds from the libraries of compound.¹⁴⁷

Pharmacophore have become one of the important CADD tool in development of drug design. Two types of pharmacophore have been used for the design of novel molecules, which includes structure-based pharmacophore, and ligand-based pharmacophore. Generated model gives an idea related to the important pharmacophoric groups required for the biological activity.¹⁴⁸

Another very important CADD tool viz. quantitative structural activity relationship (QSAR), and quantitative structural property relationship (QSPR). Both these methods are used for to predict the relationship between the physicochemical properties with biological activity of the compounds. 3D model is generating based on the outcome of

QSAR statistical parameters. This model gives useful information related to important substitution required for biological activity.^{148,149}

Another important CADD tool is molecular docking, where the 3D binding pose of the protein structure and ligand is docked. The results of molecular docking analysis are given in the form of binding of amino acid interaction as well as docking score. This tool is widely useful for structural investigation of protein-ligand interaction in the absence of experimental structural information. It is a very important tool to screen out library of compounds based on the docking score as well as ligand binding interaction.¹⁵⁰

4.2 Pharmacophore modelling: -

Scientist Paul Ehrlich gave the concept of pharmacophore modelling during the late 1800s.¹⁵¹ At that time the pharmacophore was defined as certain chemical groups or functional groups in a compound required for biological activity. Schueler gave the definition of pharmacophore in his 1960 book *Chemobiodynamics and Drug Design* and was defined as “essential structural framework required for biological activity.”¹⁵² In 1997, as per International Union of Pure and Applied Chemistry (IUPAC) pharmacophore has been defined as “A pharmacophore is the ensemble of steric and electronic features that is necessary to ensure the optimal supramolecular interactions with a specific biological target and to trigger (or block) its biological response.”¹⁵³

Pharmacophore model can be established by ligand based manner in which the diverse sets of active molecules are superimposed to each other and give the common chemical features that are required for biological activity. This approach is widely used in virtual screening, de-novo design, and other applications such as hit to lead optimization. Different varieties of automated pharmacophore based computational software is used with different *in-silico* algorithms. Various pharmacophore modelling tools with their inventor and typical characteristics are shown in **Table 9**.¹⁵⁴

Ligand-based pharmacophore has become an important computational approach for drug design. It is applicable in the absence of target protein structure. In this approach all the active ligands are superimposed to each other and give the important structural features

which are required for biological activity. Currently, various automated pharmacophore software includes HipHop, HypoGen (Accelrys Inc. <http://www.accelrys.com>), DiscoTech, GASP, GALAHAD (Tripos Inc. <http://www.tripos.com>), PHASE (Schrodinger Inc., <http://www.schrodinger.com>), and MOE (Chemical Computing Group, <http://www.chemcomp.com>). These programs differ based on the algorithms used for model generation.

4.2.1 DiscoTech: -

In DiscoTech each molecule is characterized by ligand point and site point. All the features, which are comes from the ligand sides are called as ligand point. Ligand point includes positively charged atom, negatively charged atom, HBD, HBA, and hydrophobic. Any features which arises from protein structure are called site point. DiscoTech module follows ligand conformational flexibility. In DiscoTech software generate maximum conformer for each ligand and among all these conformers all molecules are align on conformer which having low energy. Each molecule with each low energy conformer being treated as a rigid body during the alignment step. Due to the geometric increment involved in the nature of pharmacophore theory with (1) expanding number of molecules, (2) expanding number of conformations, and (3) expanding number of features.¹⁵⁵

Table 9. Various programs for pharmacophore modelling (including ligand-based and structure-based methods)

Ligand-based methods						
Software	Year and inventor(s)	Key techniques			Other typical characteristics	Remarks
		Handling conformational flexibility	Molecular alignment			
HipHop	1996 Barnum D. et al.	Pre-enumerating method by Poling algorithm	Feature-based method	Identifying common features by a pruned exhaustive search (qualitative model)	Integrated into the Catalyst, and now Discovery Studio, Accelrys Inc. Website: www.accelrys.com	
HypoGen	2000 Li H.; Sutter J.; Hoffmann R. et al.	Pre-enumerating method by Poling algorithm	Feature-based method	Designed to correlate structure and activity (quantitative model)	Integrated into the Catalyst, and now Discovery Studio, Accelrys Inc. Website: www.accelrys.com	
HypoRefine	2004 Maynard A.J.; Waldman M.; Sutter J.	Pre-enumerating method by Poling algorithm	Feature-based method	An extension to the HypoGen. Exclusion volumes are involved.	Integrated into the Catalyst, and now Discovery Studio, Accelrys Inc. Website: www.accelrys.com	
DISCO	1993 Martin Y.C. et al	Pre-enumerating method by Concord and Confort	Bron-Kerbosh via clique-	Considering 3D conformations of compounds as sets of inter-point	Integrated into the Sybyl, Tripos Inc. Website: www.tripos.com	

		Sybyl interface	detection algorithm	distances	
GASP	1995 Jones G.; Willett P.; Glen R.C.	On-the-fly	Atom-based method	A flexible genetic algorithm is used for pharmacophore identification	Integrated into the Sybyl, Tripos Inc. Website: www.tripos.com
GALAHAD	2006 Clark R.D.; Richmond N. J. et al.	Both pre- enumerating method and on the fly	Atom-based method	A more sophisticated genetic algorithm (developed on real-world data sets) is used for pharmacophore modeling	Integrated into the Sybyl, Tripos Inc. Website: www.tripos.com
PHASE	2006 Dixon S.L. et al.	Pre-enumerating method Schrödinger's ConfGen technology	Feature- based method (called sites)	Very flexible and user friendly. SMARTS pattern matching is used for feature location. Excluded volumes are included.	Marketed by Schrödinger Inc. Website: www.schrodinger.com

MOE	2004 Chemical Computing Group Inc. (CCG)	Pre-enumerating method by various ranging from molecular dynamics to stochastic methods and systematic search	Property-based algorithm	A pharmacophore is defined manually by applying schemes using a Pharmacophore Query Editor	Released by Chemical Computing Group, Inc. Website: www.chemcomp.com
GAMMA	1997 Handshuh S.; Gasteiger J.	On the fly	Atom-based method	The conformational search and the pattern identification are performed simultaneously by utilizing the genetic algorithm technique	Not commercialized
MPHIL	1997 Holliday J.; Willet P.	On the fly	Atom-based method (rigid)	Based on clique detection and genetic algorithm	Not commercialized
RAPID	1998 Finn P.W. et al.	Pre-enumerating method	Atom-based method	A rigid alignment based on mapping triangles of 3D atom coordinates	Not commercialized

CLEW	1998 Dolata D.P. et al.	N/A*	Feature-based method	Utilizing machine learning method and geometrical fitting to discover pharmacophores from a set of active and inactive compounds	Not commercialized
SCAMPI	1999 Chen X. et al.	On the fly	Feature-based method	Handling large heterogeneous data sets	Not commercialized
ALADDIN	1989 Van Drie J.H.; Martin Y.C.	N/A*	N/A*	Design and pharmacophore recognition of molecules from geometric, steric, and substructure searching of 3D structures	Not commercialized
DANTE	1996 Van Drie J.H.	N/A*	N/A*	Shrink-wrap pharmacophores. Inferring pharmacophores automatically from	Not commercialized

				structure–activity data, which includes information about the shape of the binding cavity	
Apex-3D	1995 Golender V.	Pre-enumerating method	Feature-based method	An expert system developed to represent, elucidate, and utilize knowledge on structure-activity relationships	Early commercialized by Biosym Inc. (Accelrys, Inc), now it has been replaced by Catalyst (Accelrys, Inc)
CoMFA	1988 Cramer III R. D. et al.	Pre-enumerating method	Molecular field based method	An industry standard 3D QSAR method	Commercially distributed by Tripos, Inc. Website: www.tripos.com
COMSIA	1994 Klebe G. et al.	Pre-enumerating method	Molecular field based method	Similar to CoMFA, but introducing Gaussian-type physicochemical property	Commercially distributed by Tripos, Inc. Website: www.tripos.com
XED	1994 Vinter J.G.	Pre-enumerating method	Molecular field based method	Using field points to describe the van der Waals and electrostatic potential that surround	Marketed by Cresset Biomolecular

			molecules		
APOLLO	1989 Snyder J. P. et al.	Pre-enumerating method	Feature-based method (vector points)	Identifying from a set of ligands their interaction points belonging to the receptor site and creating pseudoreceptor	Not commercialized
PharmaGist	2008 Schneidman-Duhovny D.; Dror O. et al.	On the fly	Feature-based method	A webserver for ligand-based pharmacophore detection	Webserver: http://bioinfo3d.cs.tau.ac.il/PharmaGist

4.2.2 GASP: - Genetic Algorithm Superposition Program

GASP module follows the genetic algorithm and quite differs from DiscoTech. In GASP each molecule is treated as a single conformer by random rotation and random translation before the superimposition is made. Based on the generated conformer, pharmacophoric features are determined (HBD, HBA, and ring aromatic). The molecule having least number of pharmacophoric features is chosen as the base molecule and other molecules are superimpose on it.

A chromosome of GASP encoded the molecules which are mapped on the particular pharmacophoric features by angle of rotation of the rotatable bonds. For a data set of N compounds, the chromosome consists of $2N-1$ where, N binary strings to represent the conformations of the molecules and N-1 integer strings that represent the mapping from the base molecule to each of the other molecules. Thus, number of pharmacophoric features in the base molecule determines the length of integer.

The fitness function in GASP pharmacophore model given by the molecules having least conformer and each molecule align based on mapping. Genetic operators (GA) are used to sort out the maximum fitness function and best structural overlay. Each run of GA in the GASP module generates pharmacophore and each feature in the pharmacophore must be present in each molecule. GA is not able to determine the global minimum solution; it is possible that each run of GASP gives the different global minimum molecules. Therefore, GASP will be run for several times for same data set of the molecule and generated model can be ranked based on their fitness scores.¹⁵⁶

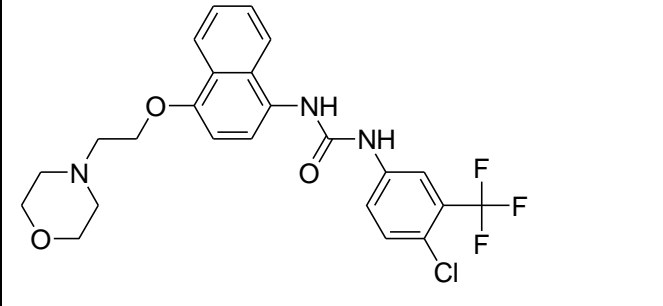
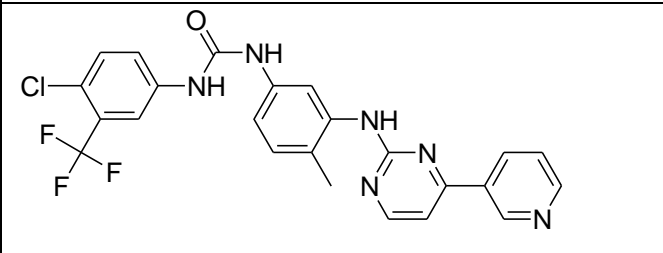
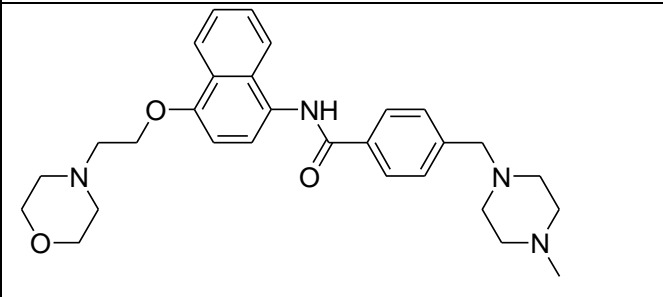
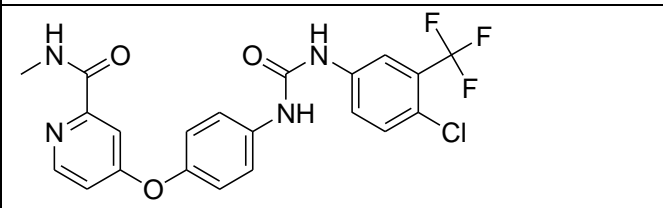
4.3 Materials and Methods: -

4.3.1 Selection of Dataset

10 different previously reported B-Raf^{V600E} kinase inhibitors with diverse sets of chemical classes were used for generation of Pharmacophore model. All molecules were selected in the range of potent, least potent, and moderately active. All these structures were drawn in SKETCH function of Sybyl X, and energy minimization of SKETCH compounds were calculated by the Gasteiger-Huckel method. Structures used for pharmacophore generation with their reported IC₅₀ on B-Raf enzyme are shown in **Table 10**.

Table 10: Reported B-Raf Inhibitors used to develop Pharmacophore model

Compound No.	Structure of Compound	IC ₅₀	Ref
140		4.21 nm	²⁷
141		0.669 nm	²⁷
142		0.3 nm	³⁴
143		48.3 nm	³⁴
144		57.8 nm	³⁷
145		672 nm	³⁷

146		1 nm	¹⁵⁷
147		180 nm	¹⁵⁷
148		100 μm	¹⁵⁷
149	 Sorafenib	22 nm	-

4.3.2 Pharmacophore model generation

The DiscoTech module of sybyl X software was used for generation of the pharmacophore model and furthermore it was refined with GASP module of sybyl X software. All 10 molecules were imported and run against the DiscoTech module for generating the conformer of all molecules. Based on the conformer analysis of DiscoTech generate models, the model having the top scoring function (D_{MEAN} value) was refined with GSAP. All generated conformers were used for alignment optimization by using GA parameters. Based on the alignment functioned, four different pharmacophore model were generated. All the parameters were kept as default except population size, fitness increment, mutation weight, and number of alignment. Model having the good fitness score were subjected to validated using test and decoy database (B-Raf decoy set).

4.3.3 Validation of the pharmacophore model

The generated pharmacophore model should be statistically significant, and predictive power of the model were proven by the two well-known statistical methods viz. GH Score (Gunner Henry Score) and ROC curve (Receiver Operating Characteristic).

4.3.3.1 Gunner Henry Score (GH Score)

The generated pharmacophore model was validated by using the list of active and inactive molecules (Decoy set).

A database of 200 decoy set (inactive B-Raf inhibitors), and 21 active B-Raf inhibitors were selected for the validation of pharmacophore model. The UNITY module of sybyl X software was used to screen the pharmacophore model on database of 221 molecules. The validation of model depends on how pharmacophore model retrieved already active B-Raf inhibitors and did not retrieve decoy molecules, which are inactive on B-Raf.

GH Score was calculated by following equations:

$$\%A = HA/A * 100$$

$$\%Y = HA/HT * 100$$

$$E = (HA/HT) * (D/A)$$

$$GH = (HA (3A + HT) / 4 HT A) * (1 - (HT - HA / D - A))$$

where,

HA: Active Retrieved.

HT: Total Number of Hit Retrieved.

A: No.Of Active Compound.

D: Total number of database.

E: Enrichment Factor

%A: percent active

%Y: percent yield

GH: Goodness of Hit/Gunner Henry

4.3.3.2 Receiver operating characteristic (ROC) curve

The ROC is a well-known method used to evaluate the predictive power of model with the help of test set molecules and discriminate between two populations. In ROC curve, two important terms viz. selectivity and specificity gives an idea about the predictive power of the

model. The ROC curve is the graph of sensitivity (Se) versus 1- specificity (Sp). On the basis of graphical curve, to calculate the values of Se, Sp, and AUC. The equations are shown in below:

$$Se = \frac{TP}{TP+FN}$$

where,

TP: Number of true positive

FN: Number of false negative

$$Se = \frac{FP}{FP+TN}$$

where,

FP: Number of false positive

TN: Number of true negative

$$AUC = \sum_{X=Z}^N Se(x)[(1 - Sp)(x) - (1 - S)(x - 1)]$$

where,

X: rank position

Se(x): percent of true positive versus total positive

(1-Sp)(x): percent of the false positives versus total negatives.

4.4 Results and Discussion

4.4.1 Pharmacophore Model

Ten different diverse sets of B-Raf inhibitors were used and generate DiscoTech and their results are given in **Table 11**. Model having highest score and highest D_{MEAN} value were selected for further analysis. Model **6** showed highest score and highest D_{MEAN} value and it was used for refinement using GASP. By the use of different default parameters of GASP module, **4** different models were generated. Among all these models, model **2** showed highest fitness score and D_{MEAN} score which indicated model **2** was best pharmacophore model.

Results of GSAP refinement pharmacophore are shown in **Table 12**. The best model contained three acceptor atoms, one donor atom, one hydrophobic, three donor sites, and one acceptor site. A 3D and 2D image of pharmacophore model are shown in **fig. 4**. The obtained pharmacophoric features were used for the design of novel B-Raf^{V600E} inhibitors.

Table 11. Results of DiscoTech Pharmacophore model

Model no.	Rowname	Size	Hits	Score	Tolerance	Dmean
1	Model_001	8	10	1.5465	0.25	4.163
2	Model_002	8	10	1.5466	0.25	4.1635
3	Model_003	8	10	1.5475	0.25	4.1678
4	Model_004	8	10	1.5456	0.25	4.1584
5	Model_005	8	10	1.5465	0.25	4.1626
6	Model_006	8	10	1.5475	0.25	4.168
7	Model_007	8	10	1.5464	0.25	4.1622

Table 12. Results of GASP pharmacophore after refining of DiscoTech model (Model_006)

Model no.	Rowname	FITNESS	SIZE	HITS	DMEAN	ACTIVITIES
1	Model_001	3249.71	9	10	3.6011	0
2	Model_002	3263.36	9	10	3.6002	0
3	Model_003	2726.34	9	10	3.6	0
4	Model_004	3246.97	9	10	3.6017	0

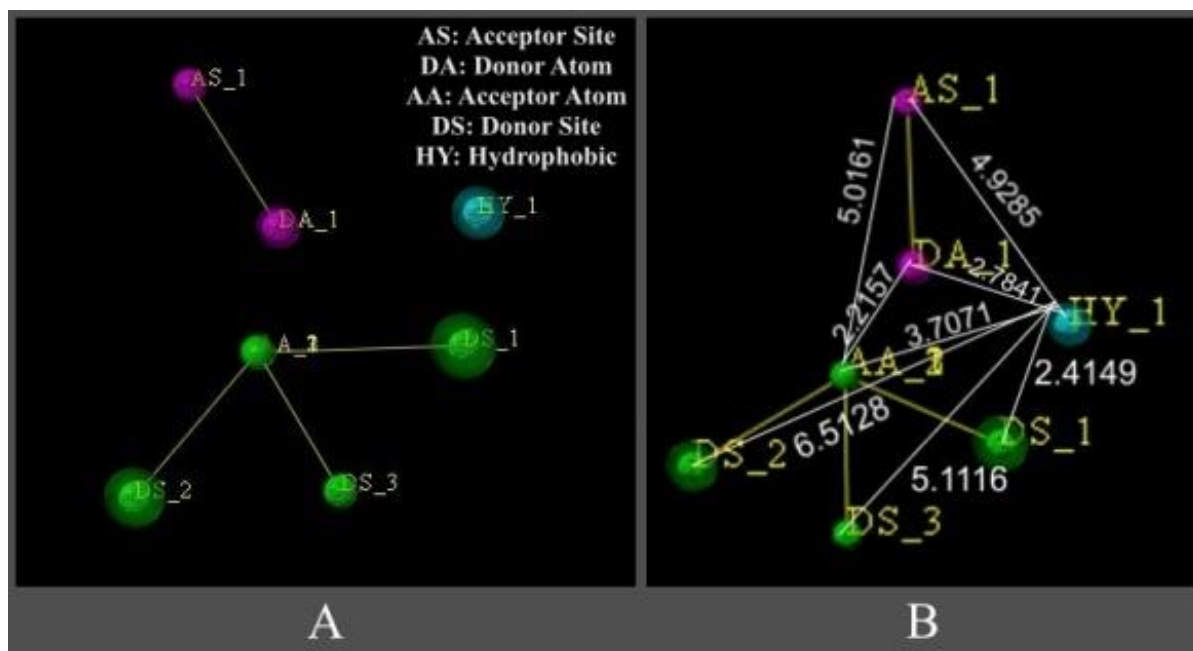


Fig. 4 Pharmacophore model A) 3D pharmacophore model B) 2D pharmacophore model with distance between two features in Å.

4.4.2 Validation of Pharmacophore Model

4.4.2.1 Gunner Henry Score (GH Score)

GH score was calculated by using the dataset of active and decoy molecules of B-Raf enzyme. Here, various variables were calculated based on results of UNITY module of sybyl X. These variables include %A (Active retrieved), %Y (Selectivity), Enrichment Ratio (E), and Goodness of hits (GH) score. The values of the above mentioned variables are given in **Table 13**. The value of the GH score was found to be more than 0.6 indicated that the goodness of the pharmacophore model.

Table 13. Statistical parameter for GH scoring method

Parameters	Statistical Value
% Active (%A)	95.23%
%selectivity (% Y)	90.90%
Enrichment Factor (E)	9.56
Gunner Henry (GH) Score	0.910
No. of compound in database (D)	221
No. of active in database (A)	21

Total no. of hits retrieved (Ht)	22
Total no. of active retrieved (Ha)	20

4.4.2.2 Receiver Operating Characteristic (ROC)

The datasets of active conformer of B-Raf molecules and decoy molecules was screened on pharmacophore model by using UNITY module of sybyl X software. The ROC curve was obtained from trial version of SPSS software. The result of ROC curve with AUC shown in **Fig 5**.

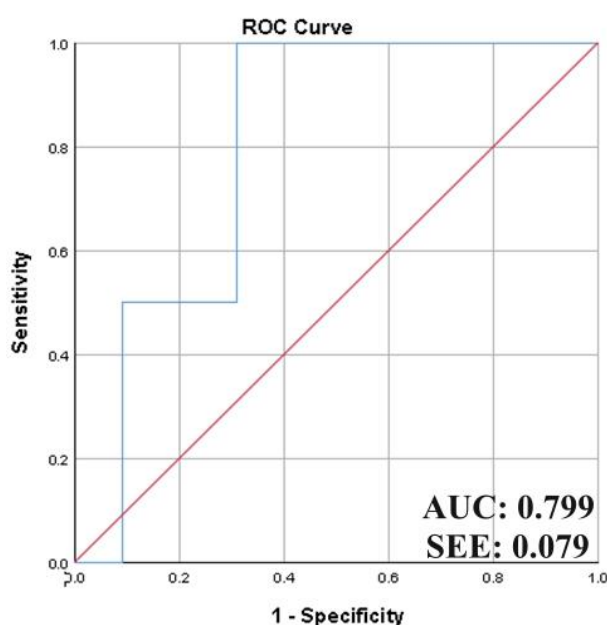


Fig. 5 ROC curve with their AUC

4.5 Virtual Screening

Once the pharmacophore model is generated, the generated pharmacophore model can be used for query for various 3D chemical databases to search hit molecules. This process to search out new hits is called as 'pharmacophore based virtual screening' (VS).

The objective to perform pharmacophore based virtual screening is to search out new virtual hits that are having chemical feature similar to the pharmacophoric template. The outcome of virtual screening to get various virtual hits which might be similar to the known active compounds or entirely novel in scaffold. The searching of compounds with different scaffolds with sharing of biological activity is usually called as 'scaffold hopping'.¹⁵⁴

Various databases are available to use for pharmacophore based virtual screening, which includes ZINC, Maybridge, NCI (National Cancer Institute), Pubchem, IBS, etc.

4.6 Material and Methods

To find the novel virtual hits for targeting B-Raf inhibitor, the generated pharmacophore model was put as a query model screened against NCI database. UNITY module of sybyl X software was used for finding of substructure. The obtained hits from the database were further filtered out various filters includes Lipinski's rule of five, Removal of duplicate structure, counter ions, fragments, etc.

4.7 Results and Discussion

The best 3D pharmacophore model was chosen for query model on NCI database for finding of virtual hits by UNITY module of sybyl X. Total 33377 molecules were obtained after pahrmacophore based virtual screening process from NCI database. The retrieved 33377 molecules were further filtered out to remove bad fragments, and remove counter ions & duplicate structure, which results into total 19502 structures were removed by applied these two filters. At last, these 19502 structures were further filter-out by Lipinski's rule of five and finally we got 11485 virtual hits which could be useful for design of novel B-Raf inhibitors. Steps for virtual screening process are shown in **Fig 6**.

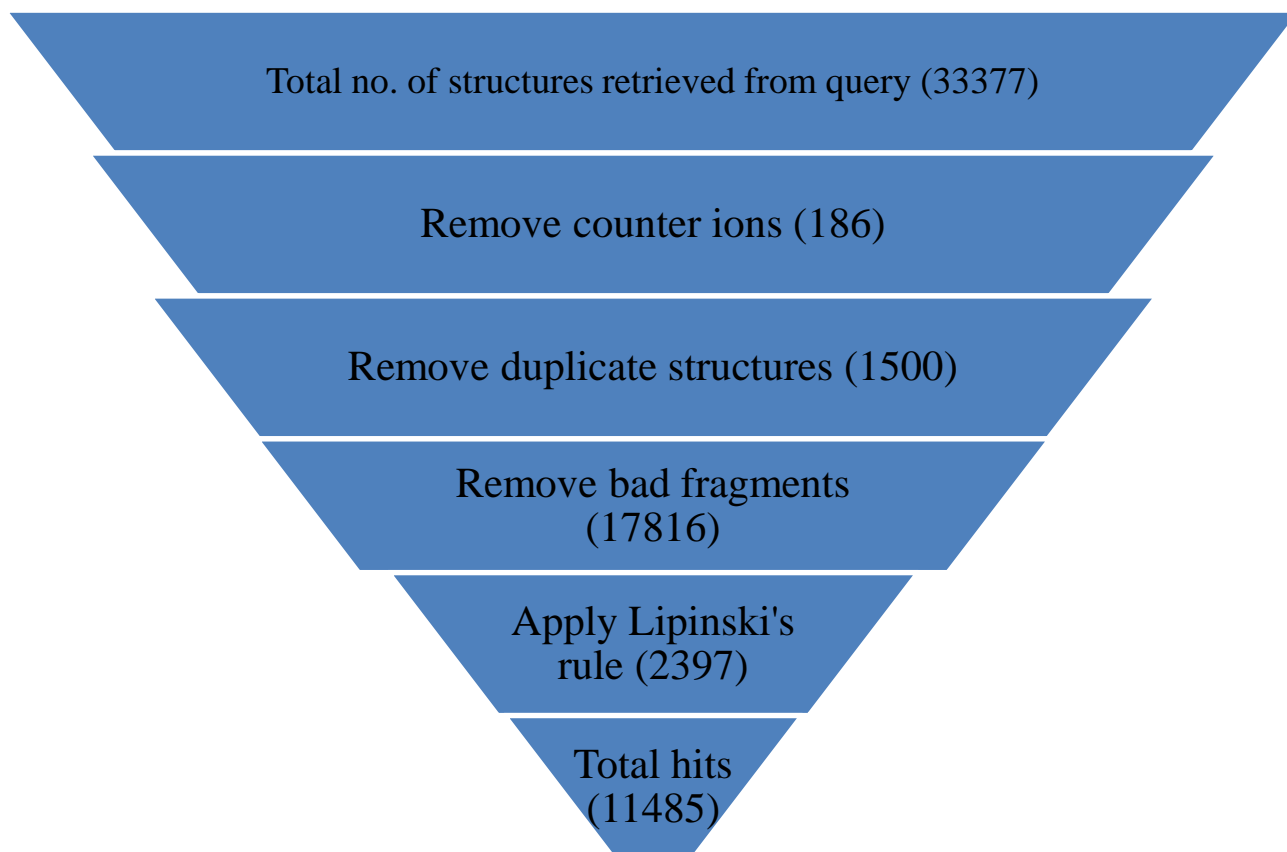


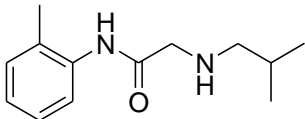
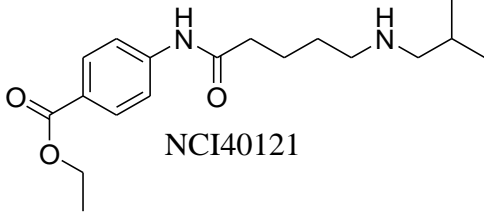
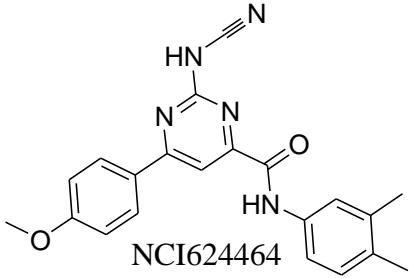
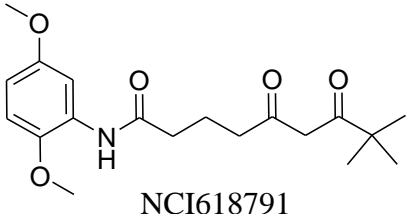
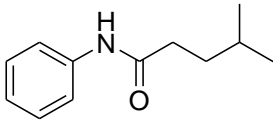
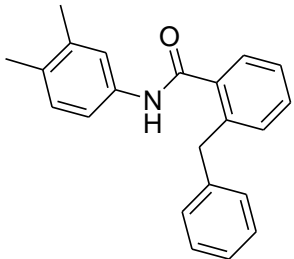
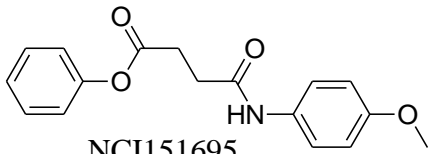
Fig. 6 Steps for virtual screening

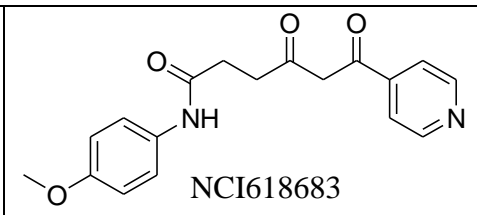
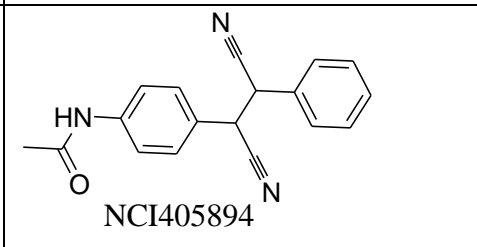
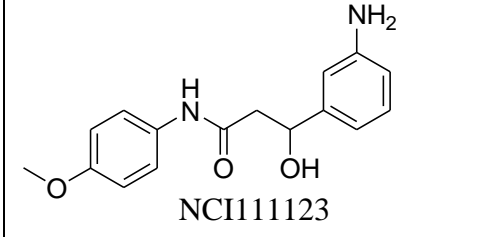
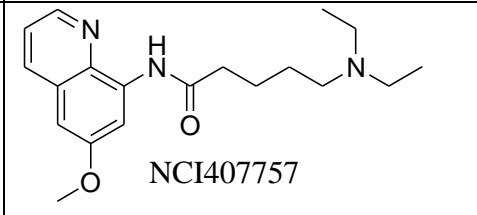
In Pharmacophore based virtual screening, obtained virtual molecules having high Q_{Fit} value which indicated that the pharmacophoric features were completely aligned with particular or fitted into the molecule that were shown in **Table 14** with their Q_{Fit} value.

Table 14: Top 20 virtual hits with their Q_{fit} value

Compound No.	Structure of Virtual Hit	Q_{Fit} value
150	 NCI123227	95.83
151	 NCI618685	95.79

152	 NCI135100	95.78
153	 NCI631822	95.78
154	 NCI630281	95.78
155	 NCI622564	95.78
156	 NCI622564	95.77
157	 NCI164245	95.75
158	 NCI135110	95.75

159	 NCI40126	95.72
160	 NCI40121	95.69
161	 NCI624464	95.68
162	 NCI618791	95.68
163	 NCI98377	95.64
164	 NCI129401	95.63
165	 NCI151695	95.62

166	 NCI618683	95.61
167	 NCI405894	95.59
168	 NCI111123	95.57
169	 NCI407757	95.55

4.7 3D QSAR (Three Dimensional Quantitative Structural Activity Relationship)

3D-QSAR is a ligand-based drug design approach which plays a vital role in the design of novel compounds. All descriptors have an essential role in correlating the effect of structural substitution on the biological activity. In the present research work, four different 3D-QSAR techniques were used which included Comparative Molecular Field Analysis (CoMFA), Comparative Molecular Similarity Indices Analysis (CoMSIA), Molecular Hologram QSAR (HQSAR) and topomer CoMFA¹⁵⁸. In CoMFA, biological activity was correlated with steric and electrostatic parameters, while in case of CoMSIA, biological activity was associated with hydrophobic, hydrogen bond donor (HBD), hydrogen bond acceptor (HBA), steric field and electrostatic parameters. In HQSAR, biological activity was correlated with the structural part of each group and atom of the molecules. The HQSAR analysis gave essential information about the effect of atom, stereochemistry, and fragments on the biological

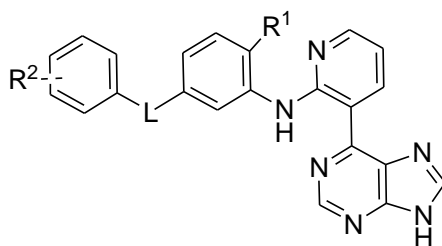
activity of molecules.¹⁵⁹ The Topomer CoMFA analysis was carried out to overcome the limitations of CoMFA. In Topomer CoMFA, molecules of the series were divided into two or more than two fragments and model was generated. Topomer CoMFA results were directly correlated with the fragments of the molecule and the outcome of this analysis was found to be very similar to the CoMFA contour maps.

4.8 Material and Methods

4.8.1 Dataset and selection of training and test set

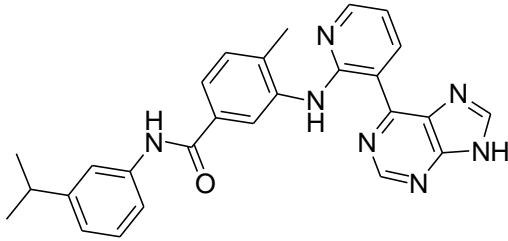
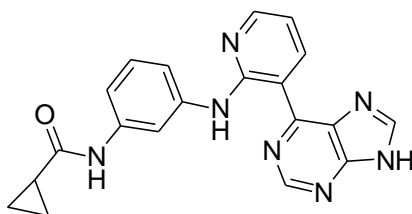
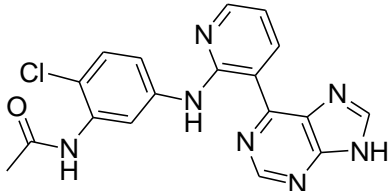
A data set of 28 synthetic molecules having purinylpyridine scaffold and reported as a B-Raf^{V600E} inhibitory activity was used for the present study as shown in Table 15²⁷. The IC₅₀ values were reported in nM and converted into PIC₅₀ (-logIC₅₀). The biological activity (pIC₅₀) were selected as a dependent variable and 3D descriptors of CoMFA, CoMSIA, and HQSAR were choose as an independent variable. All these structures were drawn in SKETCH function of Sybyl X, and energy minimization of SKETCH compounds were calculated by the Gasteiger-Huckel method.¹⁶⁰ Out of 28 molecules, 7 molecules were selected for test set and remaining 21 molecules as a training set. These training and test set were constructed in such a way that both datasets consisted of balanced combination of potent, moderate and less active molecules.

Table 15. Reported B-Raf Inhibitors with IC₅₀ and PIC₅₀ values (nM).



Compound No.	L	R ¹	R ²	IC ₅₀ (nM)	pIC ₅₀
170*	-NHCONH-	-H	4-Cl-3-CF ₃	12.0	7.921
171	-NHCONH-	-CH ₃	4-Cl-3-CF ₃	4.21	8.376
172	-NHCO-	-H	4-Cl-3-CF ₃	13.5	7.870

173	-NHCO-	-CH ₃	4-Cl-3-CF ₃	3.15	8.502
174*	-NHCO-	-CH ₃	3-CF ₃	2.17	8.664
175	-NHCO-	-CH ₃	3-CH(CH ₃) ₂	1.69	8.772
176	-NHCO-	-CH ₃	3-CN	0.717	9.145
177*	-NHCO-	-CH ₃	3-F	1.03	8.987
178	-NHCO-	-CH ₃	4-Cl-3-CH ₃	1.43	8.845
179*	-NHCO-	-CH ₃	3-Cl	1.30	8.886
180	-NHCO-	-CH ₃	3-Br-4-Cl	3.62	8.441
181	-NHCO-	-CH ₃	4-CF ₃	1.50	8.824
182	-NHCO-	-Cl	4-Cl-3-CF ₃	10.8	7.967
183	-NHCO-	-Cl	3-CF ₃	2.78	8.556
184*	-NHCO-	-Cl	3-CH(CH ₃) ₂	8.07	8.093
185	-NHCO-	-Cl	3,4-di-Cl	1.60	8.796
186*	-NHCO-	-F	4-Cl-3-CF ₃	4.82	8.317
187	-CONH-	-H	4-Cl-3-CF ₃	3.03	8.519
188*	-CONH-	-CH ₃	4-Cl-3-CF ₃	2.71	8.567
189	-CONH-	-CH ₃	3-CF ₃	2.51	8.600
190	-CONH-	-CH ₃	3-CN	0.669	9.175
191	-CONH-	-CH ₃	4-Cl-3-CH ₃	2.56	8.592
192	-CONH-	-CH ₃	3-Cl	1.77	8.752
193	-CONH-	-CH ₃	3-OCH ₃	1.20	8.921
194	-CONH-	-CH ₃	3-N(CH ₃) ₂	0.790	9.102

195		7.44	8.128
196		471	6.327
197		6430	5.192

*test set molecules

4.8.2 Molecular alignment

Molecular alignment is a fundamental process for the generation of the QSAR model. All statistical values of CoMFA, CoMSIA, and HQSAR depended on molecular alignment. In the present study, three different alignments methods were used viz. Distill based alignment, Docking based alignment, and Pharmacophore-based alignment for the generation of the 3D-QSAR model. Among all these alignment methods, distill based alignment showed good statistical values and giving good QSAR correlation with biological activity. Alignment- I (Distill based alignment), as shown in **Fig. 7a**, was generated by distill method. In this method, alignment was carried out on the common core scaffold present in all the structures. Compound **190** (most potent) was selected as a template molecule, and other molecules were aligned on the template molecule. Alignment-II (Pharmacophore-based alignment) (**Fig. 7b**), was generated by DiscoTECH module of Sybyl X, where conformers of each molecule were generated, and all conformers were aligned on each other to get a pharmacophore. Alignment-III (docking based alignment) (**Fig. 7c**), was carried out by the surflex module of Sybyl X, in which B-Raf protein (PDB ID: 5ITA) was imported, and protomol was generated by SurFlex module, and all these molecules were docked in the active site of the protein.¹⁶¹

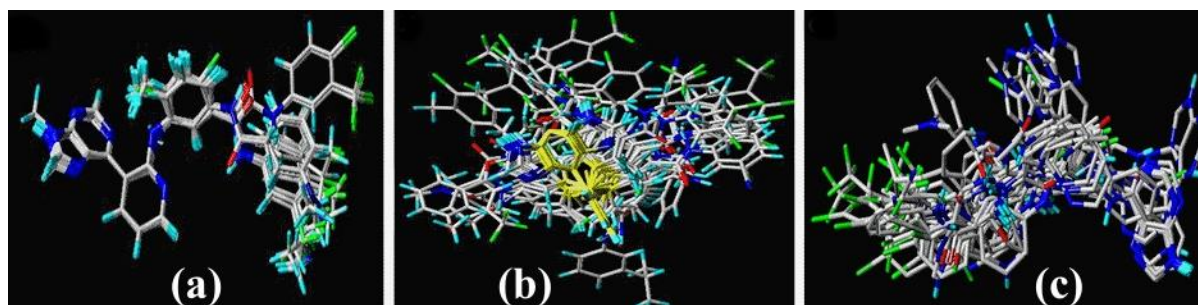


Fig 7: Different alignment methods with common core scaffold of purinylpyridine derivatives: (a) Distill based alignment; (b) Pharmacophore based alignment; (c) Docking based alignment.

4.8.3 CoMFA Studies

In CoMFA analysis, steric and electrostatic fields were calculated. In CoMFA, generated equation and energy fields were estimated at every grid point. The algorithm of CoMFA analysis was based on the principle of Lenard Jones potential and was utilized for the calculation of electrostatic while the steric property was calculated by Columbia potential. The steric and electrostatic potential values were obtained around 30.0 kcal/mol. Steric and electrostatic contour maps were generated by CoMFA model. Along with contour maps, the model also showed contour plots from the PLS model, which included score plots and loading/weight plots. Score plots showed the relationship between the activity and the structure, whereas the loading/weight plot displayed similarity/dissimilarity between the molecules.¹⁶²

4.8.4 CoMSIA Studies

CoMSIA analysis consisted a grid box which included steric, electrostatic, HBD, HBA, and hydrophobic parameters. All properties were calculated at each lattice point of grid box consisted of a probe atom with a radius of 1 Å for all five fields with +1 charge. The Gaussian function was used to determine molecular atoms and probe atoms for all grid points. In CoMSIA analysis, the Gaussian function was utilized for the distance dependence between a molecular atom and probe atom, because during analysis distances were calculated at all grid points from both inside and outside the molecular surface.¹⁶²

4.8.5 Halogram QSAR (HQSAR)

All the sub-basic fragments in the size of 4– 7 atoms were created for every molecule. The SLN (Sybyl Line Notation) for each piece of fragment created was mapped to a unique whole number. Every whole number was utilized to select a container in a whole number cluster of foreordained hologram length running from 97 to 353. The hologram length characterized the dimensionality of the descriptor space. The HQSAR descriptor factors checked molecular structural fragments in each cluster. The hydrogen of the molecules were incorporated into the generation of the molecular HQSAR model. Fragments and descriptor variables were used for generation of HQSAR model. Models were also generated by molecular substructure between 4 to 7 atoms in size and hologram bins with lengths of 97, 151, 199, 254, 307 and 353 for all molecules.¹⁵⁹

4.8.6 Topomer CoMFA

To overcome the limitation of CoMFA in alignment, topomer CoMFA methodology was utilized. It was a combination of CoMFA with topomer technology of the molecular descriptors. Topomer was directly correlated with a molecular fragment, which was generated by stereocenter as well as its position. It is very similar to CoMFA methodology to create contour maps of steric as well as electrostatic by using Tripos force field method with +1 atom charge. pIC50 was used as an independent variable to build a model using PLS, steric and electrostatic descriptors [14].

4.8.7 Partial least square analysis (PLS)

PLS analysis was carried out by comparing the regression analysis of the dependent variable and the independent variable of the dataset. PLS regression method was used to carry out the results of 3D-QSAR. Optimization of CoMFA and CoMSIA model was carried out by using the Leave-one-out (LOO) method (q^2), where the training set of the dataset predicted the activity of the model. PLS was also evaluated by using cross-validation method, the conventional coefficient (r^2), predicted correlation coefficient (r^2_{pred}), standard error of estimation (SEE) and an optimal number of components. Golbraikh and Tropsha concluded that the actual predictive power of generated QSAR model could be estimated by using external test set of the compounds which were not used for generation of QSAR model. The value of r^2_{pred} was calculated using test set of the compounds. Higher value of r^2_{pred} indicated that the predictive power of generated QSAR model was good. The ideal value of r^2_{pred} is more than 0.5 and indicated that the model is good.¹⁶⁴ In addition, N-fold validation is also carried out for all three alignment methods to generate 3D-QSAR models.

In 3D-QSAR, q^2 statistical value was most important which gave the prediction power of the model. With q^2 value more than 0.5, QSAR model was said to be considered as acceptable. Optimization of QSAR model column filtering should be at 0 kcal.mol⁻¹ which gave the exact results and least chance of correlation in the analysis.¹⁶³

In CoMFA analysis, pIC₅₀ values were used as a dependent variable, and CoMFA descriptors values were used as an independent variable. In CoMSIA analysis; steric, electrostatic, hydrophobic, HBD and HBA descriptors were used as independent variables and pIC₅₀ value was used as a dependent variable. Evaluation of CoMFA and CoMSIA models were done by determining the r^2_{pred} , based on the test set of molecules by the following equation.¹⁶⁵

$$r^2_{\text{pred}} = 1 - (\text{PRESS}/\text{SD})$$

where,

PRESS denotes as the sum of square deviation between predictive and experimental activities of the test molecules. SD denotes as the sum of square deviation between its biological activity of test molecules and activity in the mean of training molecules.

4.9 Result and Discussion

4.9.1 CoMFA analysis

In this present research, CoMFA models were generated by three different alignments methods. Results of the CoMFA model are shown in Table 16. Among three alignment methods, distill based alignment showed the best QSAR statistical data as compared to other two methods. A statistical parameter such as q^2 , r^2_{pre} , r^2_{cv} , r^2_{ncv} , F and SEE were found to be best in distill based alignment. q^2 was found to be 0.638 with six components by PLS analysis. The r^2_{pred} value of 0.653 indicated that the predictive power of the generated model was excellent. A PLS no-validation method gave r^2_{ncv} value of 0.971, F value of 99.852 and standard error estimation (SEE) value of 0.187. In addition, r^2_{cv} value of 0.637 indicated that internal predicted power of the model was good because the value was greater than 0.5. Bootstrap r^2_{bs} value of 0.978, stated the higher degree of assurance in the analysis. We also carried out N-fold validation and generated 3D-QSAR model. In distill based alignment, various statistical parameters includes r^2_{ncv} value of 0.969, F value of 110.675, SEE value of 0.166, r^2_{cv} value of 0.732, r^2_{bs} value of 0.990 and r^2_{pred} value of 0.848 (Table 16). In CoMFA analysis, the contribution values of steric and electrostatic were found to be 0.592 and 0.408,

respectively. Both values indicated contribution of steric and electrostatic properties in biological activities. The analytical capability of the CoMFA model was predicted by plotting the graph of experimental pIC_{50} and predicted pIC_{50} of all compounds as shown in Table 17. The value of the correlation coefficient (r^2) was found to be 0.970 as shown in Fig. 8a.

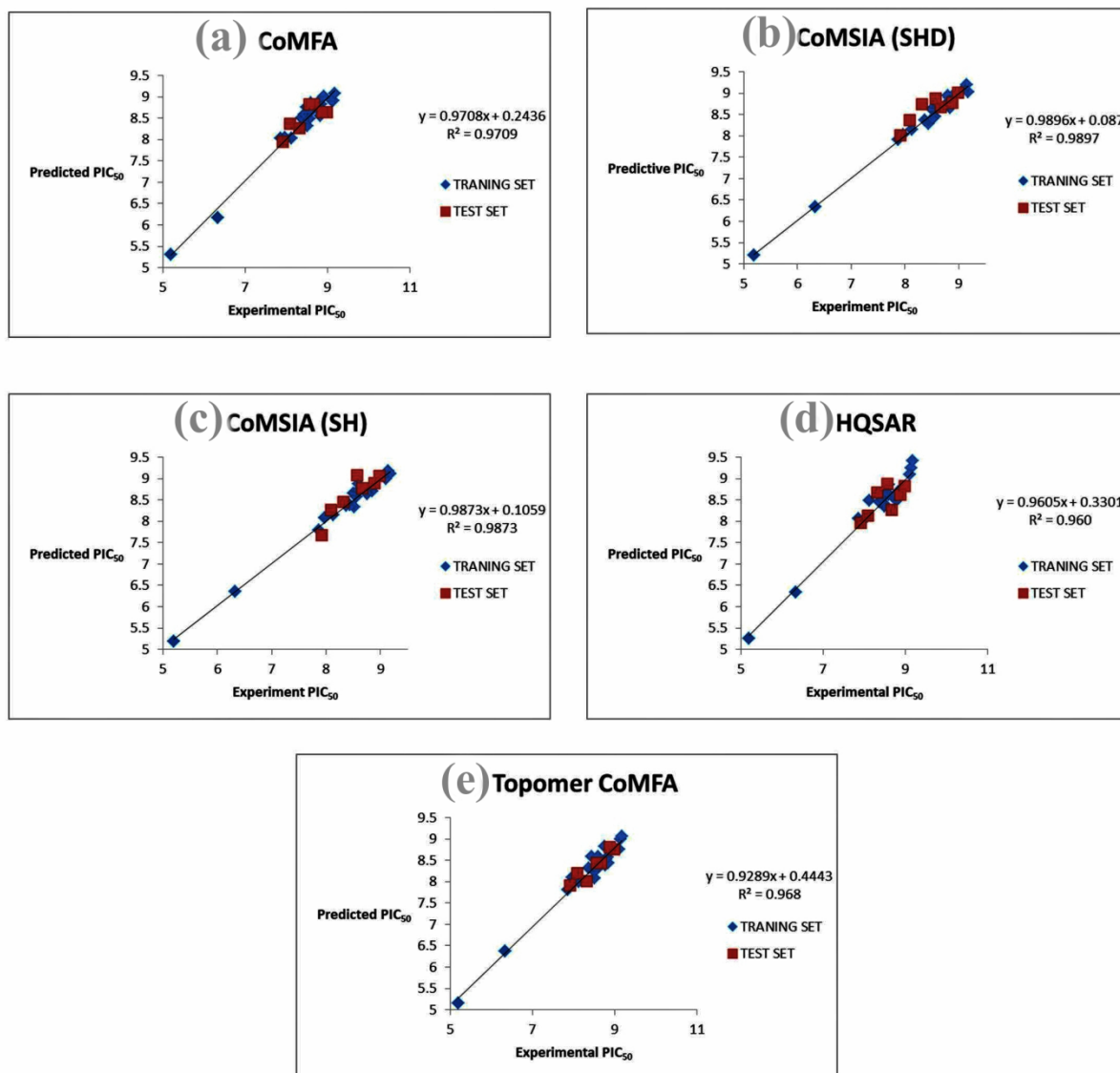


Fig 8. The plot of experimental versus predicted activity of training and test set based on: (a) CoMFA model; (b) CoMSIA model (SHD); (c) CoMSIA model (SH); (d) HQSAR model; (e) Topomer CoMFA model

4.9.2 CoMSIA analysis

The best CoMSIA model was generated by different 25 permutation and combination trials of all CoMSIA properties. A statistical comparison of 25 different combinations of CoMSIA model is shown in Fig. 9. Among all these combinations, SHD (Steric, Hydrophobic, and

HBD) and SH (Steric and Hydrophobic) showed best statistical data. CoMSIA (SHD) combination gave q^2 value of 0.796, r^2_{pred} value of 0.629, r^2_{ncv} value of 0.990, F value of 223.213, SEE value of 0.115, r^2_{cv} value of 0.824 and r^2_{bs} value of 0.993, while CoMSIA (SH) combination gave q^2 value of 0.761, r^2_{pred} value of 0.622, r^2_{ncv} value of 0.987, F value of 181.660, SEE value of 0.127, r^2_{cv} value of 0.746 and r^2_{bs} value of 0.995. The values of predictive r^2 (r^2_{pred}) of more than 0.5 proves that the predictive power of both SHD and SH CoMSIA models was acceptable (Table 16). The statistical results of N-fold validation of CoMSIA (SHD) included r^2_{ncv} value of 0.978, F value of 157.666, SEE value of 0.140, r^2_{cv} value of 0.786, r^2_{bs} value of 0.986 and r^2_{pred} value of 0.891, while in CoMSIA (SH) gave r^2_{ncv} value of 0.973, F value of 125.194, SEE value of 0.157, r^2_{cv} value of 0.750, r^2_{bs} value of 0.986 and r^2_{pred} value of 0.852 (Table 16). In CoMSIA analysis, the contribution values of steric, hydrophobic and HBD were 0.183, 0.595 and 0.222, respectively. All values indicated that steric, hydrophobic and HBD properties contributed in biological activities. The analytical capability of the both CoMSIA models were predicted by plotting the graph of experimental pIC_{50} and predicted pIC_{50} of all compounds as shown in Table 17. The value of the correlation coefficient (r^2) of both SHD and SH CoMSIA model were found to be 0.9897 and 0.9873, respectively as shown in Fig. 8b and 8c.

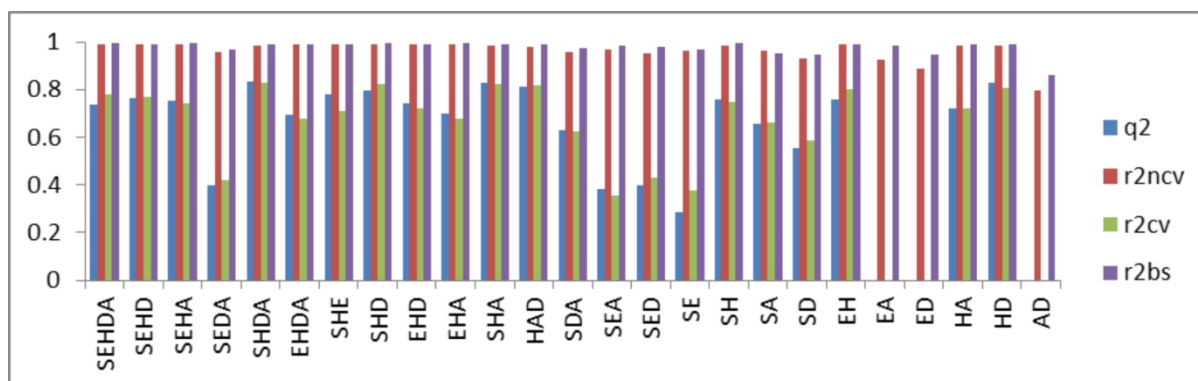


Fig 8. Statistical comparison of 25 different combinations of descriptors for the CoMSIA model.

Table 16. Statistical Parameters of a Comparative Study by Different Alignment Methods Using PLS Analysis.

Statistical Parameter	Alignment I (Distill based)			Alignment II (Pharmacophore-based)			Alignment III (Docking based)			Topomer CoMFA			
	CoMFA	CoMSIA		HQSAR	CoMFA	CoMSIA		HQSAR	CoMFA		CoMSIA		HQSAR
		(SHD)	(SH)			(SHD)	(SH)				(SHD)	(SH)	
NC	6	6	6	6	6	6	6	6	6	6	6	6	6
q ²	0.638	0.796	0.761	0.984	-0.256	-0.662	-0.339	0.992	-0.383	-0.666	-0.560	0.987	0.663
N-fold Statistical Validation													
r ² _{ncv}	0.969	0.978	0.973	0.972	0.994	0.985	0.985	0.945	0.965	0.982	0.968	0.941	0.967
r ² _{CV}	0.732	0.786	0.750	-	-0.260	-0.569	-0.796	-	-0.503	-0.748	-0.750	-	-
r ² _{pred}	0.848	0.891	0.852	0.887	-0.894	-0.912	-0.757	0.885	-0.478	-0.147	-0.345	0.883	-
SEE	0.166	0.140	0.157	0.160	0.071	0.118	0.115	0.223	0.247	0.203	0.101	0.231	0.160
F test	110.675	157.666	125.194	120.834	625.196	222.669	237.144	60.346	81.445	20.456	17.77	55.970	-
r ² _{bs}	0.990	0.986	0.986	-	0.996	0.986	0.992	-	0.979	0.998	0.989	-	-
Statistical Validation Based on splitting of test set and training set													
r ² _{ncv}	0.971	0.990	0.987	0.999	0.999	0.996	0.998	0.999	0.997	0.989	0.989	0.960	0.967
r ² _{CV}	0.637	0.824	0.746	-	-0.272	-0.760	-0.367	-	-0.323	-0.451	-0.505	-	-
r ² _{pred}	0.653	0.629	0.622	0.634	0.999	-0.542	-0.783	0.545	-0.320	-0.919	-0.249	0.557	-
SEE	0.187	0.115	0.127	0.049	0.031	0.075	0.050	0.225	0.058	0.117	0.119	0.226	0.160
F test	99.852	223.213	181.660	173.038	3101.743	531.579	1182.075	56.820	881.445	216.595	209.177	56.148	-

r_{bs}^2	0.978	0.993	0.995	-	1	0.998	0.999	-	0.999	0.996	0.995	-	-
Contribution													
Steric	0.592	0.183	0.238	-	0.514	0.211	0.344	-	0.324	0.201	0.372	-	-
Electrostatic	0.408	-	-	-	0.486	-	-	-	0.676	-	-	-	-
Hydrophobic	-	0.595	0.762	-	-	0.412	0.656	-	-	0.362	0.628	-	-
HBD	-	0.222	-	-	-	0.377	-	-	-	0.437	-	-	-
HBA	-	-	-	-	-	-	-	-	-	-	-	-	-

4.9.3 HQSAR analysis

HQSAR model was generated by test set molecules used in CoMFA and CoMSIA model optimization. In addition to this, the model was generated by using two characteristic parameters viz. fragment distinction and atom size. These two characteristic parameters were directly correlated with pIC_{50} values. Model optimization was carried out by different fragment distinction followed by atom sizes (as shown in Supporting Information Table - ST2 & ST3). The results of the HQSAR model was listed in Table 16. The optimum HQSAR model was developed by taking atom (A), bond (B), connection (C) and chirality (Ch) as fragment distinction and atom size as 4-7 with 6 as a no of components and 97 as a hologram length. Model showed a cross-validated r^2 (q^2) value of 0.984 with SEE value of 0.244 and a non-cross-validated r^2 (r^2_{ncv}) value of 0.999 with least SEE value of 0.049. The calculation of r^2_{pred} validated the predictive power of the generated HQSAR model. The r^2_{pred} value of generated HQSAR model was found to be 0.634. The statistical values of N-fold validation includes r^2_{ncv} value of 0.972, F value of 120.834, SEE value of 0.160, and r^2_{pred} value of 0.887 (Table 16). The analytical capability of HQSAR model was predicted by plotting the graph of experimental pIC_{50} and predicted pIC_{50} of all compounds shown in Table 17. The value of the correlation coefficient (r^2) of generated HQSAR model was found to be 0.960 as shown in Fig. 8d.

4.9.4 Topomer CoMFA analysis

In the topomer CoMFA, model was generated by splitting of the molecules into different fragments; aligning each fragment topomerically with the help of template molecule (compound 190) and calculation of steric and electrostatic descriptor for aligned fragments. Two fragments were used for the generation of topomer CoMFA model, which included R_1 and R_2 where, R_1 fragment was split into purine ring, while R_2 fragment was split into phenyl amine scaffold. These splitting patterns demonstrated that topomer CoMFA model produced better robustness with higher q^2 and high r^2 value followed by lower SEE. The result of topomer CoMFA is shown in Table 16. The model showed cross-validated r^2 (q^2) value of 0.663 with SEE value of 0.55 and non-cross-validated r^2 (r^2_{ncv}) value of 0.967 with SEE value of 0.16. The values of q^2 and r^2_{ncv} represented the portion of the variance in biological activity which was explained by the topomer QSAR. The correlation coefficient (r^2) value was generated from the values experimental pIC_{50} and Predicted pIC_{50} (Table 17) by plotting the graph. The value was found to be 0.968 as shown in Fig. 8e.

Table 17 Experimental and Predicted pIC₅₀ with Residual of Training and Test Sets using CoMFA, CoMSIA, HQSAR and Topomer CoMFA Models (Distill Alignment).

Compounds No.	pIC ₅₀	CoMFA		CoMSIA				HQSAR		Topomer CoMFA	
		Predicted	Residues	SHD		SH		Predicted	Residues	Predicted	Residues
				Predicted	Residues	Predicted	Residues				
170*	7.9208	7.945	-0.024	8.022	-0.1012	7.67	0.2505	7.959	-0.0382	7.91	-0.0108
171	8.3757	8.508	-0.132	8.363	0.0132	8.376	-0.0005	8.459	-0.083	8.31	-0.0657
172	7.8697	8.025	-0.1551	7.92	-0.0505	7.792	0.0772	8.069	-0.1993	7.81	-0.0597
173	8.5017	8.756	-0.2542	8.615	-0.1128	8.664	-0.1619	8.359	0.1428	8.25	-0.2517
174*	8.6635	8.822	-0.1589	8.668	-0.0041	8.767	-0.1039	8.274	0.3894	8.44	-0.2235
175	8.7721	8.856	-0.0843	8.748	0.0242	8.747	0.0253	8.497	0.2755	8.39	-0.3821
176	9.1445	8.904	0.2408	9.19	-0.0455	9.187	-0.043	9.246	-0.1016	8.99	-0.1545
177*	8.9872	8.632	0.3548	9.013	-0.0261	9.062	-0.0745	8.832	0.1549	8.75	-0.2372
178	8.8447	8.825	0.0198	8.657	0.1877	8.712	0.1331	8.536	0.3085	8.44	-0.4047
179*	8.8861	8.644	0.2424	8.768	0.118	8.892	-0.0057	8.626	0.2603	8.81	-0.0761

180	8.4413	8.591	-0.1495	8.287	0.1541	8.387	0.0541	8.528	-0.0868	8.59	0.1487
181	8.8239	8.548	0.2764	8.899	-0.0755	8.772	0.0517	8.692	0.132	8.57	-0.2539
182	7.9666	8.044	-0.077	8.033	-0.0668	8.074	-0.1078	8.001	-0.0341	8.09	0.1234
183	8.556	8.49	0.0659	8.446	0.1102	8.564	-0.0076	8.677	-0.1209	8.28	-0.276
184*	8.0931	8.362	-0.2692	8.366	-0.2733	8.276	-0.1826	8.138	-0.0453	8.2	0.1069
185	8.7959	8.686	0.1101	8.937	-0.1409	8.793	0.0032	8.496	0.3003	8.52	-0.2759
186*	8.317	8.273	0.0442	8.742	-0.4252	8.457	-0.1397	8.666	-0.349	8.02	-0.297
187	8.5186	8.313	0.2058	8.404	0.1145	8.336	0.1825	8.382	0.1367	8.08	-0.4386
188*	8.567	8.834	-0.2673	8.884	-0.3168	9.073	-0.506	8.882	-0.3145	8.44	-0.127
189	8.6003	8.652	-0.0515	8.756	-0.1553	8.876	-0.2758	8.627	-0.0267	8.59	-0.0103
190	9.1746	9.076	0.0984	9.029	0.1459	9.113	0.0612	9.422	-0.2474	9.06	-0.1146
191	8.5918	8.867	-0.2753	8.637	-0.0452	8.723	-0.1311	8.854	-0.2627	8.43	-0.1618
192	8.752	8.839	-0.0869	8.707	0.0452	8.633	0.1186	8.612	0.1397	8.82	0.068
193	8.9208	9.007	-0.0864	8.973	-0.0522	8.945	-0.0246	8.756	0.1653	8.78	-0.1408

194	9.1024	8.911	0.1913	9.104	-0.0014	8.998	0.1045	9.1	0.0025	8.75	-0.3524
195	8.1284	8.029	0.0997	8.152	-0.0234	8.149	-0.0207	8.484	-0.3559	7.99	-0.1384
196	6.327	6.169	0.1583	6.341	-0.0136	6.364	-0.0367	6.345	-0.0177	6.37	0.043
197	5.1918	5.306	-0.1145	5.204	-0.0119	5.193	-0.0014	5.259	-0.0669	5.15	-0.0418

4.9.5 Contour map analysis

3D-QSAR contour maps are one of the important analysis which give information about the favourable and disfavorable regions of the molecules for biological activity. Change in the structural substitution on core moiety resulted in the change in ADME properties, which might increase or decrease the biological activity of the molecule.

4.9.5.1 CoMFA contour maps analysis

Steric and electrostatic contour maps of the CoMFA model is shown in **Fig. 10**. CoMFA steric contour map (**Fig. 10a**) showed combination of 80% of green and 20% of yellow contribution in contour map with compound **190**. Green contours indicated that a steric contribution increased potency of molecule, while the yellow contours indicated the steric hindrance which decreased potency of compound. This relationship explained that terminal position in series of compounds were responsible for the biological activity. Terminal position of compound **190** ($IC_{50} = 0.669$ nM) consisted caynobenzene derivative which was favourable due to steric bulk of phenyl ring, while in compound **197** ($IC_{50} = 6430$ nM) consisted methyl ($-CH_3$) group which was sterically unfavourable due to less bulk. An absence of a bulky group at the terminal side of the molecule resulted in decreased in potency of the molecule. Similarly, in compound **196** ($IC_{50} = 471$ nM), cyclopropyl substitution improved activity while in compound **195** ($IC_{50} = 7.44$ nM), phenyl group with isopropyl substitution supported further increased bulkiness at the terminal position of the molecule which lead to increase in biological activity. CoMFA electrostatic contour map is shown in **Fig. 10b** which indicated red (20%) and blue (80%) contours. A blue colour region is favourable for the positively charged group while the red colour region is favourable for negatively charged groups. CoMFA electrostatic contour maps concluded that combination of positively charged group and negatively charged group were responsible for potent activity. It was proved by compound **190** ($IC_{50} = 0.669$ nM) where the presence of cyanide ($-CN$) substituted phenyl ring acts as negatively charged and positively charged respectively, while in compound **197** ($IC_{50} = 6430$ nM) only methyl group was present. Here, absence of negatively charged atom lead to decrease in the potency of compound **197**. The compounds also confirmed the relationship between red contours with the potency of the compound in the series. Compound **190** ($IC_{50} = 0.669$ nM) was found to be more potent than compound **195** ($IC_{50} = 7.44$ nM). Compound **190** consisted 3-cyano group ($-CN$) at R^2 substitution with having negative charged which resulted into higher activity than compound **195**, which

consisted of 3-isopropyl group at the R² position having positive charge and lead to decrease in biological activity.

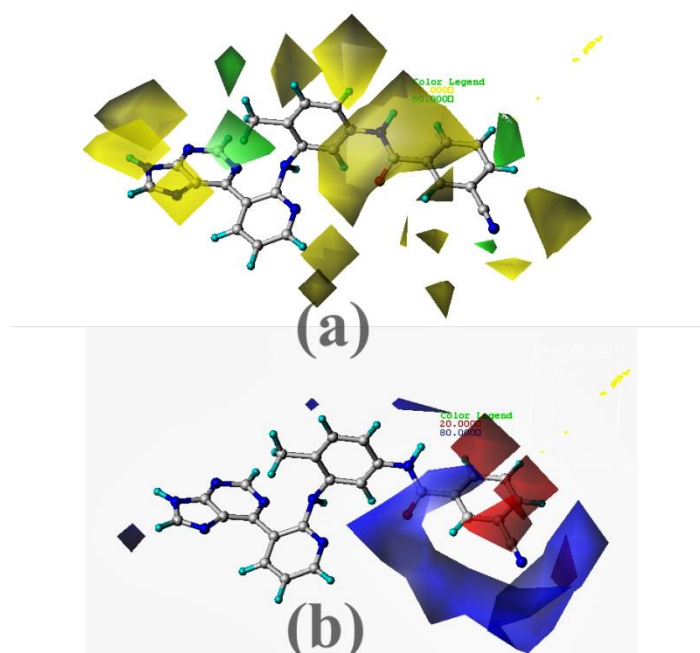


Fig 10. CoMFA contour map analysis: (a) Steric contour maps; (b) Electrostatic contour maps.

4.9.5.2 CoMSIA contour maps analysis

Contour maps of CoMSIA are shown in **Fig. 11**. CoMSIA steric contour maps (**Fig. 11a**) along with most active compound **190** showed similar results like CoMFA contour maps. Therefore, discussion or analysis for these two contour maps would be the same as CoMFA contour maps analysis.

Hydrophobic contours explained that yellow and grey contours stand for hydrophobic and hydrophilic groups respectively as shown in **Fig. 11b**. In compound **190** ($IC_{50} = 0.669$ nM), position L amide linkage ($-CONH-$) contained carbonyl group which gave positive contribution for hydrophobic functional group, whereas in compound **182** ($IC_{50} = 10.8$ nM) with $-NHCO-$ (reverse amide) which lead to $-NH-$ group instead of carbonyl group leading to decrease in activity. Compound **190** (IC_{50} 0.669 nM) consisted of phenyl ring at terminal side of the molecule which contributed to increase in hydrophobicity of the molecule and ultimately lead to increased activity, while in compound **197** (IC_{50} 6430 nM), presence of $-CH_3$ group with less hydrophobic property as compared to the phenyl ring lead to decrease in potency of the molecule. Compound **197** ($IC_{50} = 6430$ nm), **196** ($IC_{50} = 471$ nM), **195** ($IC_{50} =$

7.44nM) indicated that as the hydrophobicity of the molecule increases the potency of the compound gradually increases. Grey contour map indicated favourable for hydrophilic groups. In compound **190**, R² position contained 3-CN group which showed hydrophilic nature, while in case of compound **189** (IC₅₀ = 2.51 nM), presence of 3-CF₃ acted as a hydrophobic group which lead to decreases in potency of the compound.

Hydrogen bond donor (HBD) contour maps (**Fig. 11c**) explained that cyan colour indicated favourable positions for the HBD groups while the purple colour indicated unfavourable for the HBD groups. In compound **190** (IC₅₀ = 0.669 nM), purple colour contour map presented on –NH– group of amide functional group while cyan colour presented on carbonyl group of amide which indicated that –CONH– group was favourable for the HBD which lead to increase in the potency of the compound, while in case of compound **176** (IC₅₀ = 0.717 nM), instead –CONH– group, –NHCO– group was present which lead to slight decrease in the potency of the compound **176** compared to compound **190**.

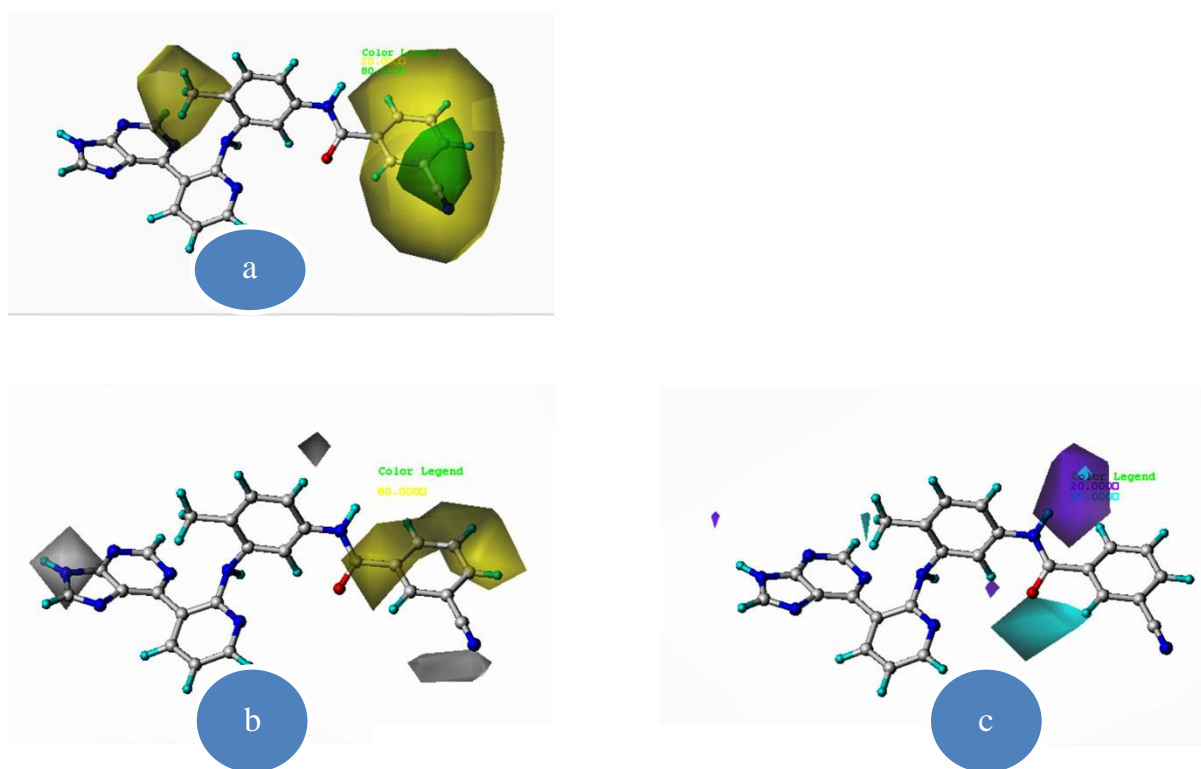


Fig 11. Contour maps of CoMSIA analysis: (a) Steric; (b) Hydrophobic; (c) Hydrogen bond donor (HBD);

4.9.5.3 HQSAR contribution maps

Useful properties were derived from HQSAR model to contribute an individual atom of the molecule in the biological activity. HQSAR gave information on those structural fragments,

which could be useful for structure optimization as shown in **Fig. 12**. HQSAR contribution maps are shown in **Fig. 13**. In the contribution maps, role of individual atom on biological activity was reflected by colours. Green or yellow colour on the contribution maps showed positive contribution; while the presence orange and red colour indicated negative contribution. Fragments or atoms showed intermediate contribution in the biological activity were exhibited by white colour.

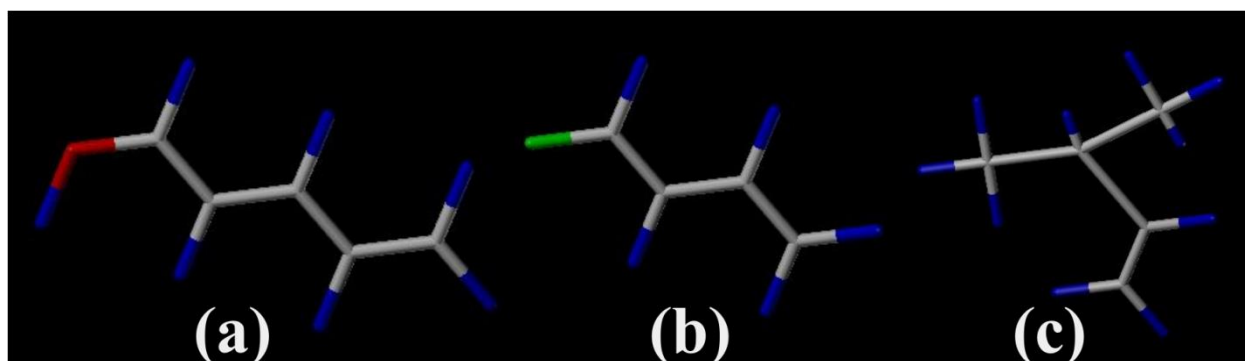


Fig 12. Important fragments of purinylpyridine derivatives obtained from HQSAR model.

Contribution maps of the most active compound **190** and least active compound **197** as B-Raf inhibitors are shown in **Fig. 13a** and **13b**, respectively. It was observed that both structures contained 2-arylamino-3-purinylpyridine as a common structural fragment, which was reflected by yellow and green colours because they were essential to all molecules. Comparing the contribution analysis of most potent compound (**190**, $IC_{50} = 0.669$ nM) as well as of least potent compound (**197**, $IC_{50} = 6430$ nM); the study showed that, presence of bulkier groups on terminal side of compound was responsible for biological activity. In compound **190**, cyanide substituted aryl ring linked with amide group on the terminal side of the molecule, which showed intermediate contribution in biological activity due to the presence of white colour. In compound **197**, methyl group was directly linked with the amide linkage on the terminal side and gave negative contribution to biological activity due to the presence of red colour on the methyl group. This contribution analysis were also proved by CoMFA and CoMSIA steric as well as electrostatic contour map analysis where the presence of bulker group on terminal side lead to the increase in biological activity, while the presence of the negatively charged group as a substitution on bulker group showed an increase in the biological activity. In compound **190**, presence of the cyanide substitution on phenyl ring at terminal side of the molecule was responsible for the good biological activity, while in

compound **197**, presence of less bulky group as well as positively charge group reduced biological activity.

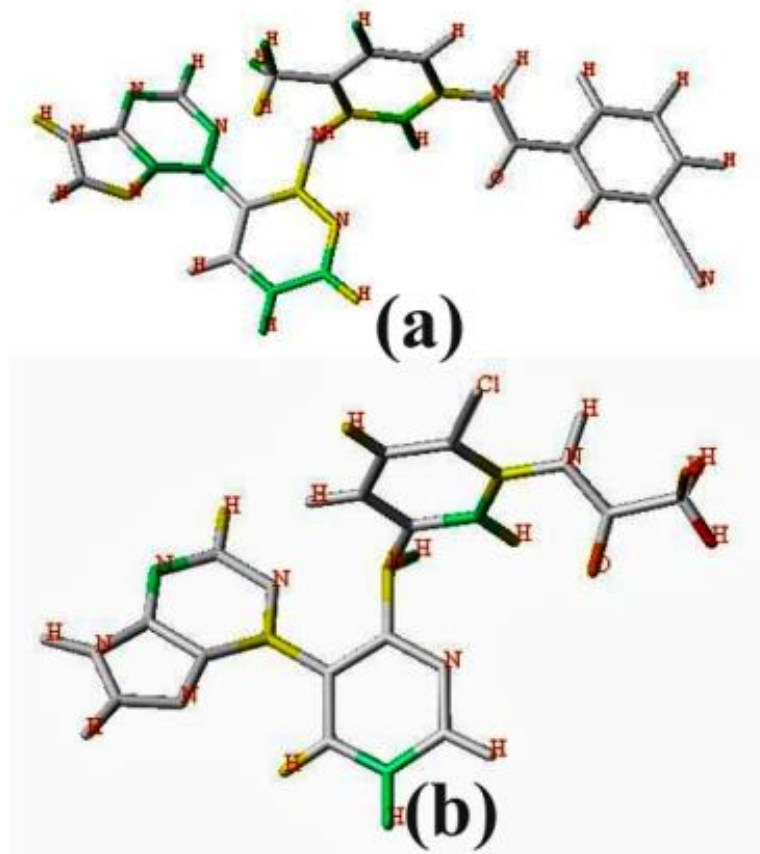


Fig 13. Atom contribution map for: (a) Compound **190**; (b) Compound **197**. The green or yellow colour indicates that positive contribution while grey or white colour indicates intermediate contribution in the biological activity.

4.9.5.4 Topomer CoMFA contour analysis

Contour maps of topomer CoMFA model were same as of CoMFA contour maps. Topomer CoMFA contour maps gave information about which splitting part of the molecule affected biological affinity. The highest active compound **190** and least active compound **197** were utilized for comparison study of CoMFA and Topomer CoMFA. The splitting part of R^1 and R^2 are shown in **Fig. 14**. The steric contour maps showed yellow colour for disfavorable groups, while green colour was showed for favourable for biological activity. Similarly, in electrostatic contour maps, blue and red colour indicated positively and negatively charged groups, respectively. **Fig. 14a** showed steric and electrostatic contour maps of Compound

190 and **197** of R¹ fragment. Similarly, **Fig. 14b** showed steric and electrostatic contour maps of R² fragment.

The contour maps analysis of R¹ fragment (**Fig. 14a**) did not show any significant contribution in both types of contour maps viz. steric as well as electrostatic because R¹ fragment contained purine ring, which was present as a core scaffold in the series of all compounds. The R¹ electrostatic contour maps did not show any colour contribution. Based on the analysis of R¹ contour maps we concluded that the core ring scaffold showed a neutral contribution in the biological activity.

Fig. 14b showed steric and electrostatic contribution of the R² fragment. On the terminal side of the compound **190** (IC₅₀ = 0.669 nM), the green colour contribution was more prominent as compared to substituted phenyl ring. Similarly, yellow colour contributions was more in the least potent compound **197** (IC₅₀ = 6430 nM) on the terminal side of the methyl group. The comparison of steric contour maps analysis of R² fragment with potent and least potent compound concluded that the presence of a bulkier group on the terminal side of the molecules was responsible for biological activity. In compound **190**, on the cyano-substituted phenyl ring, the presence of green contour map showed increased in the biological affinity, while in compound **197**, yellow contour map showed on methyl group which reduced the biological activity.

Electrostatic contour map analysis of the R² fragment showed that in compound **190**, the presence of the negatively charged group on phenyl ring was favourable for the biological activity. Compound **197** showed red colour contour map on the terminal side of the methyl group, which gave a negative correlation in the biological activity.

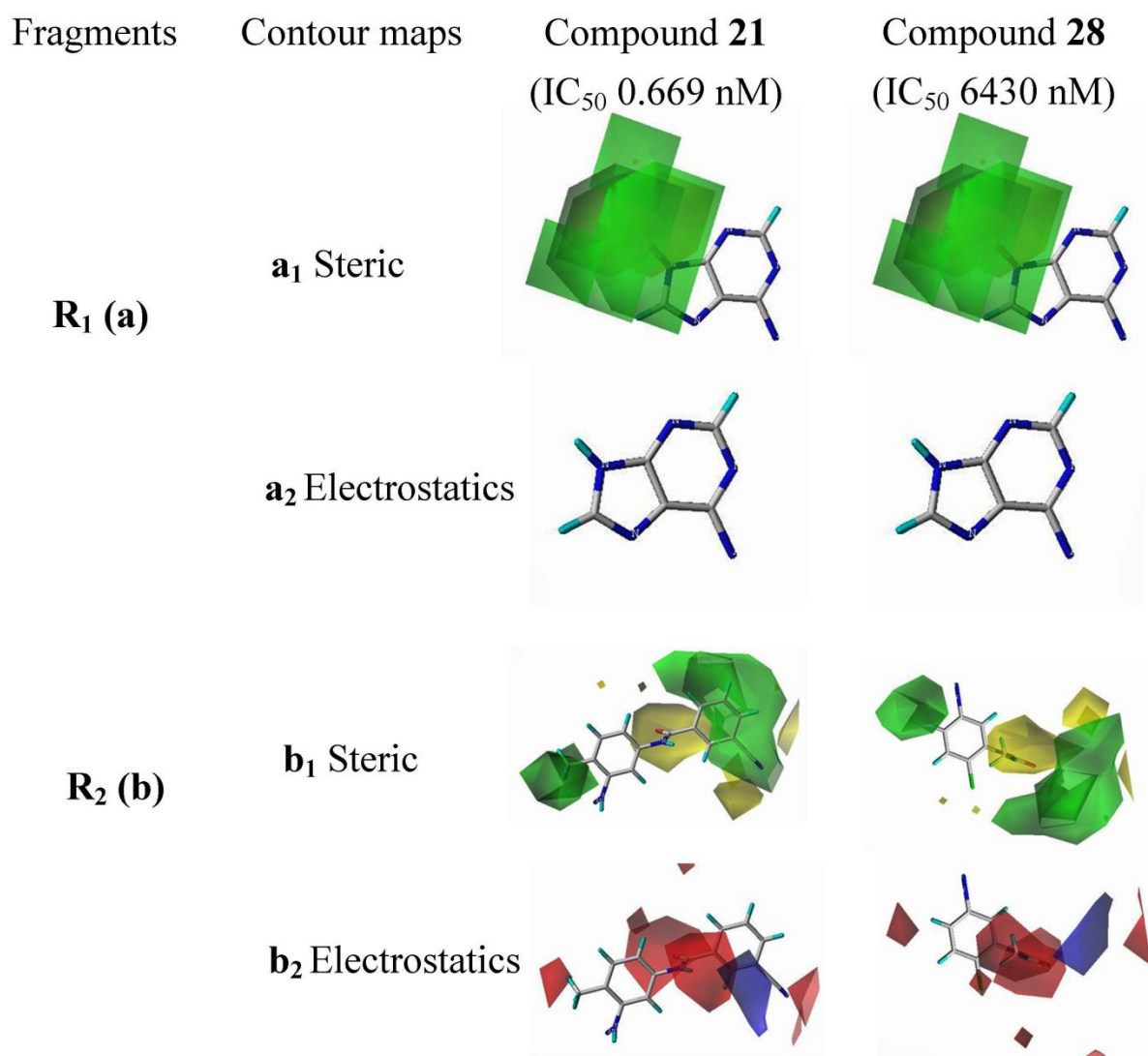


Fig 14. 3D contour maps of Topomer CoMFA model for: (a) R¹; (b) R² of potent compound **190** (IC₅₀ = 0.669 nM) and least potent compound **197**, (IC₅₀ = 6430 nM). **a1** and **b1** shows steric contour maps, while **a2** and **b2** shows electrostatic contour maps. Colour coding of all these contour maps were same as CoMFA and CoMSIA steric and electrostatic contour maps.

4.9.6 Overall outcome of 3D-QSAR

3D-QSAR analysis on purinylpyridine series gave an idea regarding design of novel derivatives as B-Raf inhibitors in the treatment of melanoma cancer. Results of contour maps analysis of compound **190** gave an idea that on terminal side, -CONH- linkage was crucial for B-Raf inhibitory activity. Incorporation of the bulky groups on both sides of -CONH- linkage were suitable for the kinase inhibitory activity. The novel molecule could be designed which have HBD, and HBA functional groups adjacent to each other and both groups could be

linked with bulky groups. Based on 3D-QSAR analysis, we concluded that novel molecule could be designed in such a way that during orientation of the design novel molecules, the core scaffold went inside the kinase domain of the protein. The outcomes of this research work was incorporated in the most active compound **190** of this series and is shown in **Fig. 15**, which could be useful to understand whole study and to design the novel molecules as B-Raf inhibitors for the treatment of melanoma cancer in future.

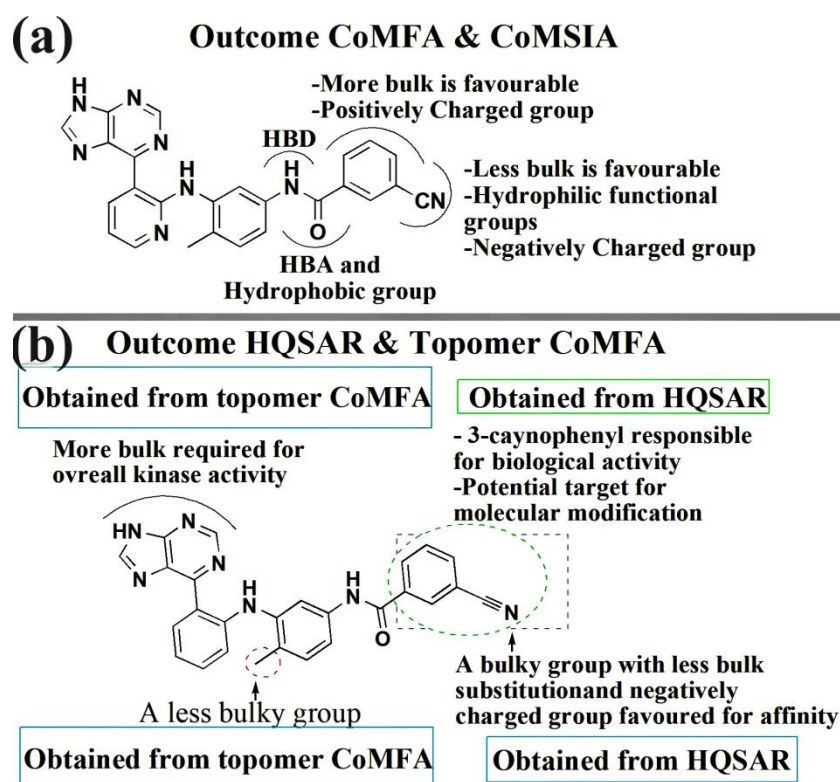


Fig. 15 General outcome of 3D-QSAR study: (a) CoMFA & CoMSIA contour maps output; (b) output of HQSAR contribution maps and Topomer CoMFA contour maps.

7.1 *In Vitro* Pharmacological Screening

7.1.1 Cell Viability Assays

Cell-based assays are widely used to check the potency of design compounds on cell proliferation or for their cytotoxic effects. The major principle of cell based assays are measuring of receptor binding, expression of gene or protein, trafficking of cellular constituents, or monitoring of cell functions. There are different types of cellular assay methods used to determine the number of viable eukaryotic cells at the end of experiment. These methods include: tetrazolium reduction, resazurin reduction, protease markers, and ATP detection.¹⁶⁹

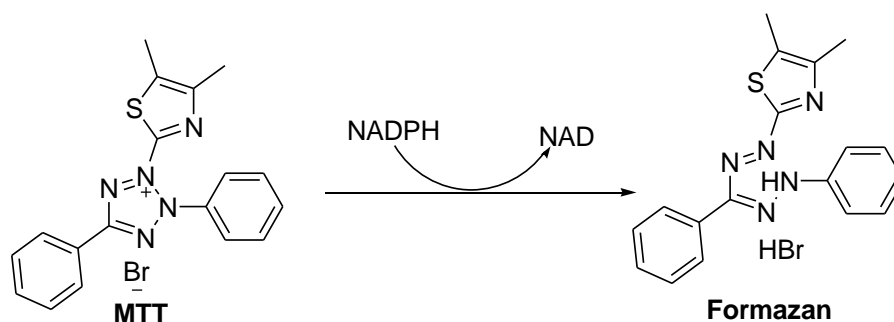
These methods are used to measure general metabolism or enzymatic activity in viable cells. In these types of assays, incubation of reagent with cells, which leads to formation of the colour or fluorescent product that can be analysed by plate reader. In all types of cell-based assay, methods the absorbance of results are directly correlated with number of cells are present.¹⁷⁰⁻¹⁷²

7.1.2 Tetrazolium Reduction Assay

Different types of tetrazolium compounds have been used for the detection of eukaryotic cells. Most commonly used compounds include 3-(4,5-dimethylthiazol-2-yl)-2,5-diphenyltetrazolium bromide (MTT), 3-(4,5-dimethylthiazol-2-yl)-5-(3-carboxymethoxyphenyl)-2-(4-sulfophenyl)-2H-tetrazolium (MTS), 2,3-Bis-(2-methoxy-4-nitro-5-sulfophenyl)-2H-tetrazolium-5-carboxyanilide salt (XTT), and 2-(4-Iodophenyl)-3-(4-nitrophenyl)-5-(2,4-disulfophenyl)-2H-tetrazolium (WST-1). All these compounds are divided into two basic categories based on its charge formation: 1) Positively charged, and 2) Negatively charged. MTT is a positively charged compound and easily penetrates eukaryotic cells and MTS, XTT, and WST-1 are negatively charged compounds which are not easily penetrate in cells. The negatively charged compounds are used with electron acceptor intermediates and that can be transfer electrons from the cytoplasm or plasma membrane which helps the reduction of tetrazolium into formazan and formation of colour.¹⁷¹

7.1.2.1 MTT Tetrazolium Assay

The MTT tetrazolium assay was the first cell viability assay developed in 96 well plate which was suitable for HTS technique. The MTT is prepared in growth medium, added into the 96 well plate containing cells, and incubate for 1 to 4 hours. The quantity of formazan is measured by taking absorbance at 575 nm using ELISA plate reader. The cellular mechanism of the formation of formazan crystals depends upon the presence of mitochondrial enzyme dehydrogenase.¹⁷³



Due to the accumulation of MTT, the formazan crystals are insoluble inside the cells and in the growth medium. So, formazan crystals are mandatory to solubilize before recording absorbance readings. Various solubilization methods are used to dissolve formazan crystals. Various solubilization methods includes acidified IPA, DMSO, DMF, and combination of detergent and organic solvent.

The amount of signal generated is depends upon several parameters which includes the concentration of MTT, length of incubation period, the number of viable cells and their metabolic activity.

7.2 Materials and Methods

7.2.1 Materials

7.2.1.1 Reagents

Trypan blue Dye (Hyclone)

DMSO cell culture grade (SRL)

Trpsin 1X Gamma irradiated (Himedia)

FBS (Fetal Bovine Serum, South American origin) (Himedia)

DMEM (Dulbecos Modified Eagels medium, high glucose with glutamine) (Himedia)

IPA (Iso Propyl alcohol) (SRL)

MTT dye

7.2.1.2 Glassware and Plastic wares

96-well microtiter plate (Flat Bottom, U Bottom, V Bottom),

Tissue culture flasks (75 cm² T Flask vented and 150 cm² T Flask vented),

Falcon tubes (15 ml, 50 ml), Cryotubes (2ml).

Micro tips (Blue 1000 µl, Yellow 200 µl, White 10µl (Volex).

Centrifuge tubes (1.5 ml, 2.0 ml)

Haemocytometer cell counting chamber.

7.2.1.3 Description of cell lines used in the cytotoxicity study

Organism: Homo sapiens (human)

Tissue: skin; malignant melanoma

Morphology: epithelial

Growth properties: adherent

Medium: Culture Medium: DMEM (high glucose), 10% fetal bovine serum (FBS).

7.2.2 Experimental Protocol

Cells were grown in DMEM media in T25/T75 flask and incubate in CO₂ incubator at 37°C.

The flask was confluent with cells and indicated that cells are ready for plating.
Counting of cells play an important role in this assay
Ideally 10,000 cells were added in each 96 well plate and incubate for 24 h.

After 24 h, all synthesized compounds were added in different series of concentration.
All compounds were used in doublet and incubate for 48 h.

MTT was added after 48 h and plate was incubated for 4 h for the formation of formazon crystal and dissolve in DMSO.
Absorbance was taken at 575 nM.

7.3 Results and Discussion

All synthesized benzoxazole derivatives were evaluated for cancer cell line A375 (melanoma). These compounds were also screened for *in-vitro* toxicity studies on HEK293T (normal kidney cell line). All compounds with their IC₅₀ values are reported in

Table 23. All compounds were found to be non-toxic on normal kidney cell line (HEK293T) with IC₅₀ value of >100 μM.

Table 23: Anti-proliferative activity of synthesized compounds with their IC₅₀ value

Compound No.	Compound Code	IC ₅₀ (μM)	
		A375	HEK293T
202a	HB-JC-01	>100	>100
202b	HB-JC-02	>100	>100
202c	HB-JC-03	<1	>100
202d	HB-JC-04	<1	>100
202e	HB-JC-05	3.9	>100
202f	HB-JC-06	6.7	>100
202g	HB-JC-07	48.78	>100
203a	HB-JC-101	<1	>100
203b	HB-JC-102	18.66	>100
203c	HB-JC-103	>100	>100
210a	HB-JC-201	9.36	>100
210b	HB-JC-202	28.8	>100
210c	HB-JC-203	26.09	>100
210d	HB-JC-204	59.59	>100
210e	HB-JC-205	10.76	>100
211a	HB-JC-206	3.53	>100
211b	HB-JC-301	66.75	>100
211c	HB-JC-302	9.64	>100
211d	HB-JC-303	4.68	>100
211e	HB-JC-304	2.34	>100
211f	HB-JC-305	3.23	>100
	Sorafenib	6.22	>100
	5-FU	0.004	>100

8. *In-Vivo* Pharmacological Screening:

8.1 Material and Methods

8.1.1 Protocol Approval

All *in-vivo* experiments were performed in compliance with relevant laws and institutional guidelines. In present research work, the Institutional Ethics Committee (IAEC) of Institute of Pharmacy, Nirma University permitted to work on in-vivo animal study. (vide Protocol Number IP/PCEM/MPH/23/2018/013).

8.1.2 Induction of Skin Cancer¹⁷⁴

Female Swiss-albino having the weight of 25-30 gm were chosen for the study. All animals were maintained under controlled temperature (25 ± 2 °C), humidity ($55 \pm 5\%$) and 12 hours light-dark cycle as per the CPCSEA guidelines.

Female Swiss-albino mice were kept for 1 week for adjustment period. During this period simultaneously, all mice were treated with hair removal cream to remove the hairs from the caudal region of skin of its back. After removal of skin, all mice were held for 2 days to understand the condition and all mice were divided into 5 groups, six animals.

5 groups are divided as following:

NC- Normal control animals given only Vehicle.

DC- Skin cancer induced animals applied with DMBA and Croton oil to induce disease.

Standard- Disease induced animals treated with 5% 5-FU solution.

Compound HB-JC-206 Disease induced animals treated with 5% solution of the sample Compound HB-JC-206.

Compound HB-JC-304 Disease induced animals treated with 5% solution of the sample Compound HB-JC-304.

Skin cancer was induced by applying 50 μ l solution of 1mg/ml concentration (5mg of DMBA in 5 ml Acetone) DMBA by topical route of administration on caudal region of skin. The application of DMBA on mice was given twice in a week for two weeks. After completion of the two weeks of DMBA application, 1% croton oil solution (in acetone) was applied thrice in a weeks from 3rd to 16th week. On the 7th week of the model, the drug treatment was started and continue till 16th week. The washout period between application of drug/compounds and croton oil with the gap of 1 hour.

8.1.3 Tissue and Serum Preparation

At the end of the 16th week, blood was collected from the retro orbital from each mice and evaluated for various biochemical parameters. After blood collection, all mice were euthanized with the help of diethyl ether, sacrifice and caudal region was collected, stored in 10% v/v of formalin for histopathological study. After sacrifice the animals collected blood samples were centrifuge in refrigerate centrifuge at 10000 RPM for 10 minutes at 4°C. After completion of this process supernatant was collected and stored at -20°C. These serum samples were used to evaluate various biochemical parameters.

The collected caudal region skin tissues were homogenate with the help of phosphate buffer (pH 7.4). 500 mg of tissue samples were subjected to homogenization with 5 ml of phosphate buffer in homogenizer. Apart from this 2 ml of homogenate was collected for to check Malondialdehyde (MDA) level and remaining homogenates were centrifuge in refrigerate centrifuge at 10000 RPM for 10 minutes at 4°C. After completion of this process supernatant was collected and stored at -20°C. These serum samples were used to evaluate various tissue parameters.

8.1.4 Measurement of the various parameters

8.1.4.1 Biochemical Parameters

Various biochemical parameters were performed to measure the effectiveness of the treatment.

8.1.4.1.1 Serum Lactate Dehydrogenase (LDH) Level

Principle

Lactate is oxidised into pyruvate in the absence of oxygen. Due to anerobic condition this conversion occurs in presence of NAD with the help of LDH enzyme. Rate of conversion of NAD to NADH is directly correlated with the presence of LDH enzyme. LDH parameter was performed using LDH-SLR Kinetic kit, which was procured from ACCUCARE.

Reagents

1. Reagent I (Buffer): Imidazol (65mmol/L), Pyruvate (0.6 mmol/L)
2. Reagent II (Substrate): NADH (0.18 mmol/L)

Procedure

Working reagent was prepared by mixing reagent I and reagent II in the ratio of 9:1. Add 1 ml of this reagent solution followed by adding 25 µl of blood serum and incubated for 1 min. measure the change in the absorbance for 2 min at 320 nm. The enzyme activity was calculated with help of following equation.

LDH Activity (U/L) = $\Delta A/\text{min} * 6592$

8.1.4.1.2 Serum Gamma Glutanyl Transferase (GGT) Level

Principle

Gamma-glutamyl transferase is a cellular enzyme present in various body parts includes kidney, pancreas, liver, and prostate. Measurement of Gamma-GT is widely useful to check the liver functioning. The key principle Gamma-glutamyl is transfer red colour from gamma-glutamyl-*p*-nitroanilide to glycylglycine by Gamma-GT (Gamma-Glutamyl-Transferase). The *p*-nitro aniline formed absorbs at 405nm. The amount of *p*-nitro aniline formed is directly proportional to Gamma-GT activity.

Reagent

Reagent I: Buffer reagent

Reagent II: Substrate reagent

Procedure

Working reagent was prepared by mixing reagent I and reagent II in the ratio of 4:1. Add 1 ml of this reagent solution followed by adding 100 μl of blood serum and incubated for 1 min. measure the change in the absorbance after 1, 2, and 3 min at 405 nm. The enzyme activity was calculated with help of following equation.

Gamma GT (U/L) = $\Delta A/\text{min} * 1640$

8.1.4.1.3 Serum C-Reactive Protein (CRP) Level

Principle

CRP is an acute-phase protein present in normal serum. The levels of serum CRP increases significantly after forms of tissue, bacterial and viral infection, and malignant neoplasia. The principle behind this assay is a quantitative turbidimetric test. In human serum latex particles are coated with CRP protein. When CRP is agglutinated with sample, which leads to change in the absorbance.

Reagent

Diluent (R1): - Tris buffer 20 mmol/L, Ph 8.2. sodium azide 0.95 g

Latex (R2): - Latex particles coated with goat IgG anti-human CRP

Calibrator: - pH 7.3. sodium azide 0.95 g/L Human serum.

Procedure

Working reagent was prepared by mixing reagent I (R1) and reagent II (R2) in the ratio of 9:1. Add 1 ml of this reagent solution followed by adding 1 ml of blood serum, incubated for 10 minutes, and measure the absorbance at 540 nm after 10 seconds (A1) and after 2 minutes (A2). The enzyme activity was calculated with help of following equation.

$$\text{CRP (mg/L)} = \frac{(A2-A1)_{\text{sample}}}{(A2-A1)_{\text{calibrator}}} * \text{Calibrator concentration}$$

8.1.4.1.4 Malondialdehyde (MDA) level**Principle**

The method estimates MDA the product of lipid peroxidation process. One molecule of MDA reacts with two molecules of thiobarbituric acid (TBA) under mildly acidic conditions to form a pink coloured chromogen, whose intensity was measured colorimetrically at 535 nm. The MDA was assayed in the tissue homogenate in the form of thiobarbituric acid-reactive substances (TBARS) and expressed as nanomols of MDA per milligram of protein.

Reagents:

1. Sodium lauryl sulphate (SLS) (8%) - 8 gm of SLS in 100 ml of distilled water.
2. Acetic acid (20%) - Prepared in 0.27 M hydrochloric acid (2.29 ml HCL in 100 ml water)
3. Thiobarbituric acid (TBA) (1% in Tris hydrochloride, pH 7): (Freshly prepared) - 1gm of thiobarbituric acid in 100 ml of Tris hydrochloride buffer pH 7.

Note: Thiobarbituric acid solubilized in Tris-HCl by exposing the solution to hot steam under

the water bath for 5-10 min or by constant sonication for 30 min.

Blank	Test
0.2 ml of distilled water	0.2 ml of homogenate
0.2 ml of SLS	0.2 ml of SLS
1.5 ml of acetic acid in HCl	1.5 ml of acetic acid in HCl
1.5 ml TBA	1.5 ml TBA
0.6 ml distilled water	0.6 ml distilled water
Heated for 45 min in water bath at 95 °C and cool	
1 ml of distilled water	1 ml of distilled water
5 ml mixture of n-butanol + pyridine (15:1)	5 ml mixture of n-butanol + pyridine (15:1)

8.1.4.1.5 Reduced Glutathione (GSH) Level

Principle:

Glutathione consists of sulfhydryl groups. 5, 5- dithiobis 2- nitro benzoic acid (DTNB), a disulphide compound, gets readily attacked by these sulfhydryl groups and forms a yellow coloured anion 5-thio 2-nitrobenzoic acid which measured colorimetrically at 412 nm.

Reagents:

1. Trichloroacetic acid (TCA) (10%) - 10 gm of TCA in 100 ml of distilled water.
2. 0.3 M Na₂HPO₄ - 4.26 gm of Na₂HPO₄ in distilled water.
3. DTNB (Fresh) - 40 mg in 100 ml of 1% sodium citrate and covered with aluminium foil.

Procedure

Blank	Test
0.2 ml of distilled water	0.2 ml of supernatant homogenate
1.0 ml of TCA (10%)	1.0 ml of TCA (10%)
Mixture was kept in ice bath for next 30 min and then centrifuge for 10 min at 4 °C at 3000 RPM	
0.5 ml Supernatant	0.5 ml Supernatant
2.0 ml disodium hydrogen phosphate	2.0 ml disodium hydrogen phosphate
0.25 ml DNTB	0.25 ml DNTB

8.1.4.1.6 Superoxide dismutase (SOD) level

Principle:

The O₂⁻ substrate for SOD is generated indirectly in the oxidation of epinephrine at alkaline pH. As O₂⁻ builds in the solution, the formation of adrenochrome accelerates because O₂⁻ also reacts with epinephrine to form adrenochrome. Toward the end of the reaction, when the epinephrine is consumed, the adrenochrome formation slows down. If observed for long times, the adrenochrome disappears and insoluble brown, products form in the solution. SOD reacts with the O₂⁻ formed during the epinephrine oxidation and therefore slows down the rate of formation of the adrenochrome as well as the amount that is formed. Because of this slowing process, SOD is said to inhibit the oxidation of epinephrine.

Reagents:

1. EDTA – 0.0001 M (9.3 mg/250 ml)
2. Carbonate buffer – pH 9.7 (8.4 gm NaHCO₃ + 10.6 gm Na₂CO₃ in 500 ml)
3. Epinephrine – 0.003 M (50 mg/100 ml in HCL (pH 2) and covered with aluminium foil.

Procedure

Blank	Test
0.2 ml of distilled water	0.2 ml of supernatant homogenate
0.1 ml of EDTA	0.1 ml of EDTA
0.5 ml carbonate buffer	0.5 ml carbonate buffer
1.0 ml epinephrine	1.0 ml epinephrine

8.1.5 Histopathological Analysis

This study was carried out to evaluate induction of disease, and effectiveness of synthesized compounds along with 5-FU as a standard. The caudal region of skin was excised and stored in 10% formalin for 24 hours. These skin tissues were transferred in ethanol followed by wash of xylene. Furthermore, these tissues were covered with paraffin block. 4 µm thick section of these tissue were mounted on glass slide with the help of albumin solution. Finally these slide were stained with 10% hematoxylin for 2-5 minutes and washed with water. Simultaneously, these slide were stained with 10% eosin for 2 minutes and pass through alcohol in ascending order. These slides were treated with xylene and observed under microscope with 10X magnification.

8.2 Results and Discussion

8.2.1 Effect of 5-FU (5%), Compound HB-JC-206, and HB-JC-304 on serum LDH, GGT, and CRP level

At the end of 16th week, levels of all these biochemical components were increases in disease control group (DC) as compared to the normal control group (NC). Animal were treated with 5-FU, HB-JC-206, and HB-JC-304 in disease treated group the levels of all these components were reduced. Statistical levels of all these serum biomarkers are shown in Table 24.

Table 24. Effect of 5-FU (5%), Compound HB-JC-206, and HB-JC-304 on serum biomarkers:

Parameters	NC	DC	5-FU	HB-JC-206	HB-JC-304
LDH (U/L)	291.867 ± 48.76	287.050 ± 4.126	190.803 ± 0.882	209.067 ± 0.418	210.467 ± 1.615
GGT (U/L)	21.890 ± 1.369	74.553 ± 3.383	10.567 ± 0.573	21.857 ± 1.021	11.407 ± 0.647
CRP (mg/dl)	3.483 ± 0.174	31.057 ± 0.920	4.193 ± 0.232	6.080 ± 0.257	5.663 ± 0.185

Each column represents Mean ± SEM, n = 6 mice (Oneway ANOVA followed by Dunnett's multiple comparison test); GGT: Gamma glutamyl transferase; LDH: Lactate dehydrogenase; CRP: C-reactive protein; NC: Normal control group; DC: Skin cancer control group.

Graphical Representation of serum biomarkers are shown in Fig.19.

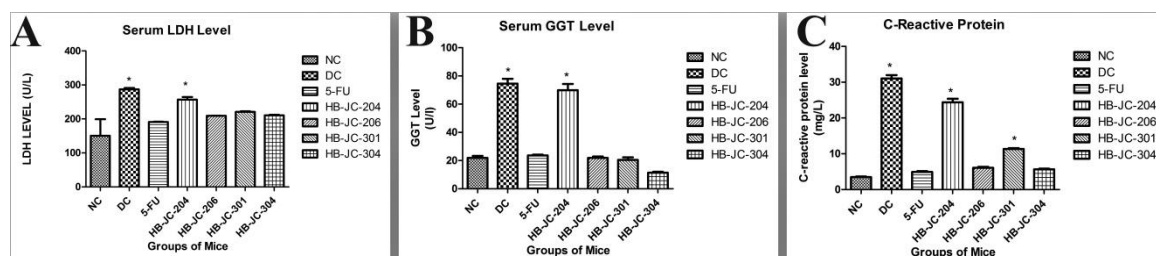


Fig. 19: Measurement of serum biomarkers after the treatment with 5-FU and compounds HB-JC-206 and HB-JC-304 where each bar represents Mean ± SEM, n = 6 mice (Oneway ANOVA followed by Dunnett's multiple comparison test), * = p < 0.05 vs normal control group: (A) Lactate dehydrogenase level; (B) Gamma glutamyl transferase level; (C) C-reactive protein level.

8.2.2 Effect of 5-FU (5%), Compound HB-JC-206, and HB-JC-304 on MDA, GSH, and SOD levels in tissue.

At the end of 16th week, there was a significant (p<0.05) increase in the MDA levels in the skin cancer control group as compared to the normal control group. Treatment with 5% 5-FU and 5% compound HB-JC-206, and HB-JC-304 in disease treated groups significantly (p<0.05) reduced the MDA levels as compared to skin cancer control group.

There were decreased GSH levels in skin cancer control group in comparison to the normal control group. Treatment with 5% 5-FU and 5% compound HB-JC-206, and HB-JC-304 in disease treated groups significantly (p<0.05) increased the GSH levels as compared to skin cancer control group.

The SOD activity obtained in skin cancer control group was found to be significantly lower in comparison to that found in normal control group. Treatment with 5% 5-FU and 5% compound HB-JC-206, and HB-JC-304 in disease treated groups significantly

($p > 0.05$) increased the SOD levels as compared to skin cancer control group. Statistical levels of all these serum biomarkers are shown in Table 25.

Table 25. Effect of 5-FU (5%), Compound HB-JC-206, and HB-JC-304 on oxidative stress parameters

Parameters	NC	DC	5-FU	HB-JC-206	HB-JC-304
MDA (nm/mg of protein)	38.880 ± 0.158	97.113 ± 1.397	50.813 ± 0.237	61.250 ± 0.129	62.630 ± 0.702
GSH (nm/mg of protein)	55.037 ± 0.947	13.630 ± 1.233	53.450 ± 0.641	33.038 ± 0.231	52.298 ± 1.666
SOD (units/mg of protein)	55.037 ± 0.947	13.630 ± 1.233	53.450 ± 0.641	33.038 ± 0.231	52.298 ± 1.666

Each column represents Mean ± SEM, n = 6 mice (Oneway ANOVA followed by Dunnett's multiple comparison test).

Graphical Representation of Oxidative Stress Parameters are shown in Fig. 20.

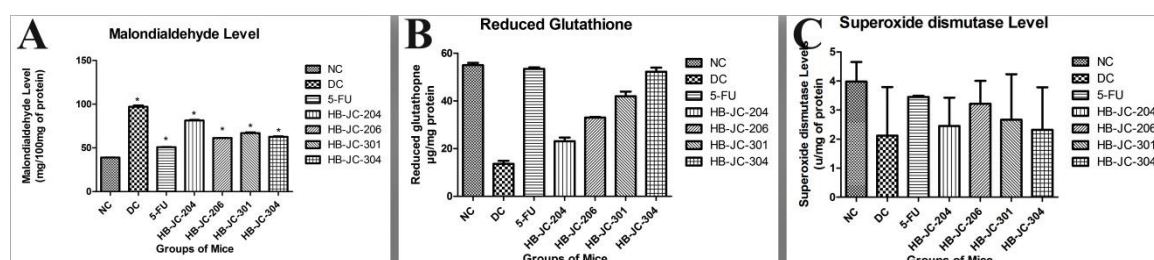


Fig. 20 Measurement of oxidative stress parameters after the treatment with 5-FU and compounds Hb-JC-206, and HB-JC-304 where each bar represents Mean ± SEM, n = 6 mice (Oneway ANOVA followed by Dunnett's multiple comparison test), * = $p < 0.05$ vs normal control group: (A) Malondialdehyde level; (B) Glutathione level; (C) Super oxide dismutase level.

8.2.3 Histopathological Analysis

In case of skin cancer control group, there was disruption of fatty layer with presence of keratin pearls. Also presence of rete ridges extending through the connective tissue was seen. There was mark presence of dysplastic and hyperplastic epithelial cells. Histopathological sections of skin from mice treated with 5% compound HB-JC-206, HB-JC-304 and 5-FU (5%) solution showed complete absence of keratin pearls, dysplastic epithelial cells and rete ridges showed effectiveness of the treatment. Photographs of caudal region of mice and histopathological analysis are shown in fig.21 and 22, respectively.



Fig. 21 Photographs of caudal region skin of the mice (A) Normal control group; (B) Disease control group; (C) Skin cancer treated with 5-FU; (D) Skin cancer treated with synthesized compounds.

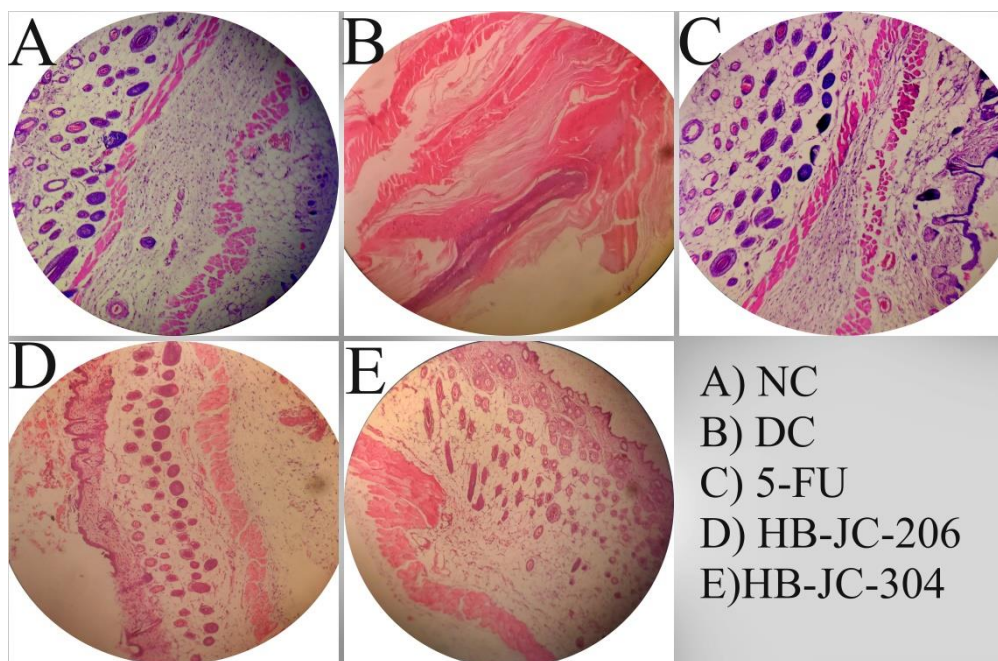


Fig. 22 Photographs of histopath analysis of caudal region skin of the mice (A) Normal control group; (B) Disease control group; (C) Skin cancer treated with 5-FU; (D) Skin cancer treated with HB-JC-206. (E) Skin cancer treated with HB-JC-304.

Conclusion

In course our research to find novel compounds acting against the skin cancer, ligand based pharmacophore modelling was performed using DiscoTech. 10 molecules were used to perform pharmacophore mapping. Total 4 models were generated after refinement with GASP and from that, Model 1 was considered as the best model on the basis of specificity, energy and hits which contained 1 donor atoms, 1 hydrophobic sites and 3 acceptor atom. Best pharmacophore model was chosen for substructure searching in NCI database. Total number of 11,485 molecules obtained after virtual screening. Pharmacophore model chosen for the virtual screening methods to retrieve the potential leads against B-Raf kinase inhibitors. Hits obtained after virtual screening showed that Benzofuran moiety had highest Q_{fit} and good molecular docking interaction. Different substituted benzoxazole moieties were designed based upon the docking and knowledge based structure activity relationship studies. 21 designed and docked molecules were synthesised in laboratory which consist of amino, and sulphonamide derivatives of benzoxazole. Structures of synthesised compounds were confirmed by the FT-IR, Mass, 1H NMR, and ^{13}C NMR. All the synthesised compounds were tested for in vitro anticancer activity on melanoma cancer cell line A-375. From the results, it was found that compound **HB-JC-206**, and **HB-JC-304** were showed most potent activity and was further evaluated for in vivo activity. Based upon all these results it was concluded that the computational tools help to derive the new potent hits, through which lead can be designed and developed in future.

References

1. World Health Organization (WHO) <http://www.who.int/en/news-room/fact-sheets/detail/cancer> (Accessed on April 28, 2019).
2. Hassanpour, S.H.; Mohammadamin D. Review of cancer from perspective of molecular. *J. Can. Res. Pra.* **2017**, *4*, 127-129.
3. Trafialek, J.; Kolanowski W. Dietary exposure to meat-related carcinogenic substances: is there a way to estimate the risk? *Int. J. Food Sci. Nutr.* **2014**, *65*, 774-780.
4. Yoo, K.Y.; Shin, H.R. Cancer epidemiology and prevention. *Korean J Epidemiol.* **2003**, *25*, 1-15.
5. National Cancer Institute (NCI). <https://www.cancer.gov/> (Accessed on April 28, 2019)
6. National Institute of Cancer Prevention and Research <http://cancerindia.org.in/cancer-statistics/> (Accessed on April 28, 2019)
7. Das, P.; Deshmukh, N.; Badore N.; Ghulaxe C.; Patel P. A Review Article on Melanoma. *J. Pharm. Sci. & Res.* **2016**, *8*, 112-117.
8. Rastrelli, M; Tropea, S; Rossi, CR; Alaibac, M. Melanoma: epidemiology, risk factors, pathogenesis, diagnosis and classification. *In Vivo* **2014**, *28*, 1005-1011.
9. Zhenyu, Ji.; Keith, T. F.; Tsao, H. Targeting the RAS pathway in melanoma. *Trends. Mol. Med.* **2012**, *18*, 27-35.
10. Mirshafiey, A.; Ghalamfarsa, G.; Asghari, B.; Azizi, G. Receptor Tyrosine Kinase and Tyrosine Kinase Inhibitors: New Hope for Success in Multiple Sclerosis Therapy. *Innov. Clin. Neurosci.* **2014**, *11*, 23-36.
11. Baines, A.T; Xu, D; Der, C.J. Inhibition of Ras for cancer treatment: the search continues. *Future Med Chem.* **2011**, *14*, 1787-1808.
12. Grimaldi, A. M.; Simeone, E.; Festino, L.; Vanella, V.; Strudel, M.; Ascierto A. P.; MEK Inhibitors in the Treatment of Metastatic Melanoma and Solid Tumors. *Am. J. Clin. Dermatol.* **2017**, *18*, 745-754.
13. Robinson, M.J; Cobb, M.H; Mitogen-activated protein kinase pathways. *Curr. Opin. Cell. Biol.* **1997**, *9*, 180-186.
14. Harris; P.A., Targeting B-RAF. The Discovery and Development of B-RAF Inhibitors, Cancer Drug Design and Discovery. *Acedamic Press*, London, **2013**.
15. Rapp, U.R; Goldsborough, M.D; Mark, G.E.; Bonner, T.I; Groffen, J.; Reynolds, F.H; et al. Structure and biological activity of v-raf, a unique oncogene transduced by a retrovirus. *Proc. Natl. Acad. Sci.* **1983**, *80*, 4218-4222.
16. Davies, H.; Bignell, G.R; Cox, C.; Stephens, P.; Edkins, S.; Clegg, S.; et al. Mutations of the BRAF gene in human cancer. *Nature* **2002**, *417*, 949-954.
17. Tran, N.H.; Wu, X.; Frost, J.A. B-Raf and Raf-1 Are Regulated by Distinct Autoregulatory Mechanisms. *J. Bio. Che.* **2005**, *280*, 16244-16253.
18. Chong, H.; Lee, J.; Guan, K.; Positive and negative regulation of Raf kinase activity and function by phosphorylation, *EMBO J.*, **2001**, *20*, 3716-3727.
19. Matallanas, D.; Birtwistle, M.; Romano, D.; Zebisch, A.; Rauch, J.; Kriegsheim A.V.; et al. Raf Family Kinases: Old Dogs Hve Learned New Tricks. *Genes Cancer*, **2011**, *2*, 232-260.
20. Jr, R..R.; RAF protein-serine / threonine kinases: Structure and regulation. *Biochem. Biophys. Res. Commun.*, **2010**, *399*, 313-317.
21. Dhomen, N.; Marais, R. New insight into BRAF mutations in cancer. *Curr. Opin. Genet. Dev.* **2007**, *31*-39.

22. Wilhelm, S.; Carter, C.; Lynch, M.; Lowinger, T.; Dumas, J.; Smith, R.A.; et al. Discovery and development of sorafenib: a multikinase inhibitor for treating cancer. *Nat. Rev. Drug. Discov.* **2006**, *5*, 835–844.
23. Wilhelm, S.M.; Carter, C.; Tang, L.; Wilkie, D.; McNabola, A.; Rong, H.; et al. BAY 43-9006 exhibits broad spectrum oral antitumor activity and targets the RAF/MEK/ERK pathway and receptor tyrosine kinases involved in tumor progression and angiogenesis. *Cancer Res.* **2004**, *64*, 7099–7109.
24. Bollag, G.; Tsai, J.; Zhang, J.; Zhang, C.; Ibrahim, P.; Nolop, K.; et al. Vemurafenib: the first drug approved for BRAFmutant cancer. *Nat. Rev. Drug Discov.* **2012**, *11*, 873–886.
25. Tsai, J.; Lee, J.T.; Wang, W.; Zhang, J.; Cho, H.; Mamo, S.; et al. Discovery of a selective inhibitor of oncogenic B-Raf kinase with potent antimelanoma activity. *Proc. Natl. Acad. Sci.* **2008**, *105*, 3041–3046.
26. Takle, A.K.; Brown, M.J.; Davies, S.; Dean, D.K.; Francis, G.; Gaiba, A.; et al. The identification of potent and selective imidazole-based inhibitors of B-Raf kinase. *Bioorg. Med. Chem. Lett.* **2006**, *16*, 378–381.
27. Yang, W.; Chen, Y.; Zhou, X.; Gu, Y.; Qian, W.; Zhang, F.; et al. Design, synthesis and biological evaluation of bis-aryl ureas and amides based on 2-amino-3-purinylypyridine scaffold as DFG-out B-Raf kinase inhibitors. *Eur. J. Med. Chem.* **2015**, *89*, 581–596.
28. Zhao, M.Y.; Yin, Y.; Yu, X.W.; Sangani, C.B.; Wang, S.F.; Lu, A.M.; et al. Synthesis, biological evaluation and 3D-QSAR study of novel 4,5-dihydro-1H-pyrazole thiazole derivatives as BRAFV600E inhibitors. *Bioorganic. Med. Chem.* **2015**, *23*, 46–54.
29. Yang, Y.S.; Li, Q.S.; Sun, S.; Zhang, Y.B.; Wang, X.L.; Zhang, F.; et al. Design, modification and 3D QSAR studies of novel 2,3-dihydrobenzo[b][1,4]dioxin-containing 4,5-dihydro-1H-pyrazole derivatives as inhibitors of B-Raf kinase. *Bioorg. Med. Chem.* **2012**, *20*, 6048–6058.
30. Wang, S.F.; Zhu, Y.L.; Zhu, P.T.; Makawana, J.A.; Zhang, Y.L.; Zhao, M.Y.; et al. Design, synthesis and biological evaluation of novel 5-phenyl-1H-pyrazole derivatives as potential BRAFV600E inhibitors. *Bioorg. Med. Chem.* **2014**, *22*, 6201–6208.
31. Li, C.Y.; Li, Q.S.; Yan, L.; Sun, X.G.; Wei, R.; Gong, H.B.; Zhu, H.L. Synthesis, biological evaluation and 3D-QSAR studies of novel 4,5-dihydro-1H-pyrazole niacinamide derivatives as BRAF inhibitors. *Bioorg. Med. Chem.* **2012**, *20*, 3746–3755.
32. Liu, J.J.; Zhang, H.; Sun, J.; Wang, Z.C.; Yang, Y.S.; Li, D.D.; et al. Synthesis, biological evaluation of novel 4,5-dihydro-2H-pyrazole 2-hydroxyphenyl derivatives as BRAF inhibitors. *Bioorg. Med. Chem.* **2012**, *20*, 6089–6096.
33. Li, Q.S.; Li, C.Y.; Lu, X.; Zhang, H.; Zhu, H.L.; Design, synthesis and biological evaluation of novel (E)- α -benzylsulfonyl chalcone derivatives as potential BRAF inhibitors. *Eur. J. Med. Chem.* **2012**, *50*, 288–295.
34. Dietrich, J.; Gokhale, V.; Wang, X.; Hurley, L.H.; Flynn, G.A. Application of a novel [3+2] cycloaddition reaction to prepare substituted imidazoles and their use in the design of potent DFG-out allosteric B-Raf inhibitors. *Bioorg. Med. Chem.* **2010**, *18*, 292–304.
35. Yu, M.; Yang, H.; Wu, K.; Ji, Y.; Ju, L.; Lu, X. Novel pyrazoline derivatives as bi-inhibitor of COX-2 and B-Raf in treating cervical carcinoma. *Bioorg. Med. Chem.* **2014**, *22*, 4109–4118.
36. Qin, H.L.; Leng, J.; Zhang, C.P.; Jantan, I.; Amjad, M.W.; Sher, M.; et al.

- Synthesis of α,β -Unsaturated Carbonyl-Based Compounds, Oxime and Oxime Ether Analogs as Potential Anticancer Agents for Overcoming Cancer Multidrug Resistance by Modulation of Efflux Pumps in Tumor Cells. *J. Med. Chem.* **2016**, *59*, 3549–3561.
37. Yanga, W.; Yadong, C.; Yanmin, Z.; Tanga, S.; Chena, H.; Tanga, W.; Lu, T. Design, Synthesis and Antitumor Activities of Bis-aryleureas and Bisarylamides Based on 1H-benzo[d]imidazole Moiety as Novel BRafV600E/VEGFR2 Dual Inhibitors. *Lett. Drug. Des. Discov.* **2014**, *11*, 1079-1089.
 38. Yang, Y.S.; Zhang, F.; Tang, D.J.; Yang, Y.H.; Zhu, H.L.; Modification, biological evaluation and 3D QSAR studies of novel 2-(1,3-diaryl-4,5-dihydro-1H-pyrazol-5-yl)phenol derivatives as inhibitors of B-Raf kinase. *PLoS One* **2014**, *9*.
 39. Blackburn, C.; Duffey M.O.; Gould, A.E.; Kulkarni, B.; Liu, J.X.; Menon, S.; Nagayoshi, M.; et al. Discovery and optimization of N-acyl and N-aryloxy-pyrazolines as B-Raf kinase inhibitors. *Bioorg. Med. Chem. Lett.* **2010**, *20*, 4795–4799.
 40. Wang, P.F.; Qiu, H.Y.; Wang, Z.F.; Zhang, Y.J.; Wang, Z.C.; Li, D.D.; et al. Identification of novel B-Raf V600E inhibitors employing FBDD strategy. *Biochem Pharmacol* **2017**, *132*, 63–76.
 41. Wang, L.; Zhang, Y.; Zhang, Q.; Zhu, G.; Zhang, Z.; Duan, C.; et al. Discovery of potent Pan-Raf inhibitors with increased solubility to overcome drug resistance. *Eur. J. Med. Chem.* **2019**, *153*, 243-255.
 42. Jung, H.; Kim, J.; Im, D.; Moon, H.; Hah, J.M. Design, synthesis, and in vitro evaluation of N-(3-(3-alkyl-1H-pyrazol-5-yl) phenyl)-aryl amide for selective RAF inhibition. *Bioorg. Med. Chem. Lett.* **2019**, *29*, 534-538.
 43. Garamvölgyi, R.; Dobos, J.; Sipos, A.; Boros, S.; Illyés, E.; Baska, F.; et al. Design and synthesis of new imidazo[1,2-a]pyridine and imidazo [1,2-a]pyrazine derivatives with antiproliferative activity against melanoma cells. *Eur. J. Med. Chem.* **2016**, *108*, 623-643.
 44. Abdelazeem, A.H.; El-Saadi, M.T.; Said, E.G.; Youssif, B.G.M.; Omar, H.A.; El-Moghazy, S.M. Novel diphenylthiazole derivatives with multi-target mechanism: Synthesis, docking study, anticancer and anti-inflammatory activities. *Bioorg. Chem.* **2017**, *175*, 127-138.
 45. Assadieskandar, A.; Yu, C.; Maisonneuve, P.; Liu, X.; Chen, Y.C.; Prakash, G.K.S.; et al. Effects of rigidity on the selectivity of protein kinase inhibitors. *Eur. J. Med. Chem.* **2018**, *246*, 519-528.
 46. Duffey, M.O.; Adams, R.; Blackburn, C.; Chau, R.W.; Chen, S.; Galvin, K.M.; et al. Discovery and optimization of pyrazoline compounds as B-Raf inhibitors. *Bioorg. Med. Chem. Lett.* **2010**, *20*, 4800-4804.
 47. Buckmelter, A.J.; Ren, L.; Laird, E.R.; Rast, B.; Miknis, G.; Wenglowksy, S.; et al. The Discovery of furo[2,3-c]pyridine-based indanone oximes as potent and selective B-Raf inhibitors. *Bioorg. Med. Chem. Lett.* **2011**, *21*, 1248-1252.
 48. Berger, D.M.; Torres, N.; Dutia, M.; Powell, D.; Ciszewski, G.; Gopalsamy, A.; et al. Non-hinge-binding pyrazolo[1,5-a]pyrimidines as potent B-Raf kinase inhibitors. *Bioorg. Med. Chem. Lett.* **2009**, *19*, 6519-6523.
 49. Liu, L.; Lee, M.R.; Kim, J.L.; Whittington, D.A.; Bregman, H.; Hua, Z.; et al. Purinylpyridinylamino-based DFG-in/ α C-helix-out B-Raf inhibitors: Applying mutant versus wild-type B-Raf selectivity indices for compound profiling. *Bioorg. Med. Chem.* **2016**, *24*, 2215–2234.
 50. El-Damasy, A.K.; Lee J.H.; Seo, S.H.; Cho, N.C.; Pae, A.N.; Keum, G. Design

- and synthesis of new potent anticancer benzothiazole amides and ureas featuring pyridylamide moiety and possessing dual B-RafV600E and C-Raf kinase inhibitory activities. *Eur. J. Med. Chem.* **2016**, *115*, 201-216.
51. Gopalsamy, A.; Shi, M.; Hu, Y.; Lee, F.; Feldberg, L.; Frommer, E.; et al. B-Raf kinase inhibitors: Hit enrichment through scaffold hopping. *Bioorg. Med. Chem. Lett.* **2010**, *20*, 2461-2434.
 52. Smith, A.; Ni, Z.J.; Poon, D.; Huang, Z.; Chen, Z.; Zhang, Q.; et al. Imidazo [1 , 2- a] pyridin-6-yl-benzamide analogs as potent RAF inhibitors. *Bioorg. Med. Chem. Lett.* **2017**, *27*, 5221–5224.
 53. Okaniwa, M.; Hirose, M.; Arita, T.; Yabuki, M.; Nakamura, A.; Takagi, T.; et al. Discovery of a Selective Kinase Inhibitor (TAK-632) Targeting Pan- RAF Inhibition: Design, Synthesis, and Biological Evaluation of C-7-Substituted 1,3-Benzothiazole Derivatives. *J. Med. Chem.* **2013**, *56*, 6478-6494.
 54. Gould, A.E.; Adams, R.; Adhikari, S.; Aertgeerts, K.; Afroze, R.; Blackburn, C.; et al. Design and Optimization of Potent and Orally Bioavailable Tetrahydronaphthalene Raf Inhibitors. *J. Med. Chem.* **2011**, *24*, 1836-1846.
 55. Khan, M.A.; El-Gamal, M.I.; Tarazi, H.; Choi, H.S.; Oh, C.H.; Design and synthesis of a new series of highly potent RAF kinase-inhibiting triarylpyrazole derivatives possessing antiproliferative activity against melanoma cells. *Future Med. Chem.* **2016**, *8*.
 56. Kim, M.; Kim, M.; Yu, H.; Kim, H.; Yoo, K.; Sim, T.; Hah, J.M.; Structure based design and syntheses of amino-1H-pyrazole amide derivatives as selective Raf kinase inhibitors in melanoma cells. *Bioorg. Med. Chem.* **2011**, *19*, 1915-1923.
 57. Kim, H.; Kim, M.; Lee, J.; Yu, H.; Hah, J.M.; Syntheses of phenylpyrazolodiazepin-7-ones as conformationally rigid analogs of aminopyrazole amide scaffold and their antiproliferative effects on cancer cells. *Bioorg. Med. Chem.* **2011**, *19*, 6760-6767.
 58. Li, X.; Shen, J.; Tan, L.; Zhang, Z.; Gao, D.; Luo, J.; et al. Design and synthesis of N-(4-aminopyridin-2-yl)amides as B-RafV600E inhibitors. *Bioorg. Med. Chem. Lett.* **2016**, *26*, 2760–2763.
 59. Yang, Y.S.; Yang, B.; Zou, Y.; Li, G.; Zhu, H.L. Design, biological evaluation and 3D QSAR studies of novel dioxin-containing triaryl pyrazoline derivatives as potential B-Raf inhibitors. *Bioorg. Med. Chem.* **2016**, *24*, 3052–3061.
 60. Kim, M.; Lee, J.; Jung, K.; Kim, H.; Aman, W.; Ryu, J.S.; Hah, J.M.; Design, synthesis and biological evaluation of benzyl 2- (1H -imidazole-1-yl) pyrimidine analogues as selective and potent Raf inhibitors. *Bioorg. Med. Chem. Lett.* **2014**, *24*, 3600–3604.
 61. Jiao, Y.; Xin, B.T.; Zhang, Y.; Wu, J.; Lu, X.; Zheng, Y.; Tang, W.; Design, synthesis and evaluation of novel 2-(1H-imidazol-2-yl) pyridine Sorafenib derivatives as potential BRAF inhibitors and anti-tumor agents. *Eur. J. Med. Chem.* **2015**, *90*, 170–183.
 62. Gamal El-Din, M.M.; El-Gamal, M.I.; Abdel-Maksoud, M.S.; Yoo, K.H.; Oh, C.H.; Design, synthesis, broad-spectrum antiproliferative activity, and kinase inhibitory effect of triarylpyrazole derivatives possessing arylamides or arylureas moieties. *Eur. J. Med. Chem.* **2016**, *119*, 122–131.
 63. Lu, B.; Cao, H.; Cao, J.; Huang, S.; Hu, Q.; Liu, D.; et al. Discovery of EBI-907: A highly potent and orally active B-RafV600E inhibitor for the treatment of melanoma and associated cancers. *Bioorg. Med. Chem. Lett.* **2015**, *26*, 819–823.
 64. Wang, X.; Berger, D.M.; Salaski, E.J.; Torres, N.; Hu, Y.; Levin, J.I.; et al.

- Discovery of highly potent and selective type I B-Raf kinase inhibitors. *Bioorg. Med. Chem. Lett.* **2009**, *19*, 6571–6574.
65. Kong, X.; Qin, J.; Li, Z.; Vultur, A.; Tong, L.; Feng, E.; et al. Development of a novel class of B-RafV600E-selective inhibitors through virtual screening and hierarchical hit optimization. *Org. Biomol. Chem.* **2012**, *10*, 7402:7417.
 66. Newhouse, B.J.; Wenglowky, S.; Grina, J.; Laird, E.R.; Voegtli, W.C.; Ren, L.; et al. Imidazo[4,5-b]pyridine inhibitors of B-Raf kinase. *Bioorg. Med. Chem. Lett.* **2013**, *23*, 5896-5899.
 67. El-damasy, A.K.; Hee, S.; Cho, N.; Bang, S.; Design, synthesis, in-vitro antiproliferative activity and kinase profile of new picolinamide based 2-amido and ureido quinoline derivatives. *Eur. J. Med. Chem.* **2015**, *101*, 754–768.
 68. Niculescu-Duvaz, D.; Niculescu-Duvaz, I.; Suijkerbuijk, B.M.; Ménard, D.; Zambon, A.; Davies, L.; et al. Potent BRAF kinase inhibitors based on 2,4,5-trisubstituted imidazole with naphthyl and benzothiophene 4-substituents. *Bioorg. Med. Chem.* **2013**, *21*, 1284-1304.
 69. Qin, J.; Xie, P.; Ventocilla, C.; Zhou, G.; Vultur, A.; Chen, Q.; et al. Identification of a Novel Family of BRAFV600E Inhibitors. *J. Med. Chem.* **2012**, *55*, 5220–5230.
 70. Qin, M.; Zhai, X.; Xie, H.; Ma, J.; Lu, K.; Wang, Y.; et al. Design and synthesis of novel 2-(4-(2-(dimethylamino)ethyl)-4H-1,2,4-triazol-3-yl)pyridines as potential antitumor agents. *Eur. J. Med. Chem.* **2014**, *81*, 47-58.
 71. Gong, Z.H.; Jian, Y.; Ji, J.F.; Yang, J.; Xiang, T.; Zhou, C.K.; Synthesis and biological evaluation of novel N-(5-phenyl-1H-pyrazol-3-yl) benzenesulfonamide derivatives as potential. *Med. Chem. Res.* **2017**, *4032*, 1–8.
 72. Ramurthy, S.; Aikawa, M.; Amiri, P.; Costales, A.; Hashash, A.; Jansen, J.M.; et al. Design and synthesis of 5,6-fused heterocyclic amides as Raf kinase inhibitors. *Bioorg. Med. Chem. Lett.* **2011**, *21*, 3286-3289.
 73. Hansen, J.D.; Grina, J.; Newhouse, B.; Welch, M.; Topalov, G.; Littman, N.; et al. Potent and selective pyrazole-based inhibitors of B-Raf kinase. *Bioorg. Med. Chem. Lett.* **2008**, *18*, 4692–4695.
 74. Rheault, T.R.; Stellwagen, J.C.; Adjabeng, G.M.; Hornberger, K.R.; Petrov, K.G.; Waterson, A.G.; et al. Discovery of Dabrafenib: A Selective Inhibitor of Raf Kinases with Antitumor Activity against B-Raf-Driven Tumors. *ACS Med. Chem. Lett.* **2013**, *4*, 358-362.
 75. Henry, J.R.; Kaufman, M.D.; Peng, S.B.; Ahn, Y.M.; Caldwell, T.M.; Vogeti, L.; et al. Discovery of 1-(3,3-Dimethylbutyl)-3-(2-fluoro-4-methyl-5-(7-methyl-2-(methylamino)pyrido[2,3-d]pyrimidin-6-yl)phenyl)urea (LY3009120) as a Pan-RAF Inhibitor with Minimal Paradoxical Activation and Activity against BRAF or RAS Mutant Tumor Cells. *J. Med. Chem.* **2015**, *58*, 4165–4179.
 76. Gopalsamy, A.; Ciszewski, G.; Shi, M.; Berger, D.; Hu, Y.; Lee, F.; et al. Hit to lead optimization of pyrazolo [1,5-a] pyrimidines as B-Raf kinase inhibitors. *Bioorg. Med. Chem. Lett.* **2009**, *19*, 6890–6892.
 77. El-Gamal, M.I.; Abdel-Maksoud, M.S.; Gamal El-Din, M.M.; Shin, J.S.; Lee, K.T.; Yoo, K.H.; Oh, C.H.; Synthesis, in vitro Antiproliferative and Antiinflammatory Activities and Kinase Inhibitory effects of New 1,3,4-triarylpyrazole Derivatives. *Anticancer Agents Med Chem.* **2017**, *17*, 75-84.
 78. Rowbottom, M.W.; Faraoni, R.; Chao, Q.; Campbell, B.T.; Lai, A.G.; Setti, E.; et al. Identification of 1-(3-(6,7-dimethoxyquinazolin-4-yloxy)phenyl)-3-(5-(1,1,1-trifluoro-2-methylpropan-2-yl)isoxazol-3-yl)urea hydrochloride (CEP-32496), a highly potent and orally efficacious inhibitor of V-RAF murine sarcoma viral

- oncogene homologue B1 (BRAF) V600E. *J. Med. Chem.* **2012**, *55*, 1082-1105.
79. Lyne, P.D.; Aquila, B.; Cook, D.J.; Dakin, L.A.; Ezhuthachan, J.; Ioannidis, S.; et al. Identification of amidoheteroaryls as potent inhibitors of mutant (V600E) B-Raf kinase with in vivo activity. *Bioorg. Med. Chem. Lett.* **2009**, *19*, 1026–1029.
80. Li, Q.S.; Lv, X.H.; Zhang, Y.B.; Dong, J.J.; Zhou, W.P.; Yang, Y.; Zhu, H.L.; Identification of novel 3,5-diarylpiperazine derivatives containing salicylamide moiety as potential anti-melanoma agents. *Bioorg. Med. Chem. Lett.* **2012**, *22*, 6596–6601.
81. Wang, X.; Berger, D.M.; Salaski, E.J.; Torres, N.; Dutia, M.; Hanna, C.; et al. Indazolylpyrazolopyrimidine as Highly Potent B-Raf Inhibitors with in Vivo Activity. *J. Med. Chem.* **2010**, *53*, 7874–7878.
82. Kim, Y.K.; Ahn, S.K.; Lee, M.; Differential sensitivity of melanoma cell lines with differing B-Raf mutational status to the new oncogenic B-Raf kinase inhibitor UI-152. *Cancer Lett.* **2012**, *320*, 215–224.
83. Tang, J.; Hamajima, T.; Nakano, M.; Sato, H.; Dickerson, S.H.; Lackey, K.E.; Knowledge-based design of 7-azaindoles as selective B-Raf inhibitors. *Bioorg. Med. Chem. Lett.* **2018**, *18*, 4610-4614.
84. Wenglowsky, S.; Moreno, D.; Rudolph, J.; Ran, Y.; Ahrendt, K.A.; Arrigo, A.; et al. Pyrazolopyridine inhibitors of B-Raf(V600E). Part 3: an increase in aqueous solubility via the disruption of crystal packing. *Bioorg. Med. Chem. Lett.* **2012**, *22*, 912-915.
85. Tang, J.; Lackey, K.E.; Dickerson, S.H.; The discovery of potent and selective 4-aminothienopyridines as B-Raf kinase inhibitors. *Bioorg. Med. Chem. Lett.* **2013**, *23*, 66-70.
86. Li, Y.; Cheng, H.; Zhang, Z.; Zhuang, X.; Luo, J.; Long, H.; et al. N-(3-Ethynyl-2,4-di fluorophenyl)sulfonamide Derivatives as Selective Raf Inhibitors. *ACS Med. Chem. Lett.* **2015**, *6*, 543–547.
87. Thaher, A.B.; Arnsmann, M.; Totzke, F.; Ehlert, J.E.; Kubbutat, M.H.; Schächtele, C.; et al. Tri- and Tetrasubstituted Pyrazole Derivates: Regioisomerism Switches Activity from p38MAP Kinase to Important Cancer Kinases. *J. Med. Chem.* **2012**, *55*, 961–965.
88. Mathieu, S.; Gradl, S.N.; Ren, L.; Wen, Z.; Aliagas, I.; Gunzner-Toste, J.; et al. Potent and Selective Aminopyrimidine-Based B-Raf Inhibitors with Favorable Physicochemical and Pharmacokinetic Properties. *J. Med. Chem.* **2012**, *55*, 2869–2881.
89. Ménard, D.; Niculescu-Duvaz, I.; Dijkstra, H.P.; Niculescu-Duvaz, D.; Suijkerbuijk, B.M.; Zambon, A.; et al. Novel Potent BRAF Inhibitors : Toward 1 nM Compounds through Optimization of the Central Phenyl Ring. *J. Med. Chem.* **2009**, *52*, 3881–3891.
90. Fu, Y.; Wang, Y.; Wan, S.; Li, Z.; Wang, G.; Zhang, J.; Wu, X.; Bisarylureas Based on 1H-Pyrazolo[3,4-d]pyrimidine Scaffold as Novel Pan-RAF Inhibitors with Potent Anti-Proliferative Activities: Structure-Based Design, Synthesis, Biological Evaluation and Molecular Modelling Studies. *Molecules* **2017**, *22*, 542-564.
91. Niculescu-Duvaz, I.; Roman, E.; Whittaker, S.R.; Friedlos, F.; Kirk, R.; Scanlon, I. J.; et al. Novel Inhibitors of B-RAF Based on a Disubstituted Pyrazine Scaffold . Generation of a Nanomolar Lead. *J. Med. Chem.* **2006**, *49*, 407-416.
92. Niculescu-Duvaz, I.; Roman, E.; Whittaker, .SR.; Friedlos, F.; Kirk, R.; Scanlon, I.J.; et al. Novel Inhibitors of the v-raf Murine Sarcoma Viral Oncogene

- Homologue B1 (BRAF) Based on a 2 , 6-Disubstituted Pyrazine Scaffold. *J. Med. Chem.* **2008**, *1*, 3261–3274.
93. Ren, L.; Wenglowky, S.; Miknis, G.; Rast, B.; Buckmelter, A.J.; Ely, R.J.; et al. Non-oxime inhibitors of B-Raf V600E kinase. *Bioorg. Med. Chem. Lett.* **2011**, *21*, 1243–1247.
94. Newhouse, B.J.; Hansen, J.D.; Grina, J.; Welch, M.; Topalov, G.; Littman, N.; et al. Non-oxime pyrazole based inhibitors of B-Raf kinase. *Bioorg. Med. Chem. Lett.* **2011**, *21*; 3488–3492.
95. Grandi, M.J.; Berger, D.M.; Hopper, D.W.; Zhang, C.; Dutia, M.; Dunnick, A.L.; et al. Novel pyrazolopyrimidines as highly potent B-Raf inhibitors. *Bioorg. Med. Chem. Lett.* **2009**, *19*, 6957–6961.
96. Huang, S.C.; Adhikari, S.; Afroze, R.; Brewer, K.; Calderwood, E.F.; Chouitar, J.; et al. Optimization of tetrahydronaphthalene inhibitors of Raf with selectivity over hERG. *Bioorganic. Med. Chem. Lett.* **2015**, *26*, 1156–1160.
97. Ren, L.; Laird, E.R.; Buckmelter, A.J.; Dinkel, V.; Gloor, S.L.; Grina, J.; et al. Potent and selective pyrazolo [1,5-a] pyrimidine based inhibitors of B-Raf V600E kinase with favorable physicochemical and pharmacokinetic properties. *Bioorg. Med. Chem. Lett.* **2012**, *22*, 1165–1168.
98. Pulici, M.; Traquandi, G.; Marchionni, C.; Modugno, M.; Lupi, R.; Amboldi, N.; et al. Optimization of Diarylthiazole B-Raf Inhibitors: Identification of a Compound Endowed with High Oral Antitumor Activity, Mitigated hERG Inhibition, and Low Paradoxical Effect. *ChemMedChem* **2014**, 1–21.
99. Wenglowky, S.; Moreno, D.; Laird, E.R.; Gloor, S.L.; Ren, L.; Risom, T.; et al. Pyrazolopyridine inhibitors of B-Raf V600E . Part 4 : Rational design and kinase selectivity profile of cell potent type II inhibitors. *Bioorg. Med. Chem. Lett.* **2012**, *22*, 6237–6241.
100. Wang, M.; Xu, S.; Wu, C.; Liu, X.; Tao, H.; Huang, Y.; et al. Design, synthesis and activity of novel sorafenib analogues bearing chalcone unit. *Bioorg. Med. Chem. Lett.* **2016**, *26*, 5450-5454.
101. Ramurthy, S.; Subramanian, S.; Aikawa, M.; Amiri, P.; Costales, A.; Dove, J.; et al. Design and Synthesis of Orally Bioavailable Benzimidazoles as Raf Kinase Inhibitors. *J. Med. Chem.* **2008**, *51*, 7049–7052.
102. Baska, F.; Szabadkai, I.; Sipos, A.; Breza, N.; Kékesi, L.; Garamvölgyi, R.; Pharmacophore and Binding Analysis of Known and Novel B-RAF Kinase Inhibitors. *Curr. Med. Chem.* **2014**, *21*, 1938-1955.
103. Smith, A.L.; DeMorin, F.F.; Paras, N.A.; Huang, Q.; Petkus, J.K.; Doherty, E.M.; Nixey, T.; et al. Selective Inhibitors of the Mutant B-Raf Pathway : Discovery of a Potent and Orally Bioavailable Aminoisoquinoline. *J. Med. Chem.* **2009**, 6189–6192.
104. Wang, L.; Zhu, G.; Zhang, Q.; Duan, C.; Zhang, Y.; Zhang, Z.; et al. Rational design, synthesis, and biological evaluation of Pan-Raf inhibitors to overcome resistance. *Org. Biomol. Chem.* **2017**, *15*, 3455–3465.
105. Wang, M.; Xu, S.; Lei, H.; Wang, C.; Xiao, Z.; Jia, S.; et al. Design, synthesis and antitumor activity of Novel Sorafenib derivatives bearing pyrazole scaffold *Bioorg. Med. Chem.* **2017**, *25*, 5754-5763.
106. Wu, Z.; Yan, M.; Hu, S.H.; Yu, Z.C.; Zhu, Y.; Cheng, Y.D.; et al. Design, synthesis and biological evaluation of indole derivatives as novel inhibitors targeting B-Raf kinase. *Chin. Chem. Lett.* **2014**, *25*, 351-354.
107. Vasbinder, M.M.; Aquila, B.; Augustin, M.; Chen, H.; Cheung, T.; Cook, D.; et al. Discovery and Optimization of a Novel Series of Potent Mutant B -

- RafV600E Selective Kinase Inhibitors. *J. Med. Chem.* **2013**, *56*, 1996–2015.
108. Wang, G.M.; Wang, X.; Zhu, J.M.; Guo, B.B.; Yang, Z.; Xu, Z.J.; et al. Docking-based structural splicing and reassembly strategy to develop novel deazapurine derivatives as potent B-Raf V600E inhibitors. *Acta Pharmacol. Sin.* **2017**, *1*, 1–10.
109. Wenglowky, S.; Ren, L.; Ahrendt, K.A.; Laird, E.R.; Aliagas, I.; Aliche, B.; et al. Pyrazolopyridine Inhibitors of B-RafV600E Part 1: The Development of Selective, Orally Bioavailable, and Efficacious Inhibitors. *ACS Med. Chem. Lett.* **2011**, *2*, 342–347.
110. Zhang, Q.; Wang, J.; Wang, F.; Chen, X.; He, Y.; You, Q.; Zhou, H. Identification of type II inhibitors targeting BRAF using privileged pharmacophores. *Chem. Biol. Drug. Des.* **2014**, *83*, 27–36.
111. Lee, J.; Nam, B.S.; Kim, H.; Oh, C.H.; Lee, S.H.; Cho, S.J.; et al. Synthesis of aminoquinazoline derivatives and their antiproliferative activities against melanoma cell line. *Bioorg. Med. Chem. Lett.* **2010**, *20*, 5722–5725.
112. Xie, Y.; Chen, X.; Qin, J.; Kong, X.; Ye, F.; Jiang, Y.; et al. Identification and synthesis of N-(thiophen-2-yl) benzamide derivatives as BRAFV600E inhibitors. *Bioorg. Med. Chem. Lett.* **2013**, *23*, 2306–2312.
113. Xin, B.; Tang, W.; Wang, Y.; Lin, G.; Liu, H.; Jiao, Y.; et al. Design, synthesis and biological evaluation of β -carboline derivatives as novel inhibitors targeting B-Raf kinase. *Bioorg. Med. Chem. Lett.* **2012**, *22*, 4783–4786.
114. Xu, Z.; Yan, G.; Wang, G.; Li, B.; Zhu, J.; Sun, P.; et al. Combining pharmacophore, docking and substructure search approaches to identify and optimize novel B-RafV600E inhibitors. *Bioorg. Med. Chem. Lett.* **2012**, *22*, 5428–5437.
115. Yao, H.; Sun, Q.; Zhu, J. Identification and Characterization of Small-Molecule Inhibitors to Selectively Target the DFG-in over the DFG-out Conformation of the B-Raf Kinase V600E Mutant in Colorectal Cancer. *Arch. Pharm. Chem. Life Sci.* **2016**, *349*, 808–815.
116. Cheng, H.; Chang, Y.; Zhang, L.; Luo, J.; Tu, Z.; Lu, X.; et al. Identification and Optimization of New Dual Inhibitors of B - Raf and Epidermal Growth Factor Receptor Kinases for Overcoming Resistance against Vemurafenib. *J. Med. Chem.* **2014**, *57*, 2692–2703.
117. Youssif, B.M.; Abdelrahman, M.H.; Abdelazeem, A.H.; Abdelgawad, M.A.; Ibrahim, H.M.; Salem, O.I.A.; et al. Design, synthesis, mechanistic and histopathological studies of small-molecules of novel indole-2-carboxamides and pyrazino[1,2-a]indol-1(2H)-ones as potential anticancer agents effecting the reactive oxygen species production. *Eur. J. Med. Chem.* **2018**, *146*, 260–273.
118. Yu, M.; Yang, H.; Wu, K.; Ji, Y.; Ju, L.; Lu, X.; Novel Pyrazoline Derivatives as Bi-inhibitor of COX-2 and B-Raf in Treating Cervical Carcinoma. *Bioorg. Med. Chem.* **2014**, *22*, 4109–4118.
119. Holladay, M.W.; Campbell, B.T.; Rowbottom, M.W.; Chao, Q.; Sprankle, K.G.; Lai, A.G.; et al. 4-Quinazolinyl-oxy-diaryl ureas as new BRAFV600E inhibitors. *Bioorg. Med. Chem. Lett.* **2011**, *21*, 5342–6.
120. Tarazi, H.; El-Gamal, M.I.; Oh, C.H.; Discovery of highly potent V600E-B-RAF kinase inhibitors: Molecular Modeling Study. *Bioorg. Med. Chem.* **2019**, *27*, 655–63.
121. Liu, B.; Yuan, X.; Xu, B.; Zhang, H.; Li, R.; Wang, X.; et al. Synthesis of novel 7-azaindole derivatives containing pyridin-3-ylmethyl dithiocarbamate moiety as potent PKM2 activators and PKM2 nucleus translocation inhibitors. *Eur. J. Med.*

- Chem.* **2019**, *170*, 1-15.
122. Abdelatef, S.A.; El-Saadi, M.T.; Amin, N.H.; Abdelazeem, A.H.; Omar, H.A.; Abdellatif, K.A. Design, synthesis and anticancer evaluation of novel Spirobenzo[h]chromene and spirochromane derivatives with dual EGFR and B-RAF inhibitory activities. *Eur. J. Med. Chem.* **2018**, *150*, 567-78.
 123. Abdel-Maksoud, M.S.; El-Gamal, M.I.; Gamal El-Din, M.M.; Oh, C.H. Design, synthesis, in vitro anticancer evaluation, kinase inhibitory effects, and pharmacokinetic profile of new 1,3,4-triarylpyrazole derivatives possessing terminal sulfonamide moiety. *J. Enz. Inhib. Med. Chem.* **2019**, *34*, 97-09.
 124. El-Gamal, M.I.; Park, B.J.; Oh, C.H.; Synthesis, in vitro antiproliferative activity, and kinase inhibitory effects of pyrazole containing diarylureas and diarylamides. *Eur. J. Med. Chem.* **2018**, *156*, 230-9.
 125. Li, H.L.; Su, M.M.; Xu, Y.J.; Xu, C.; Yang, Y.S.; Zhu, H.L.; Design and biological evaluation of novel triaryl pyrazoline derivatives with dioxane moiety for selective BRAFV600E inhibition. *Eur. J. Med. Chem.* **2018**, *155*, 725-35.
 126. Philp, J.; Lawhorn, B.G.; Graves, A.P.; Shewchuk, L.; Rivera, K.L.; Jolivet, L.J.; et al. 4,6-Diaminopyrimidines as Highly Preferred Troponin I-Interacting Kinase (TNNI3K) Inhibitors. *J. Med. Chem.* **2018**, *61*, 3076-88.
 127. Ruan, B.F.; Lin, M.X.; Shao, Q.; Wang, T.H.; Zhang, Q.; Dong, Y.L.; et al. Modification, Biological Evaluation and SAR Studies of Novel 1H-Pyrazol Derivatives Containing N, N'-Disubstituted Urea Moiety as Potential Anti-Melanoma Agents. *Chem Biodivers.* **2018**, *15*, e1700504.
 128. Sun, S.; He, Z.; Huang, M.; Wang, N.; He, Z.; Kong, X.; Yao, J. Design and discovery of thioether and nicotinamide containing sorafenib analogs as multikinase inhibitors targeting B-Raf, B-RafV600E and VEGFR-2. *Bioorg. Med. Chem.* **2018**, *26*, 2381-91.
 129. Wang, Z.F.; Wang, P.F.; Ma, J.T.; Chai, Y.Z.; Hu, H.M.; Gao, W.L.; et al. Design of potent B-RafV600E inhibitors by multiple copy simulation search strategy. *Chem. Biol. Drug. Des.* **2018**, *91*, 567-74.
 130. Wang, Y.; Wan, S.; Li, Z.; Fu, Y.; Wang, G.; Zhang, J.; Wu, X. Design, synthesis, biological evaluation and molecular modeling of novel 1H-pyrazolo[3,4-d]pyrimidine derivatives as BRAFV600E and VEGFR-2 dual inhibitors. *Eur. J. Med. Chem.* **2018**, *155*, 210-28.
 131. Wang, C.R.; Wang, Z.F.; Shi, L.; Wang, Z.C.; Zhu, H.L.; Design, synthesis, and biological evaluation of pyrazole derivatives containing acetamide bond as potential BRAFV600E inhibitors. *Bio. Med. Chem. Lett.* **2018**, *28*, 2382-90.
 132. Wang, P.F.; Zhang, Y.J.; Wang, D.; Hu, H.M.; Wang, Z.C.; Xu, C.; et al. Design, synthesis, and biological evaluation of new B-RafV600E kinase inhibitors. *Bioorg. Med. Chem.* **2018**, *26*, 2372-80.
 133. Wang, P.F.; Wang, Z.F.; Qiu, H.Y.; Huang, Y.; Hu, H.M.; Wang, Z.C.; Zhu, H.L. Identification and Biological Evaluation of New Type II B-RafV600E Inhibitors. *ChemMedChem* **2018**, *13*, 2558-63.
 134. Zhang, H.Q.; Gong, F.H.; Ye, J.Q.; Zhang, C.; Yue, X.H.; Li, C.G.; et al. Design and discovery of 4-anilinoquinazoline ureas as multikinase inhibitors targeting BRAF, VEGFR-2 and EGFR. *Med. Chem. Commun.* **2014**, *4*, 979-986.
 135. Zhang, C.H.; Zheng, M.W.; Li, Y.P.; Lin, X.D.; Huang, M.; Zhong, L.; et al. Design, Synthesis, and Structure-Activity Relationship Studies of 3-(Phenylethynyl)-1H-pyrazolo[3,4-d]pyrimidin-4-amine Derivatives as a New Class of Src Inhibitors with Potent Activities in Models of Triple Negative Breast Cancer. *J. Med. Chem.* **2015**, *58*, 3957-3974.

136. Wenglowsky, S.; Ahrendt, K.A.; Buckmelter, A.J.; Feng, B.; Gloor, S.L.; Gradl, S.; et al. Pyrazolopyridine inhibitors of B-RafV600E. Part 2: structure-activity relationships. *Bioorg. Med. Chem. Lett.* **2011**, *21*, 5533-7.
137. Tsai, J.; Lee, J.T.; Wang, W.; Zhang, J.; Cho, H.; Mamo, S.; et al. Discovery of a selective inhibitor of oncogenic B-Raf kinase with potent antimelanoma activity. *Proc. Natl. Acad. Sci.* **2008**, *105*, 3041–3046.
138. Hoeflich, K.P.; Herter, S.; Tien, J.; Wong, L.; Berry, L.; Chan, J.; et al. Antitumor efficacy of the novel RAF inhibitor GDC-0879 is predicted by BRAF V600E mutational status and sustained extracellular signal-regulated kinase/mitogen-activated protein kinase pathway suppression. *Cancer Res.* **2009**, *69*, 3042–3051.
139. Montagut, C.; Sharma, S.V.; Shioda, T.; McDermott, U.; Ulman, M.; Ulkus, L.E.; et al. Elevated CRAF as a potential mechanism of acquired resistance to BRAF inhibition in melanoma. *Cancer Res.* **2008**, *68*, 4853-4861.
140. Khazak, V.; Astsaturov, I.; Serebriiskii, I.G.; Golemis, E.A.; Selective Raf inhibition in cancer therapy. *Expert Opin Ther Targets* **2007**, *11*, 1587–1609.
141. Takle A.K.; Brown, M.J.; Davies, S.; Dean, D.K.; Francis, G.; Gaiba, A.; et al. The identification of potent and selective imidazole-based inhibitors of B-Raf kinase. *Bioorg. Med. Chem. Lett.* **2006**, *16*, 378–381.
142. King, A.J.; Patrick, D.R.; Batorsky, R.S.; Ho, M.L.; Do, H.T.; Zhang, S.Y.; et al. Demonstration of a genetic therapeutic index for tumors expressing oncogenic BRAF by the kinase inhibitor SB-590885. *Cancer Res* **2006**, *66*, 11100–11105.
143. Nakamura, A.; Arita, T.; Tsuchiya, S.; Donelan, J.; Chouitar, J.; Carideo, E.; Galvin, K.; et al. Antitumor activity of the selective pan-RAF inhibitor TAK-632 in BRAF inhibitor-resistant melanoma. *Cancer Res.* **2013**, *73*, 7043–55.
144. Girotti, M.R.; Lopes, F.; Preece, N.; Niculescu-Duvaz, D.; Zambon, A.; Davies, L.; et al. Paradox-Breaking RAF Inhibitors that Also Target SRC Are Effective in Drug-Resistant BRAF Mutant Melanoma. *Cancer Cell* **2017**, *31*, 85-96.
145. <http://clinicaltrials.gov> (Accessed on 10th April 2019).
146. Qing, X.; Lee, X. Y.; Raeymaeker J. D.; Tame J. R.; Zhang K.Y.; Maeyer M.D.; Pharmacophore modeling: advances, limitations, and current utility in drug discovery. *J. Rec. Lig. Chan. Res.* **2014**, *7*, 81–92.
147. Li, A.P. Screening for human ADME/Tox drug properties in drug discovery. *Drug Discov Today.* **2001**, *6*, 357–366
148. Kapetanovic I.M. Computer-aided drug discovery and development (CADD): in silico-chemico-biological approach. *Chem. Biol. Interact.* **2008**, *171*, 165–176.
149. Karelson M.; Lobanov, V.S.; Katritzky, A.R. Quantum-Chemical Descriptors in QSAR/QSPR Studies. *Chem. Rev.* **1996**, *96*, 1027–1044.
150. Lee, M.; Kim, D. Large-scale reverse docking profiles and their applications. *BMC Bioinformatics.* **2012**, *13*, S6.
151. Ehrlich, P. Über den jetzigen Stand der Chemotherapie. *Ber. Dtsch. Chem. Ges.* **1909**, *42*, 17–47.
152. Schueler, F.W. *Chemobiodynamics and Drug Design*. New York; McGraw-Hill: **1960**
153. Wermuth, C.G. Ganellin, C.R.; Lindberg. P.; Mitscher. L.A.; Glossary of terms used in medicinal chemistry (IUPAC recommendations 1998). *Pure Appl Chem.* **1998**, *70*, 1129–1143.
154. Yang, S. Y. Pharmacophore modeling and applications in drug discovery: challenges and recent advances. *Drug. Disc. Today.* **2010**, *15*, 11-12
155. Patel Y.; Gillet, V. J.; Bravi G.; Leach, R. A. A comparison of the

- pharmacophore identification programs: Catalyst, DISCO and GASP. *J. Comput.-Aided Mol Design.* **2002**, *16*, 653-681.
156. Jones, G.; Willett, P.; Glen, R.C.; A comparison of the pharmacophore identification programs. *J. Comput.-Aided Mol.Design*, **1995** 532-540.
157. Dietrich, J.; Hulme, C.; Hurley, L.H. The design, synthesis, and evaluation of 8 hybrid DFG-out allosteric kinase inhibitors: a structural analysis of the binding interactions of Gleevec, Nexavar, and BIRB-796. *Bioorg. Med. Chem.* **2010**, *18*, 5738-5748.
158. Verma, J.; Khedkar, V.M.; Coutinho, E.C. 3D-QSAR in drug design--a review. *Curr Top Med Chem.* **2010**, *10*, 95-115.
159. Zhang, S.; Lin, Z.; Pu, Y.; Zhang, Y.; Zhang, L.; Zuo, Z. Comparative QSAR studies using HQSAR, CoMFA, and CoMSIA methods on cyclic sulfone hydroxyethylamines as BACE1 inhibitors. *Comput Biol Chem.* **2017**, *67*, 38-47.
160. Sybyl X (2011) Molecular modelling software, Tripos Certara, V.1.2, St. Louis.
161. Borisa, A.; Bhatt, H. 3D-QSAR (CoMFA, CoMFA-RG, CoMSIA) and molecular docking study of thienopyrimidine and thienopyridine derivatives to explore structural requirements for aurora-B kinase inhibition. *Eur. J. Pharm. Sci.* **2015**, *79*, 1-12.
162. Nilewar; Shrikant, S.; Kathiravan; Muthu. K. 3D CoMFA, CoMSIA, topomer CoMFA and HQSAR studies on aromatic acid esters for carbonic anhydrase inhibitory activity. *J. Chemo.* **2014**, *28*, 60-70.
163. Tong, J.; Zhan, P.; Wang, X. S.; Wu, Y. Quionolone carboxylic acid derivatives as HIV-1 integrase inhibitors: Docking-based HQSAR and topomer CoMFA analyses. *J. Chemom.* **2017**, *31*, e2934.
164. Zambre, V.P.; Murumkar, P.R.; Giridhar, R.; Yadav, M.R.; Development of highly predictive 3D-QSAR CoMSIA models for anthraquinone and acridone derivatives as telomerase inhibitors targeting G-quadruplex DNA telomere. *J Mol Graph Model.* **2010**, *29*, 223-239.
165. Clark M.; Cramer R, D. The Probability of Chance Correlation Using Partial Least Squares (PLS). *Mol. Info.* **1993**, *12*, 137-145.
166. Meng, X. Y.; Zhang, H.X.; Mezei, M.; Cui, M. Molecular Docking: A powerful approach for structure-based drug discovery *Curr Comput Aided Drug Des.* **2011**, *7*, 146-157.
167. Hein, D.W.; Alheim, R.J.; Leavitt J.J.; The Use of Polyphosphoric Acid in the Synthesis of 2-Aryl- and 2-Alkyl-substituted Benzimidazoles, Benzoxazoles and Benzothiazoles¹. *J. Am. Chem. Soc.* **1957**, *79*, 427-429.
168. Charles, M.D.; Schultz, P.; Buchwald, S.L. Efficient Pd-Catalyzed Amination of Heteroaryl Halides. *Org. Lett.* **2005**, *7*, 3965-3968.
169. Liu B.; Gao Y.; Wang X.; Wang Y.; Fu L. Germacrone Inhibits the Proliferation of Glioma Cells by Promoting Apoptosis and Inducing Cell Cycle Arrest. *Mol Med Rep.* **2014**, 1046-1050
170. Bhuva H.; Kini S. Synthesis, Anticancer Activity and Docking of Some Substituted Benzothiazoles as Tyrosine Kinase Inhibitors. *J Mol Graph Model* **2010**, *29*, 32-37
171. Jessy M.; Gubba D.; Dinakaran V.; Jesil A.; Ramaiah J.; Synthesis and Characterisation of Novel 2,4-Diphenyloxazole Derivatives and Evaluation of their In Vitro Antioxidant and Anticancer Activity. *J Pharm Res* **2013**, *6*, 210-213
172. Tao Y.; Jaegal S.; Yanyan Y.; Se Eun B.; Ji Hye K.; Ho Sik R.; et al. 3-(4-(tert-Octyl)phenoxy)propane-1,2-diol Suppresses Inflammatory Responses via

Inhibition of Multiple Kinases. *Biochem Pharmacol*, **2012**, 83, 1540-1551.

173. Manjula S.; Malleshappa N.; Noolvi K.; Parihar V.; Reddy M.; Ramani V.; et al. Synthesis and Antitumor Activity of Optically Active Thiourea and their 2-aminobenzothiazole Derivatives: A Novel Class of Anticancer Agents . *Eur. J. Med. Chem* **2009**, 44, 2923-2929.
174. Chaube U.J.; Vyasa V.K.; Bhatt H.G. Design and synthesis of potent N-phenylpyrimidine derivatives for the treatment of skin cancer. *RSC Adv.*, **2016**, 6, 10285-10297.

ORIGINALITY REPORT

8%

SIMILARITY INDEX

4%

INTERNET SOURCES

5%

PUBLICATIONS

5%

STUDENT PAPERS

PRIMARY SOURCES

1	Fatima Arshad, Mohemmed Faraz Khan, Wasim Akhtar, Mohammad Mumtaz Alam et al. "Revealing quinquennial anticancer journey of morpholine: A SAR based review", European Journal of Medicinal Chemistry, 2019 Publication	2%
2	Submitted to Institute of Technology, Nirma University Student Paper	1%
3	www.cancer.gov Internet Source	1%
4	journals.plos.org Internet Source	1%
5	article.sciencepublishinggroup.com Internet Source	1%
6	repository.ubaya.ac.id Internet Source	1%
7	shodhganga.inflibnet.ac.in Internet Source	1%

8

Weimin Yang, Yadong Chen, Xiang Zhou, Yazhou Gu, Wenqi Qian, Fan Zhang, Wei Han, Tao Lu, Weifang Tang. "Design, synthesis and biological evaluation of bis-aryl ureas and amides based on 2-amino-3-purinylypyridine scaffold as DFG-out B-Raf kinase inhibitors", European Journal of Medicinal Chemistry, 2015

Publication

1%

9

Yingjun Li, Huimin Cheng, Zhang Zhang, Xiaoxi Zhuang et al. "(3-Ethynyl-2,4-difluorophenyl)sulfonamide Derivatives as Selective Raf Inhibitors ", ACS Medicinal Chemistry Letters, 2015

Publication

1%

Exclude quotes Off

Exclude matches < 1%

Exclude bibliography Off